

THE MOMENTUM FLUX
IN TWO-PHASE FLOW

by

GERRY B. ANDEEN

B.S. (M.E.) University of Michigan (1962)

S.M. (M.E.) Massachusetts Institute of Technology (1963)

SUBMITTED IN PARTIAL FULFILLMENT
OF THE REQUIREMENTS FOR THE
DEGREE OF DOCTOR OF SCIENCE

at the

MASSACHUSETTS INSTITUTE OF TECHNOLOGY

October, 1965

Signature of Author *Gerry B. Andeen* Department of Mechanical Engineering

Certified by *[Signature]* Thesis Supervisor

Accepted by *[Signature]* Chairman, Departmental Committee on Graduate Students

THE MOMENTUM FLUX
IN TWO-PHASE FLOW

by

Gerry B. Andeen

Submitted to the Department of Mechanical
Engineering in October, 1965, in partial
fulfillment of the requirements for the
degree of Doctor of Science

ABSTRACT

The average momentum flux at a section of a pipe with two-phase upflow has been measured by the impulse technique. Steam-water and air-water mixtures were tested in one-inch and one-half inch nominal pipes. Homogeneous velocities ranging from 150 to 1200 ft/sec. and qualities from 5% to 85% were tested.

The results are compared to the results of models currently in practice for predicting pressure drop and critical flow. The influence of the void fraction, the velocity profile, phase distribution and fluctuations upon the momentum flux are discussed.

Thesis Supervisor: Peter Griffith

Title: Associate Professor of Mechanical Engineering

BIOGRAPHICAL SKETCH

I was born in Chicago in 1940, of little importance to me since we didn't live there long enough for me to remember it. I went to grade school in Minneapolis and caught gophers. You see, gophers always have two entrances to their burrows. If you pour water down one entrance, a wet gopher will come up into an old pan over the other.

I attended high school in Connecticut as the family moved there, and I learned that I never really learned to spell. The problem is that spelling is hardly ever phonetic. Take "nite," for example, neither kind is spelled the way they both sound. You can see why I studied engineering at the University of Michigan. The only prehistoric characteristic of engineering is awkward units, and no student pays attention to units anyway.

In 1962 I graduated from Michigan and came to MIT where I have been since. In fact, with the exception of summer industrial jobs, and an NROTC cruise, I have been in school continuously. For this, I owe thanks to the Scott Paper Company Foundation as an undergraduate and to the National Science Foundation as a graduate student. I have been elected to several honorary societies and, of course, am a student member of the ASME.

ACKNOWLEDGMENTS

The author wishes to thank Professor Peter Griffith and the other members of the committee, Professor J. L. Smith, Jr., and Professor S. W. Gouse, Jr., for their guidance throughout the project. Special thanks are also due to Professors Rohsenow, Brown, Bergles, Suo, and Richardson for their thoughtful and constructive suggestions.

Appreciation is expressed to the Engineering Project Laboratory Staff for their efforts in assembling the experimental apparatus.

Financial support for the project was provided by the U.S. Atomic Energy Commission, AEC Contract AT(30-1) - 3496.

The MIT Computation Center provided computer time for data reduction.

TABLE OF CONTENTS

	Page
CHAPTER I INTRODUCTION	1
1.1 Pressure Drop in a Pipe	1
1.2 Momentum Flux Models	3
1.3 Differences between Models	6
1.4 Direct Measurement	7
1.5 Fluctuation	8
1.6 Critical Flow	8
CHAPTER II ANALYTICAL CONSIDERATIONS	10
2.1 The Momentum Multiplier	10
2.2 Possible Bounds on the Momentum Multiplier Value	10
2.2.1 Martinelli's Bounds	11
2.2.2 Requirements for Minimum Possible Momentum Flux	12
2.2.3 Minimum Momentum Flux at Specified Void Fraction	13
2.2.4 Minimum Momentum Flux Model	14
2.2.5 Unsteady Minimum Momentum Flux	16
2.3 Deviations from Minimum Possible Value	17
2.3.1 Void Fraction	17
2.3.2 Velocity Distribution	19
2.3.3 Phase Distribution	22
2.3.4 Time Variation	24
2.4 Differential Deviation from Single Phase	29
CHAPTER III EXPERIMENTAL PROGRAM	30
3.1 Feasibility	30
3.2 Design Requirements	30

TABLE OF CONTENTS
(continued)

3.3	Original Design	31
3.3.1	Tank and Internals	31
3.3.2	Turning Tee	34
3.3.3	Feed System	35
3.4	Modified Design	38
3.4.1	Tank and Internals	38
3.4.2	Tee	39
3.4.3	Feed System	40
3.5	Void Fraction Data	40
3.6	Testing	41
3.7	Data System	41
3.7.1	Observation	42
3.7.2	Tape Recorder	42
3.7.3	Brush Recorder	42
3.8	Data Reduction	43
3.8.1	Average Force Data	43
3.8.2	Fluctuating Data	43
CHAPTER IV	RESULTS	44
4.1	Average Momentum Flux Data	44
4.2	Rose's Results	45
4.3	Vance's Results	46
4.4	Void Fraction Measurements	47
4.5	Fluctuations	48
4.5.1	Brush Recorder	49
4.5.2	Spectral Analysis	49
4.6	Choke Flow	50
4.7	Non-Adiabatic Flow	51
4.8	Discussion of Effects	52
4.8.1	Void Fraction Deviation	52

TABLE OF CONTENTS
(continued)

4.8.2	Velocity Distribution	52
4.8.3	Entrainment	53
4.8.4	Fluctuations	53
4.9	Interpolation and Extrapolation	54
CHAPTER V	SUMMARY	57
5.1	The Two-Velocity Slip Model	57
5.2	The Homogeneous Model	57
5.3	Deviations from Minimum Momentum Flux	58
5.4	Implications	59
APPENDIX A	MOMENTUM EQUATION DERIVATIONS	60
APPENDIX B	CAUSES OF ZERO SHIFT	64
APPENDIX C	FUNCTIONS TO FIT CURVES FOR DATA REDUCTION PROGRAM	66
APPENDIX D	EQUATION OF MOTION OF THE TEE	68
APPENDIX E	DATA	69
APPENDIX F	DATA OF VANCE	70
REFERENCES		71
FIGURES		

LIST OF FIGURES

Fig. Number	Title
1	Comparison between Homogeneous and Slip Models
2	Cross Section of Pressure Vessel Showing Internals
3	Schematic of Test Apparatus
4	LVDT Arrangement
5	Electrical Apparatus
6	Jet Surface Profiles
7	Turning Tee Design
8	Core Traverse
9	Beam Constant
10	Static Test
11	Weigh Tank Calibration
12	Steam Calibration Test
13	Beam Response
14	Filter Performance
15	Pluck Tests
16	Quality-Void Fraction Relationship
17	Air-Water Liquid Fraction
18-19	Effect of Void Fraction on Slip Model Momentum Multiplier
20	Entrainment Model
21	Anderson and Mantzoranis Model

Fig. Number	Title
22	Reichardt's Hot-Wire Data
23-28	Fluctuating Model
29	Rose's Void Fraction Data
30	Rose's Momentum Flux Data
31-40	Steam-Water Data
	31 - Atmospheric Pressure, One-Inch Pipe
	32 - Atmospheric Pressure, One-Half Inch Pipe
	33 - 30 psia, One-Inch Pipe
	34 - 30 psia, One-Half Inch Pipe
	35 - 60 psia, One-Inch Pipe
	36 - 60 psia, One-Half Inch Pipe
	37 - 90 psia, One-Inch Pipe
	38 - 90 psia, One-Half Inch Pipe
	39 - 120 psia, One-Inch Pipe
	40 - 120 psia, One-Half Inch Pipe
41-42	Air-Water Data
43	Data of Vance
44	Brush Records
45	Fluctuation Magnitude
46	Spectral Analysis

NOMENCLATURE

A	Area
B	Body force
$^{\circ}\text{C}$	Degrees Centigrade
C_1	Constant in equation (2-22)
C_2	Constant in equation (2-22)
C_3	Constant in equation (2-28)
C_4	Constant in equation (2-28)
C_5	Constant in equation (2-45)
C_6	Constant in equation (2-46)
C.S.	Control Surface
C.V.	Control Volume
F	Force
F_s	Surface force
F_{τ}	Shear force
G	Mass velocity
H_1	Defined, equation (2-5)
H_2	Defined, equation (2-10)
K	Orifice Coefficient (C-4)
M	Momentum Flux
MM	Momentum Multiplier
P	Pressure

R	Potentiometer Reading (C-2)
Re	Reynolds Number
T	Length of Time
V	Velocity
V'	Fluctuating Velocity with Zero Mean
X	Quality
YK	Defined equation (4-6)
ZK	Defined equation (4-7)
a	Location or position in area
b	Magnitude of sinusoidal perturbation, equation (2-34)
c	Coefficient of Damping
c'	Coefficient of Damping
d	Indicates differential
e	Voltage
f	Subscript indicates liquid
g	Gravitational acceleration
g	Subscript indicates gas
g_c	Gravitational constant
h	Width of arriving flow, equation (3-1)
i	Subscript indicates i^{th} term
k	Spring constant
k'	Spring constant
l	Length
m	Mass

m'	Mass
\dot{m}	Mass flow rate
n	Exponent in equation (4-3)
r	Radius
r_o	Outside radius
t	Time
v	Specific volume ($1/\rho$)
x	Displacement
y	Displacement
z	Displacement

Greek Letters

α	Void fraction
β	Decay constant
γ	Mean liquid fraction deviation equation (2-52)
δ	Calculus of variations differential
ϵ	Entrainment, equation (2-29)
S_1	Constant defined in equation (2-3a)
S_2	Constant defined in equation (2-4a)
S_3	Constant defined in equation (2-9a)
η_f	Local liquid mass flow fraction
η_g	Local gas mass flow fraction
θ	Thom's constant, equation (2-21)
λ_1	Constant, see 2.2.2
λ_2	Constant, see 2.2.2

λ_3	Constant, see 2.2.3
μ	Coefficient of viscosity
π	Ratio of circle circumference to radius
ρ	Density
ϕ	Bankoff's constant, equation (2-20a)
ω	Sinusoidal frequency, equation (2-34)

Other symbols

∂	Partial differential
f	Indicates function of the variables following
\mathcal{V}	Volume
\rightarrow	Indicates vector quantity
$\bar{\quad}$	Indicates averaged quantity

CHAPTER I

INTRODUCTION

The two-phase momentum flux has come to attention primarily through its relationship to pressure changes in systems involving phase change, water tube boilers, nuclear reactors, refrigerating evaporators and condensers, rockets, condensing ejectors, and the like. In addition to being of direct application, knowledge of the momentum flux would also result in additional basic knowledge and understanding of the nature of two-phase flows and the applicability of various models. This basic understanding of the momentum flux is, among other applications, particularly relevant to the critical flow phenomena.

1.1 Pressure Drop in a Pipe

The ability to predict two-phase pressure change to nearly the same degree of accuracy as is possible with single-phase flow has eluded investigators. This is fascinating from a motivational point of view as accurate determination of the two-phase pressures are of fundamental importance in the design of evaporators, condensers, and particularly nuclear reactors. That the technological need has not brought about a dependable solution is sufficient testimony to the difficulty of the problem.

The two-phase pressure change, like the single-phase change, can be considered to be composed of several, individual contributing terms. A development of the general momentum equation (see Appendix A) shows these contributing terms to be a frictional pressure drop, an hydrostatic pressure change, a momentum flux change, and an acceleration transient. Each of the terms is considerably more difficult to evaluate in the two-phase case than for a single phase. In particular, the hydrostatic pressure change is elementary for the single phase while it requires a knowledge of phase distribution for the two-phase phenomena. In single phase, fully developed, incompressible flows, the difference is easily computed assuming a similarity of velocity profiles. Further, the momentum pressure change is only significant in proportion to the frictional pressure change at high Mach numbers. It is seen that for general use the pressure change in a single phase flow, neglecting transient terms, is due primarily to one difficult term, the frictional term.

The relative simplicity of the single phase flow may well be one of the important reasons for the retarded development of two-phase technology. In the single phase, a simple pressure difference measurement is easily related to the one term needing correlation, the frictional term. This is simply not so for the two-phase system, but it did serve as a starting point for two-phase study. Certain holdovers unfortunately serve as mental blocks, and time after time

the hydrostatic and momentum flux terms were simply estimated and subtracted out in investigating the two-phase friction term. It was not considered important to consider these terms more carefully, even though they often served as the largest portion of the pressure change. Through careless consideration of the overall equation, only a half-way job can be done on the frictional correlation.

A second reason for the retarded development of two-phase technology, also due to the single phase study influence, is the tendency to consider the flow on the average. This is acceptable in the single phase as there are no natural deviations from the average steady flow, except in a careful consideration of turbulent flow. Averaging is not generally acceptable in two-phase flow because of the non-linear nature of the momentum flux and the occurrence of slugs, waves, and other natural fluctuations. As with turbulent flow, the first level of complication is a recognition and treatment of the natural fluctuations.

1.2 Momentum Flux Models

A model is a proposal giving the phase and velocity distribution as a function of space and time. For the purposes here, it is information from which one may calculate a momentum flux. A model may, of course, include several experimental parameters, in the limit being an actual photograph of the phenomena, or it may be a

highly simplified approximation. Several models have been proposed by investigators of two-phase flow pressure change in order to reduce their data for friction correlation. It should be noted that all are steady or averaged in time models.

The most simple model is the homogeneous. It merely assumes that the phases are mixed in the ratio of the flowing quality at a single velocity. The assumption is popular in that it is simple to deal with. Unfortunately, it assumes that the average velocity of the liquid and the gas are the same. Through measurement of the void fraction, the percentage of gas-occupied area at a section, this has been shown to be a gross error; the average gas velocity is often many times the average liquid velocity. Incidentally, the original purpose of the void fraction measurement was to establish the hydrostatic term.

Introduction of the void fraction as an experimental parameter, leading to a calculation of a velocity for the liquid and another for the gas, gives the two-velocity or slip model. Martinelli (1)* made a moderately successful two-phase pressure change correlation in which he calculated the momentum flux by the slip model. He presented an empirical chart of void fraction versus quality. Even recent investigation (2), apparently inspired by Martinelli's relative success, retains the two-velocity model for the momentum flux calculation.

* Numbers in parentheses refer to references at end of report.

They differ only in that Thom, the recent investigator, presents a mathematical relationship between void fraction in quality. The two velocity model is by far the most popular model, perhaps because it is the most simple model which manages to avoid obvious errors such as discrepancy in the void fraction.

At higher qualities and gas velocities, much of the liquid flow seems to become entrained as droplets in the gas stream. Thus was developed the entrainment model. An entrainment factor, of empirical origin, denotes the fraction of the liquid flow which is traveling at the gas velocity. The entrainment model also establishes the velocities to preserve the empirical void fraction. Magiros and Duckler (3) essentially adopt the entrainment model when they recommend that momentum be neglected in the liquid film and calculated on the basis of entrainment in the gas core.

Bankoff (4) demonstrated additional sophistication by proposing that the density and velocity profiles need not, and in fact do not, take step changes across a section. He proposed a profile for the density and another for the velocity and proceeded to show that slip between the average velocities was indeed the result. Bankoff investigated the low quality, bubbly flow, region. The power law profiles he suggested were essentially guesses based on satisfying the void fraction data.

Anderson and Mantzoranis (5) did essentially the same thing

as Bankoff in the annular flow region. Their results were highly tailored to fit empirical data and the profiles they suggest are suspect on the basis of physical reasoning. Silvestri (6) has made measurements of both the density and velocity profiles in the entrained liquid gas region. He was unsuccessful in integrating the values to predict reasonable momentum flux differences. The difficulties with complete profile specification are to find the profiles, or enough empirical data to reasonably specify them, and to deal with the problem of non-linear averaging.

1.3 Differences between Models

The selection of a model is not critical when the difference between them for the purposes for which they are to be used is small. Unfortunately, the difference in momentum predicted by the models is large. Figure 1a shows a plot of momentum pressure change versus quality as predicted by the homogeneous and by the two-velocity model, void fraction as given by Martinelli. The two models predict significantly different results at the lower qualities. Figure 1b shows the ratio of the homogeneous to the two-velocity model. Thus it can be seen that in cases where momentum flux differences play any significant role, as in rapid heating or cooling, the accurate determination of the correct model, the correct momentum flux, is of vital importance.

1.4 Direct Measurement

Four experiments are described in the literature which directly measure the momentum flux. All used the turning tee method used by this experimenter. Linning (7) first made the measurement and reduced his data to slip ratio data according to the two-velocity model. Semenov (8) did essentially the same thing, followed by Vance (9) who reproduced Linning's experiment. Semenov and Vance, both patterned their data reduction after Linning, using the two-velocity model to predict slip. As will be emphasized later, the momentum flux is more than a function of the slip ratio, and the momentum flux cannot be returned to a slip ratio which is representative of the true void fraction data. The experimenters mentioned had steady force measuring devices and were not equipped to consider fluctuating forces.

The other investigation is that of Rose (10) who attempted to evaluate each of the pressure drop terms by independent measurement in the bubbly flow regime. Rose measured the void fraction and compared his momentum flux data with that predicted by his measured void fraction in the two-velocity model and with that predicted by the homogeneous model. Although one does not necessarily expect the two-velocity model to hold as well in bubbly flow as it does in annular flow, (the two-velocity model is often called the "annular model"), the data does point out that the slip model does violate

experimental data. Rose's data is shown in Figures 29 and 30 and will be discussed in more detail.

Outside of the bubbly flow regime, the total number of experimental points is about fifty, mostly due to Vance. Considerably more direct measurement discussed in relation to the flow models is awaited.

1.5 Fluctuation

As has been mentioned, the time unsteadiness is of vital importance in two-phase flow as waves and slugs occur naturally. Some attempts have been made to correlate these natural fluctuations (8), and many investigators have presented some of their fluctuating data in its raw form. Silvestri (6) among others is able to recognize flow regimes by the fluctuating nature of some quantity. Although virtually all researchers have observed the unsteady nature, as has been mentioned, every effort has been made to neglect it through averaging. Even systematic investigations as with limited data reduction such as that of Semenov (8) are rare.

The void fraction and the momentum flux are excellent variables for the investigation of fluctuations as they can be measured at a section.

1.6 Critical Flow

Critical flow of two-phase mixtures have been predicted on the

basis of the homogeneous and two-velocity models (11). Fauske (11) claims, without giving his reasoning, that critical flow is bounded by the predictions based on these models. At the critical flow, the momentum flux change is of greatest importance. The investigation of the momentum flux should then lend some information to the validity of the critical flow modeling and the critical flow itself.

CHAPTER II

ANALYTICAL CONSIDERATIONS

2.1 The Momentum Multiplier

The momentum flux can be reduced with respect to the flow rate by the consideration of a momentum multiplier defined as

$$MM = \frac{A \iint \rho V^2 dA}{g_c (\iint \rho V dA)^2} = \frac{\text{Force}}{G^2 A} \quad (2-1)$$

This is the same momentum multiplier defined and presented by Martinelli (1). It is important to note that the momentum multiplier is not a dimensionless quantity and that the dimensions used by Martinelli are not the same as those presented in this paper.

The consideration of the momentum flux at a particular flow rate is the same as the consideration of the momentum multiplier at the same flow rate. With this fact in mind, the terms will be used interchangeably.

2.2 Possible Bounds on the Momentum Multiplier Value

In any investigation it is of interest to know of any limits that bound the values of inquiry. The knowledge of bounds is helpful in evaluating the validity of the empirical data and in forming models or parameters by which the data may be correlated and understood.

2.2.1 Martinelli's Bounds Martinelli suspected that the actual momentum multiplier lay between those predicted by the homogeneous and two-velocity models. The given reasoning was that "the water-vapor mixture ... will be partially in the form of fog and partially separated liquid and vapor." To be more exact, the reasoning is that the two models represent idealization from which deviations always occur toward the other. Homogeneous flow is always moderated by slip, so that the average gas velocity exceeds the average liquid velocity. The two-velocity model cannot exist either, if only for the step velocity gradient between the phases and the resulting deviation will be toward the homogeneous. Apparently Fauske (11) would hold to a similar argument as he predicts that the two models give bounds to critical flow values.

That the two-velocity model gives a minimum momentum multiplier value is valid as will be shown shortly. It is impossible to conceive of a model whereby a smaller momentum multiplier value may be achieved. That the homogeneous model represents an upper bound is not similarly true, but represents only the opinion of the investigators as to the nature of the phenomena. If one conceives of the flow of one of the phases in a smaller and smaller area, the momentum multiplier grows larger without bound. As the investigators have given no physical reasoning as to why all deviations should be lower in value than the homogeneous, it does not seem reasonable to accept this as a real bound.

2.2.2 Requirements for Minimum Possible Momentum Flux The density, ρ , and the velocity, V , are allowed to be unknown functions of the position, a , in the cross sectional area, A , and of time, t . We wish to find the requirements on these functions such that the minimum possible average momentum flux is given as a result.

$$M = \lim_{T \rightarrow \infty} \frac{1}{T} \int_0^T \iint_A \rho(a,t) V^2(a,t) da dt \quad (2-2)$$

The only constraint to be considered is that of average continuity of each phase.

$$\frac{\dot{m}_f}{S_1} = \lim_{T \rightarrow \infty} \frac{1}{T} \int_0^T \iint_A (\rho(a,t) - \rho_g) V(a,t) da dt \quad (2-3)$$

$$S_1 = \frac{\rho_f}{\rho_f - \rho_g} \quad (2-3a)$$

$$\frac{\dot{m}_g}{S_2} = \lim_{T \rightarrow \infty} \frac{1}{T} \int_0^T \iint_A (\rho_f - \rho(a,t)) V(a,t) da dt \quad (2-4)$$

$$S_2 = \frac{\rho_g}{\rho_f - \rho_g} \quad (2-4a)$$

Following the method of calculus of variations

$$H_1 = \lim_{T \rightarrow \infty} \frac{1}{T} \int_0^T \iint_A \left[\rho(a,t) V^2(a,t) + \lambda_1 (\rho(a,t) - \rho_g) + \lambda_2 (\rho_f - \rho(a,t)) V(a,t) \right] da dt \quad (2-5)$$

where λ_1 and λ_2 are constants.

$$\delta H_1 = \lim_{T \rightarrow \infty} \frac{1}{T} \int_0^T \int_A \left\{ [2P(a,t) V(a,t) + \lambda_1 (P(a,t) - P_g) \right. \quad (2-6)$$

$$\left. + \lambda_2 (P_f - P(a,t))] \delta V + [V^2(a,t) + \lambda_1 V(a,t) - \lambda_2 V(a,t)] \delta P \right\} da dt$$

In order that $\delta H = 0$

$$2P(a,t) V(a,t) + \lambda_1 (P(a,t) - P_g) + \lambda_2 (P_f - P(a,t)) = 0 \quad (2-7)$$

and

$$V^2(a,t) + \lambda_1 V(a,t) - \lambda_2 V(a,t) = 0 \quad (2-8)$$

Equations (2-7) and (2-8) along with the two continuity equations, (2-3) and (2-4), specify the conditions on $P(a,t)$, $V(a,t)$, λ_1 , and λ_2 for the minimum possible momentum flux.

2.2.3 Minimum Momentum Flux at Specified Void Fraction In addition to the continuity constraints of equations (2-3) and (2-4), an average void fraction constraint may be added.

$$\frac{\alpha}{S_3} = \lim_{T \rightarrow \infty} \frac{1}{T} \int_0^T \int_A P_f - P(a,t) da dt \quad (2-9)$$

$$S_3 = \frac{1}{A(P_f - P_g)} \quad (2-9a)$$

Equation (2-5) is modified by the additional constraint

$$H_2 = \lim_{T \rightarrow \infty} \frac{1}{T} \int_0^T \int_A [P(a,t) V^2(a,t) + \lambda_1 (P(a,t) - P_g) \quad (2-10)$$

$$+ \lambda_2 (P_f - P(a,t)) V(a,t) + \lambda_3 (P_f - P(a,t))] da dt$$

where λ_3 is an additional constant.

$$\delta H_2 = \lim_{T \rightarrow \infty} \frac{1}{T} \int_0^T \iint_A \left\{ \left[2 \rho(a, t) V(a, t) + \lambda_1 (\rho(a, t) - \rho_f) + \lambda_2 (\rho_f - \rho(a, t)) \right] \delta V + \left[V^2(a, t) + \lambda_1 V(a, t) - \lambda_2 V(a, t) - \lambda_3 \right] \delta \rho \right\} da dt \quad (2-11)$$

Again setting $\delta H = 0$ gives

$$V^2(a, t) + \lambda_1 V(a, t) - \lambda_2 V(a, t) - \lambda_3 = 0 \quad (2-12)$$

and equation (2-7) as before. Thus equations (2-7) and (2-12) along with the constraints, equations (2-3), (2-4), and (2-9) specify the conditions for the minimum momentum at a given void fraction.

Although it is difficult to find the solutions to the equations by direct means, it is quite simple to test a suspected solution. Because of its flat velocity profiles, we suspect that the two-velocity model may be a solution for the minimum momentum flux at a given void fraction. That this is true is easily verified. Thus Martinelli's minimum bound is shown to be valid by continuity considerations alone.

2.2.4 Minimum Momentum Flux Model It is suspected that the void fraction in the two-velocity model might be adjusted to give the minimum momentum flux and that the result might satisfy the minimum possible momentum flux requirements. It is noted that as the void

fraction approaches zero or one, the momentum flux value of this model approaches infinity (Figures 18 and 19). Also of note is the fact that void fraction values are not singular, that another void fraction in addition to the homogeneous void fraction gives the homogeneous momentum flux value.

$$M = \left[\frac{m_f^2}{(1-\alpha)\rho_f} + \frac{m_g^2}{\alpha\rho_g} \right] \frac{1}{A g_c} \quad (2-13)$$

In order that $\frac{dM}{d\alpha} = 0$

$$\alpha = \frac{\left(\frac{u_g}{u_f}\right)^{\frac{1}{2}} X}{1 + \left[\left(\frac{u_g}{u_f}\right)^{\frac{1}{2}} - 1\right] X} \quad (2-14)$$

$$= \frac{1}{1 + \left(\frac{1-X}{X}\right) \left(\frac{u_g}{u_f}\right)^{\frac{1}{2}}} \quad (2-14b)$$

A substitution shows that the two-velocity model at the void fraction given in equation (2-14) satisfies the requirements for the minimum possible momentum.

At the value of void fraction giving the minimum possible momentum flux, the slip ratio is found to be

$$\frac{V_g}{V_f} = \left(\frac{u_g}{u_f}\right)^{\frac{1}{2}} \quad (2-15)$$

a result common in two-phase flow. It can be found by considering the kinetic energy per unit cross sectional area to be the same in each phase. It was also derived by Fauske (11) by a more tortuous route. Fauske's critical flow model is thus the flow with minimum momentum flux.

2.2.5 Unsteady Minimum Momentum Flux It should be recognized that the two-velocity model at the specified void fraction represents only one of many solutions to the minimum momentum flux requirements. The other solutions are all of a time varying nature, however, leaving the two-velocity model as the only steady-state solution.

That time varying solutions exist can be demonstrated by physical reasoning. Consider a liquid jet leaving a nozzle in a steady flow at some angle upward, against gravity. Surface tension acts to break up the stream into droplets which, when they pass through the same elevation as the nozzle, have the same average momentum as at the nozzle. If the stream is enclosed in a frictionless wall duct including a gas phase introduced to give the minimum possible two-phase momentum flux at the jet, the flow will have an unsteady, minimum average momentum flux as it passes the nozzle elevation. Many of the unsteady solutions can be visualized by changing the angle of the jet giving more or less time for the fluid to form droplets.

2.3 Deviations from Minimum Possible Value

Generally speaking, deviation from the minimum possible momentum flux value is caused by deviation of the density and velocity profiles from their minimum functions. These deviations may be classified in one or more of four categories: void fraction phase distribution changes, velocity profile alterations, entrainment phase distribution changes, or time variations. An attempt will be made to investigate the influence of each of the types of deviation.

2.3.1 Void Fraction The large deviation between the homogeneous and two-velocity model momentum fluxes is due entirely to difference in void fraction assumption. The homogeneous void fraction

$$\alpha = \frac{X \frac{v_f}{v_g}}{1 + \left(\frac{v_f}{v_g} - 1 \right) X} = \frac{1}{1 + \left(\frac{1-X}{X} \right) \frac{v_f}{v_g}} \quad (2-16)$$

$$\frac{V_g}{V_f} = 1 \quad (2-17)$$

is considerably greater than minimum momentum flux void fraction. A graphical comparison is provided in Figure 16 at atmospheric pressure.

Several other values of void fraction versus quality have been suggested and are shown on the same figure. Martinelli's curve was reduced from actual data and has been given without mathematical correlation.

Zivi (12) developed the relation

$$\alpha = \frac{\left(\frac{v_g}{v_f}\right)^{\frac{2}{3}} X}{1 + \left[\left(\frac{v_g}{v_f}\right)^{\frac{2}{3}} - 1\right] X} = \frac{1}{1 + \left(\frac{1-X}{X}\right) \left(\frac{v_f}{v_g}\right)^{\frac{2}{3}}} \quad (2-18)$$

$$\frac{V_g}{V_f} = \left(\frac{v_g}{v_f}\right)^{\frac{1}{3}} \quad (2-19)$$

on the basis of a minimum kinetic energy flux.

Bankoff (4) gave the relation

$$\alpha = \frac{\phi \left(\frac{v_g}{v_f}\right) X}{1 + X \left(\frac{v_g}{v_f} - 1\right)} \quad (2-20)$$

$$\phi = 0.71 + .0001 P \quad (2-20a)$$

on the basis of his assumed density and velocity profiles in bubbly flow. One notes that Bankoff's model certainly fails outside of the low quality region and does not satisfy the known point that the void fraction is unity at single-phase gas flow.

Thom (2) proposes that the general form,

$$\alpha = \frac{\Theta X}{1 + X(\Theta - 1)} \quad (2-21)$$

where Θ should be determined by experimental evidence, best fits all the known data.

The relations of the form

$$\alpha = \frac{C_1 X}{1 + C_2 X} \quad (2-22)$$

are symmetric about the $X = (1 - \alpha)$ axis (the expressions are identical when X is replaced by $(1 - \alpha)$ and α by $(1 - X)$). This is at variance to the Martinelli result which is clearly skewed. The Bankoff model, although intended for low quality is also pleasingly skewed, a shape which seems necessary to best fit the data.

The void fractions reviewed are between the homogeneous and the minimum momentum flux void fractions. They are, excluding the Bankoff model, sufficiently close to the minimum momentum value that they all give nearly the same momentum flux. This is to be expected since they are in the region where $dM/d\alpha$ is small. At lower qualities ($X < .05$) the Martinelli curve does depart by a sufficient difference to make a noticeable difference in the momentum flux. It can be said, with the exception of the Bankoff model and the Martinelli curve at low quality, that the selection of void fraction correlation makes no difference in the momentum flux value. They are all sufficiently close to the minimum momentum flux value (see Figures 18 and 19).

2.3.2 Velocity Distribution In a single-phase flow the minimum momentum velocity profile is the uniform profile where

$$V = \frac{G}{\rho} \quad (2-23)$$

The corresponding momentum flux is

$$M = \frac{AG^2}{\rho} \quad (2-24)$$

Integration of universal velocity profiles indicates that the fully developed turbulent flow is 1%-10% greater than the flat profile value (13)(5). Further, the integration is of an averaged curve and, depending upon the fluctuations present, the actual value should be higher still. The laminar velocity profile is

$$V = \frac{2G}{\rho} \left(1 - \left(\frac{r}{r_0} \right)^2 \right) \quad (2-25)$$

and results in a momentum flux of

$$M = \frac{4}{3} \frac{AG^2}{\rho} \quad (2-26)$$

or 33% greater than the minimum possible. The laminar value is the maximum considering steady flow where viscosity is the only physical force producing factor present.

A laminar model has been investigated. The assumptions made were the following: 1) the phases flow in annular layers with a smooth interface between them (this minimizes the surface energies), 2) pressure is constant across a cross section, 3) no slip boundary conditions, and 4) shear stress matching between the phases. The

Navier-Stokes equation reduces to

$$\frac{dP}{dz} + \rho g = \frac{\mu}{r} \frac{d}{dr} \left(r \frac{dV}{dr} \right) \quad (2-27)$$

whose solution is

$$V = \frac{\frac{dP}{dz} + \rho g}{4\mu} r^2 + C_3 r + C_4 \quad (2-28)$$

in each phase.

The void fraction is a function of the flow as well as of the quality and the void fraction is on the opposite side of the minimum momentum flux void fraction from the homogeneous. This is indicative of very high slip ratios. The momentum flux value exceeds the homogeneous value except below 8% quality. At higher qualities, the values are prohibitively high. One can safely conclude that the laminar model bears such small relation to reality as to be useless; the results are not presented graphically.

Anderson and Mantzorianis (5) made the same assumptions as were made for the laminar model. They did not, however, satisfy the laminar flow equations in each phase but used Van Karman's (14) "universal velocity profile." They determined a factor giving the ratio of the actual momentum to the two-velocity momentum. Essentially, they predicted a 1% to 10% increase in the flux.

The work of Anderson and Mantzorianis presents a few conceptual difficulties. For example, they draw the velocity and shear stress

profiles as in Figure 21. Within the liquid phase it is impossible to have a positive sloping shear stress and a concave downward velocity profile. They admitted to the difficulty saying that "the assumption must involve some error Nevertheless the universal velocity profile is used here as the best approximation to the truth ..." They go even further to define the double velocity profile also shown in the sketch. The double profile amounts to two universal profiles back to back in the liquid region. There is no substantial reason for the assumption other than it might accidentally predict some results.

Note that velocity profile moves the momentum flux value toward the homogeneous model value without altering the measured void fraction. That the momentum flux values are like the homogeneous model does not imply that the flow is homogeneous, but that other factors have made their addition to the flux predicted by the slip model.

2.3.3 Phase Distribution The phenomena of phase distribution has no analogy in the single-phase flow. Here it specifically refers to the phenomena of entrainment, a portion of the liquid phase traveling at the gas velocity. The void fraction may still be specified independently. Entrainment is defined as

$$\epsilon = \frac{\text{entrained } m_f}{\text{total } m_f} \quad (2-29)$$

Real entrained flows have been observed (6) (20) to have very laminar-like velocity profiles in the core region. Here, however, the effect of entrainment is being viewed for its mass distribution effect between the two average velocities of the slip model. The steep profiles are not considered.

The two-phase momentum multiplier is

$$MM = \left(\frac{X(X+(1-X)\epsilon) u_g}{\alpha} + \frac{(1-X)^2(1-\epsilon)^2 u_F}{\left(1-\alpha - \frac{\epsilon \alpha u_F (1-X)}{u_g X}\right)} \right) \frac{1}{g_c} \quad (2-30)$$

One notes that when $\epsilon = 0$, the momentum multiplier reduces to the two-velocity slip model value

$$MM = \left(\frac{X^2 u_g}{\alpha} + \frac{(1-X)^2 u_F}{(1-\alpha)} \right) \frac{1}{g_c} \quad (2-31)$$

However, when $\epsilon = 1$, the value is

$$MM = \frac{X u_g}{\alpha g_c} \quad (2-32)$$

which is larger than the homogeneous value,

$$MM = (X u_g + (1-X) u_F) \frac{1}{g_c} \quad (2-33)$$

This is because to satisfy the void fraction, some liquid must stand on the wall, reducing the effective tube size. Entrainments larger than 1.0 are possible with back flow in the annular water at the wall. Figure 20 shows the results of the entrainment model

with entrainments of 0, 20, 40, 60, 80, and 100 percent along with the homogeneous result.

2.3.4 Time Variation In a single-phase flow, the average momentum flux may be higher than that predicted by an integration using the average velocity profile. This is because the momentum is a function of the square of the velocity. Consider a flow, with a uniform instantaneous velocity profile, varying sinusoidally about a mean value with amplitude b .

$$\dot{m} = \dot{m}_{\text{mean}} + b \sin \omega t \quad (2-34)$$

The average momentum flux is proportional to

$$M \approx \dot{m}^2 + \frac{b^2}{2} \quad (2-35)$$

as opposed to the steady value of

$$M \approx \dot{m}^2 \quad (2-36)$$

Schlichting(13) reproduces turbulent flow measurements of Reichardt as in Figure 22. Using a hot-wire anemometer, Reichardt obtained the average velocity profile and a profile of the root mean square of the fluctuating velocities in the axial and the transverse directions. Considering the velocity to be composed of a steady average and a fluctuating velocity, whose average is zero,

$$V = \bar{V} + V' \quad (2-37)$$

and that the momentum flux is proportional to the velocity squared,

$$M \approx \iint_A (\bar{V}^2 + 2\bar{V}V' + V'^2) da \quad (2-38)$$

the average momentum flux is proportional to two terms

$$\bar{M} \approx \iint_A (\bar{V}^2 + \bar{V}'^2) da \quad (2-39)$$

An integration of Reichardt's data shows that the fluctuating component amounts to slightly over one percent of the steady velocity profile integration.

In calibrating his apparatus, Rose (10) consistently measured higher momentum fluxes than he was able to support by integration of universal velocity profile. The difference is of the same magnitude as that which is attributed to fluctuation according to Reichardt's data.

The fluctuating velocity is expected to be large at the air-water interface in annular flow. This is visually evident in the fluid to one observing liquid waves propagating up the wall and in the gas from Reichardt's data. This fluctuation may well explain the inability of Silvestri to integrate steady measured profiles to reasonable momentum pressure drop data.

In the two-phase fluctuation generally, some model must be selected to relate parameters before a calculation similar to

equation (2-35) can be made. For example, one may assume the homogeneous model in which the solution is the same as for a single phase. One may assume that the void fraction remains constant and that the flow variations occur in each phase independently, similar to Reichardt's turbulent data. In a slug flow model the void fraction will have some functional relation to the fluctuating flow rates.

The model taken to represent varying void fraction conditions was the two-velocity model with the following assumptions: 1) constant gas velocity

$$\frac{\dot{m}_g \bar{u}_g}{\alpha} = \text{constant} \quad (2-40)$$

and 2) constant volume flow rate

$$\dot{m}_f \bar{u}_f + \dot{m}_g \bar{u}_g = \text{constant.} \quad (2-41)$$

For computation, step variations in the parameters were used. Any number of steps (i) can be chosen per cycle, but the percentage of time at each step (t_i) must be chosen so as to total unity.

$$\sum_i t_i = 1. \quad (2-42)$$

Void fractions selected must be time weighted to give the known overall average value, $\bar{\alpha}$.

$$\sum_i t_i \alpha_i = \bar{\alpha} \quad (2-43)$$

The continuity relations are written in terms of the local qualities

η_{fi} and η_{gi} where

$$\eta_{fi} = \frac{\dot{m}_{fi}}{\dot{m}_{Total}} \quad , \quad \eta_{gi} = \frac{\dot{m}_{gi}}{\dot{m}_{Total}} \quad (2-44a \& b)$$

Equations (2-40) and (2-41) are now

$$\frac{\eta_{gi} \sigma_g}{\alpha_i} = C_5 \quad (2-45)$$

and

$$\eta_{fi} \sigma_f + \eta_{gi} \sigma_g = C_6 \quad (2-46)$$

Of course,

$$\sum_i \eta_{gi} t_i = \bar{X} \quad (2-47)$$

and

$$\sum_i \eta_{fi} t_i = (1 - \bar{X}) \quad (2-48)$$

which give

$$C_5 = \frac{\bar{X} \sigma_g}{\alpha} \quad (2-49)$$

and

$$C_6 = (1 - \bar{X}) \sigma_f + \bar{X} \sigma_g \quad (2-50)$$

so that all η_{gi} and η_{fi} can be evaluated. The resulting momentum multiplier is

$$MM = \frac{1}{g_c} \sum_i t_i \left[\frac{\eta_{fi}^2 v_f}{(1-\alpha_i)} + \frac{\eta_{gi}^2 v_g}{\alpha_i} \right] \quad (2-51)$$

Note that η_{fi} and η_{gi} may have been selected in place of α_i along with t_i to determine the value of the other parameters.

Figures 23 through 28 show computed results of the time varying model using two steps ($i = 2$). The results are given in terms of γ an average deviation from the average liquid fraction ($1-\bar{\alpha}$)

$$\gamma = \sum_i \frac{|\bar{\alpha} - \alpha_i| t_i}{1 - \bar{\alpha}} \quad (2-52)$$

The time at each step was varied as well as the value of γ . Figure 23 shows the effect of changing the time at each step while holding γ constant. Figures 24 and 25 show the effect of variable γ while the time at each step remains constant. Figure 26 shows the value of the momentum at each step and the resulting average. Figures 27 and 28 show the ratio of the fluctuation in amplitude to the average value as γ varies.

Assuming that the model and the ensuing calculations have some validity, the last curve is particularly significant. By comparing the given figure with actual experimental data, a sample of which is given in Figure 45, one can estimate the correct values of γ .

2.4 Differential Deviation from Single Phase

The single-phase limits are points where the two-phase models can be checked against single-phase theory. This, of course, is well recognized and virtually all the models give the single phase limits in void fraction and momentum flux if they claim to be valid in the region. Bankoff's model, of course, deviates at the high qualities as discussed because it was intended to apply only to the bubbly flow regime.

In addition to the limiting values, the slope of the values with respect to quality can also be estimated with a little additional reasoning. A differentially small addition of a gas to a single-phase liquid can be imagined best as well dispersed throughout the flow (unless artificially made otherwise). Thus at the low quality limit the homogeneous flow is seen to predict the slopes of the void fraction and momentum multiplier. A differential addition of a liquid, not wetting the walls, can be expected to produce the same result. A differential addition of a wetting liquid could eventually be expected to be found at the wall. Thus the two-velocity model would best predict the slope of values for this phenomenon.

CHAPTER III
EXPERIMENTAL PROGRAM

An experimental program was undertaken to obtain direct measurements on the momentum flux in two-phase pipe flow.

3.1 Feasibility

Two methods were initially considered to measure the momentum flux at a section. The first involved condensing the vapor portion of a pipe flow exhausting into a large chamber. The measurement of the pressure difference between the end of the pipe and the exit of the chamber would then relate the negligible chamber exit section momentum flux to the entering flux of interest. The second, the method actually used, involved turning the two-phase fluid as described in Appendix A, in a tee. Calculations indicated that the second method would give more accurate results. It would also be flexible to measuring two-component as well as two-phase flow where one phase can condense. As a further incentive, turning arrangements had been successful for other investigators.

3.2 Design Requirements

An apparatus to measure the momentum flux by the method considered must accurately measure the force on the turning tee. It must provide facilities for making the force measurement under a

variety of conditions and must monitor those conditions.

It was decided to work principally with steam-water with adaptation to air-water. This decision was based upon the relative ease of availability of the fluids and their significance in regard to two-phase flow application and current studies.

Laboratory steam was available at 200 psia. This pressure and the corresponding saturation temperature set the upper bounds for which the apparatus was to be designed for both operation and safety. Unfortunately, this upper bound is well below values common in industrial practice. Since, however, momentum effects are accentuated at lower pressures, it was felt that the data could be safely extrapolated from the experimental to higher pressures. Atmospheric pressure was the lower bound on the apparatus.

The parameters to be experimentally varied were the flow rate of each of the phases, the pressure, and the inlet pipe diameter.

3.3 Original Design

The final apparatus evolved, through several design changes, from less successful earlier attempts.

3.3.1 Tank and Internals With the turning tee method, it is necessary that the tee be surrounded by an atmosphere at the pressure being tested. Further, the vessel must be large enough so that exit flow from the tee cannot be diverted so as to affect the measurement being made.

A 0.3125-inch wall steel tank having an internal diameter of 16 inches and a length of 36 inches with welded, dome-shaped heads was selected as the pressure containment vessel. The vessel was designed as a refrigerant receiver tank for use at 300 psi. It was hydrostatically tested to 500 psi.

Several fittings already available were used as steam exit, water exit, gage glass mounts, and thermocouple well header. Additional access ports made in the tank include the inlet pipe fitting, an instrumentation fitting and a 10-inch man hole. The man hole provided an entrance through which parts could be inserted and adjustments made. A 9-inch diameter, 1-inch thick tempered glass plate was inserted and sealed by an O-ring in the man hole flange cover. The glass provided a 7-1/2 inch unsupported diameter window for viewing the internal mechanism in actual operation. External mounting fittings were provided with the tank.

Measurement of the forces in the high temperature, pressure, steam-water environment posed a difficult problem. Temperature compensated strain gages presented a possible solution which would have required a great deal of calibration to prove merit on an unsupported measurement. The solution adopted is that of placing a displacement transducer external to the tank where it is not affected by the adverse environment. The transducer would then measure the deflection of a beam, a displacement proportional to the force on the tee. A Linear

Variable Differential Transformer (LVDT) was selected as the transducer so that the transmission of information could be by magnetic means through the wall of the pressure vessel. The primary LVDT coil was fed a 15 KC signal with a peak and peak amplitude of 16 volts.

The pressure vessel wall at the position of the transducer consists of stainless steel, number ten gage tubing (for hypodermic use) with an inside diameter of 0.113 inches and an outside diameter of 0.133 inches. The LVDT used is a Sanborn Linearsyn Differential Transformer Model 590T-025. As shown in Figure 4, the coil assembly has an inside diameter of 0.136 inches while the core has an outside diameter of 0.100 inches. The core was silversoldered to another stainless steel tube serving as the displacement pushrod.

The electrical output of the coil assembly as a function of the core traverse position is shown in Figure 8. The voltage output is considerably smaller than that which would be achieved in the absence of the stainless steel pressure vessel wall. The end effect of the pushrod is sufficiently far from the core effect and excellent linearity occurs in the test distance.

Fittings to clamp the deflecting beam were welded into the tank. Two beams were initially tried, one a brass beam of 1/8 x 1/2 inch squared section and the other a steel beam of 3/16 x 1/2 inch squared section. The two beams were tried for their different spring rates,

from the point of view of frequency response and sensitivity. The steel beam was selected for its higher natural frequency and sufficient sensitivity. The tee was attached to the beam by a threaded stainless steel 10-30 rod. Both the beam and the tee connections are threaded and locked by nuts.

3.3.2 Turning Tee The function of the turning tee, as can be seen from the momentum equation analysis in Appendix A, is simply to turn the flow through a right angle. As long as this is accomplished, the tee internals are of little importance. In exploratory experiments, the tee used by Rose (10) in bubbly air-water flow, was tested in the present apparatus. Rose's tee, being soft soldered, did not stand the temperatures involved. Further, it was found that Rose's tee, being a double pipe elbow, was suitable only for flows approximating a single phase because of the extreme secondary flow patterns encountered in other regimes. Thus it was decided to use a tee of radially symmetric design with flow exiting from between parallel plates to insure perpendicularity to the inlet direction.

It was decided to design the tee as a flat plate deflector with guide walls to prevent splash back not normal to the inlet direction. As might be expected, the solution for a two-phase jet striking an overhead plate has not been attempted for two-phase flow. Thus it was decided to design on the basis of a single phase and modify as was deemed necessary by performance. Note that by designing on the

basis of a deflecting plate rather than in a more gradual turning nozzle, it was hoped to increase the time response of the tee.

The problem of a radially symmetric jet striking a surface has not been solved. Two approaches are taken here which bound the solution. First, a continuity approach, where the depth of the tee aperture at each radius is determined by the criteria that it pass the same flow in a radial direction as entered the tee, provides the minimum guide wall dimension. The two-dimensional jet solution (15)

$$y = \frac{h}{2} + \frac{h}{\pi} \log \coth \frac{\pi}{4} \left(\frac{2z}{h} - 1 \right) \quad (3-1)$$

h = thickness of arriving flow

provides the other limit. The actual solution must approach the continuity solution at the exit of the tee, and the two-dimensional solution at the inlet. As an approximation to the actual solution, the two-dimensional solution was modified to a radially symmetric solution by the criteria that flow area normal to the inlet be the same. This solution is asymptotic to the two-dimensional solution at the inlet and the continuity solution at the exit as shown in Figure 6. The resulting tee design is that of Figure 7a and b. The material was aluminum.

3.3.3 Feed System City water is supplied at the system pressure by an Aurora Model E5T two-stage, vane pump designed to deliver 5 gpm

at 200 psi. The pump is bypassed so that any intermediate pressure and flow may be achieved without overloading the pump.

The liquid flow is measured by a Fischer & Porter 3000 Series Flowrator Meter measuring 5.70 gpm at full scale. The flowmeter was calibrated by weigh tank measurement presented in Figure 11.

The water was preheated in an Economy Steam and Water Mixer rated at 500 gallons per hour. The steam for the contact mixer was supplied at 200 psia from the laboratory supply through a 1/2-inch pipe. Pressure at the point of temperature measurement was read on a 1% accuracy, 200 psi max. pressure gage (#410R-TD Helicoid Test Gage 8-1/2"). The flow rate of the steam was obtained from a heat balance on the mixer. Copper Constantan thermocouples were provided to establish the temperatures necessary for this balance.

The main steam is supplied from the laboratory steam supply through a two-inch line. The flow rate of the steam is determined by flange tap orificing according to the ASME Power Test Code (16). Two sharp-edged orifices were used of 0.4-inch and of 1.0-inch diameter. Pressure readings are provided by the same Helicoid gage used to measure the heater steam pressure and the temperature by another thermocouple. The differential pressure across the orifice was measured by high pressure manometers filled with mercury or with Meriam #3 Manometer Fluid having a specific gravity of 2.95.

Air is supplied from the laboratory supply at 125 psi. It is measured by a laboratory setup equipped with mercury and oil manometers, a .3102-inch diameter orifice in a 2.067-inch diameter pipe, a thermometer, and a pressure gage. A shop air supply at 300 psi could also be used.

The steam and water are mixed in a jet pump mixing fixture, the inner chamber supplying the steam and the outer the water. The fixture, a McDaniels Suction tee, is fitted with one-inch female pipe connections. A valve is provided in both the steam and water lines immediately proceeding the mixing chamber for control and to introduce a large impedance just before mixing. The impedance is intended to minimize feedback into the feed systems. The exit of the mixing fixture feeds a length of insulated pipe leading to the pressure vessel and tee.

The pressure in the tank is monitored by a #410R 4-1/2" Helicoid gage reading to 200 psi. The pressure is determined for calculational purposes by measuring the saturation temperature in the vessel by a Copper-Constantan thermocouple set in an eight-inch well near the beam. The exhaust steam, after passing through a control valve, is condensed in a two-inch line by contact mixing with tap water and dumped. Water level is determined by a sight glass and valve controlled in a half-inch dump line.

3.4 Modified Design

3.4.1 Tank and Internals The initial assembly proved to have two difficulties: considerable frictional hysteresis and an annoying zero shift during operation. Figure 15a and b shows the decay of the beam vibration following the release of an initial deflection, a pluck. Figure 10 shows a static test in which the hysteresis is of disturbing proportions. Friction between the LVDT core and the stainless steel tube vessel wall was blamed for the hysteresis when it was estimated that a quarter of a pound of normal force there could cause the effect. Also suspect was the clamping arrangement for the beam connection to the pressure vessel. The clamping was further suspect of being somewhat responsible for the zero shift at operating temperatures.

Two modifications were made. One end of the beam was bent into a dogleg and welded to the pressure vessel wall. This was to eliminate any buckling problems and to render the attachment more immobile, absorbing deflections in the elastic beam material. The second change involved an alignment mechanism so that the pushrod could always be aligned with the stainless steel tube within the LVDT coil. A flexible wire, too short to buckle, was built into the alignment mechanism so that no torque could be transmitted to the pushrod providing a normal force at the LVDT core. Figure 2 shows a diagram of the final apparatus.

Figures 10 and 15c show that the modification eliminated the column damping and the hysteresis. An operational zero shift persisted, however. Differential thermal expansions, and differential strains from pressure and water level change were investigated (Appendix B). Thermal expansion differences were shown to be of primary effect with a possible assistance from pressure changes.

The elimination of the zero shift lay either in a complete redesign of the apparatus, reducing the lengths subject to the differential strains and compensating somehow for differential expansion, or in the definition of an operational procedure to account for the change. Of course, the operational solution was chosen. Thermocouples were placed in the wall of the pressure vessel so that equilibrium could be detected through time spaced measurements. At the operating equilibrium, a zero point would be measured and the run would commence. The procedure has worked well and the zero value can be checked many times during a run.

3.4.2 Tee The original tee gave an estimated 5% runback (liquid leaving through the entrance). A new tee was designed, the change being a larger aperture, a larger overall radius, and a larger flat distance on the radius. The redesigned tee is given in Figure 7c and d. Further opening between the deflection plate and the guide walls was provided by the insertion of washers to open the slot from 0.10 inches to 0.35 inches. The tee, also constructed

from aluminum, weighs 0.84 pounds. It has performed to satisfaction at all operating conditions.

3.4.3 Feed System At flow rates only one-third of its specified value, the contact heater become noisy in operation. The noise was detectible in a flowmeter oscillation, an oscillation of the feed system that was considered undesirable. One positive effect was that it led to a consideration of the effect of oscillations on the average momentum flux.

A recirculating line, returning water from the pressure vessel to the feed system, replaced the contact heater. A centrifugal pump made up the small pressure difference in the circuit. The recirculated water, mixed with any makeup water needed is returned to the system preceeding the flowmeter. The final arrangement is shown in Figure 3. The recirculation loop successfully eliminated the undesirable noise and was further beneficial in reducing the number of measurements to be made, and in reducing the difficulty of holding specified conditions.

3.5 Void Fraction Data

A direct measurement of the void fraction for air-water was made by isolating a section of the inlet pipe with quick closing valves. The isolated section was plexiglass pipe of 0.75-inch diameter and 75 cm. length. The ratio of liquid volume to total volume was taken to be the liquid fraction.

3.6 Testing

Several tests to verify the performance of the apparatus have already been mentioned. They will merely be listed here.

Test	Purpose
Core Traverse, Fig. 5	Test operation, determine operating range
Pluck Tests, Fig. 15	Determine damping nature and factors
Static Calibrations, Fig. 10	Calibrate flowmeter

The spring constant of the beam was determined by direct measurement of the deflection under a steady load (Figure 9).

The most significant test is the single-phase steam test for it evaluates the principle and the function of the apparatus against known results. Steam flow was measured by the orifice and the momentum flux was measured by the tee. The single-phase momentum flux as calculated from the measured flow is compared with the measured result in Figure 12. The results are excellent.

3.7 Data System

The data consists of all the pressure, temperature, and flow readings necessary to establish the thermodynamic state of the two-phase flow and the temperature equilibrium state of the pressure vessel, and the LVDT output voltage measuring the deflection of the

beam. The pressure, temperature, and flow conditions are steady state and are not monitored continuously. The LVDT output is monitored in several ways as indicated in Figure 5 as its fluctuating nature as well as the average value is of interest.

3.7.1 Observation All of the pressure, temperature, manometer, and flow readings were recorded for each run. The LVDT signal was read from a vacuum tube volt meter after being averaged by a resistor capacitor circuit with a 15 second time constant. In addition, the flow was visually observed and the LVDT output was viewed on an oscilloscope to detect any irregularities. This data is sufficient to determine the average momentum multiplier values.

3.7.2 Tape Recorder For many runs the LVDT output was recorded by a frequency modulated tape deck. As shown in Figure 5, the LVDT signal was first biased and amplified before recording. The purpose of recording the data was for automatic spectral density later.

3.7.3 Brush Recorder The signal was often recorded directly by a Brush recorder. The same signal was also passed through a standard tee filter (17) (18) designed to zero out the natural beam frequency (43.8 cps) and recorded on the second band of the recorder. A diagram of the filter and its experimental frequency response are shown in Figure 14. Also shown is the combined response of the beam and the filter. Samples of the Brush recordings are shown in Figure 44.

3.8 Data Reduction

3.8.1 Average Force Data The recorded data was reduced on the computer to the parameters presented in Chapter IV. Appendix C gives the equations and approximations used in the computer program.

3.8.2 Fluctuating Data Appendix D gives the equation of motion for the beam, the frequency response of which is plotted in Figure J. This is to be compared with the analog computer spectral analysis, samples of which are shown in Figure 46. A Philbrick Researcher's SK Analog computer was used for the analysis with a filter, Dynamic Analyzer Model 5D101A, made by Spectral Dynamics Corporation of San Diego. Unfortunately, the extremely long averaging times and narrow, sharp bandwidths required for accuracy at low frequencies limit the accuracy of the actual analog analysis.

CHAPTER IV

RESULTS

4.1 Average Momentum Flux Data

The average momentum flux data, both raw and reduced, are presented in chart form in Appendix E. Figures 31 through 42 give a graphical presentation of the data. The figures locate the data on a mass velocity versus quality map, scribed with lines of constant homogeneous velocity; and present the momentum flux information as a momentum multiplier versus quality. The lines of homogeneous and minimum possible momentum multiplier values are given for reference. An individual figure is presented for each pressure and pipe size tested; atmospheric pressure, 30 psia, 60 psia, 90 psia, and 120 psia in nominal one-half and one-inch pipes for steam-water, and atmospheric pressure in a one-half inch pipe for air-water.

The temperature of the mixing water at the tee did not have any observable effect on the data. It was concluded that the entrance pipe was of sufficient length to diameter ratio to assure the thermal equilibrium and steady flow development conditions standard for adiabatic two-phase flow.

The two pipe sizes tested had no noticeable effect upon the momentum multiplier values.

Flow rate at a particular quality has a noticeable influence on the momentum multiplier values. In an attempt to correlate this effect, the data was coded according to the homogeneous velocity. It is not meant to suggest that the flow is actually homogeneous; the parameter was selected for calculational purposes as a quantity which varies at each quality in the same way as the mass flow rate. Some lines of constant homogeneous velocity have been drawn through the data on the figures of momentum multiplier versus quality. Further mention will be made later concerning the velocity effect for purposes of extrapolation and interpolation.

A few of the data points fall below the minimum possible momentum multiplier line. They are clearly in error. The principle cause of error is the difficulty of measuring the low forces involved. All of the points in error are characterized by low momentum flux and subsequent difficulty of measurement. Points with a small force measurement, generally less than one-half pound, are plotted with bounds of one-tenth of a pound error in each direction. One-tenth of a pound measurement error is sufficient to explain most of the points which fall into the region of impossibility.

4.2 Rose's Results

The bubbly flow regime momentum flux measurements of Rose (10) are presented in Figure 30. The homogeneous and absolute minimum momentum multipliers are also shown on the figure along with other

predicted values. Rose experimentally determined the void fraction, the results being presented here in Figure 29. The void fraction data was approximated by

$$\alpha = 21.59 X^{0.574} \quad (4-1)$$

$$X < 0.001$$

and by

$$\alpha = 4.07 X^{0.333} \quad (4-2)$$

$$0.001 < X < 0.004$$

for calculational purposes. The momentum multiplier calculated from these void values according to the two-velocity model is also presented on Figure 30.

Rose's data did not show a systematic variation with the mass velocities he tested, and thus no velocity correlation has been made.

4.3 Vance's Results

Vance (9) made some careful measurements of the momentum flux in horizontal flow with an apparatus very similar to that proposed by Griffin (19). His results, due to the apparatus, are steady rather than average results. Along with the appropriate reduction, the data is shown in Appendix F. The data is taken at widely varying pressures and it is difficult to present the data on a graph. Figure 43 makes an attempt by plotting momentum multiplier versus quality and showing the range of the homogeneous and minimum

possible value for the same pressure and quality.

The question of the relationship between horizontal and vertical flow can be answered by comparison of Vance's results to the results of this investigation. At the flows tested, it is not expected that the difference due to inclination would be detected since the frictional forces are considerably greater than the body forces throughout the flow. One cannot, however, form a definite conclusion on this basis since some lever mechanism may be involved whereby a small body force would dominate much larger forces in influencing flow formation. The similarity of this investigation's data with that of Vance affirms the predominance of the friction forces in determining the flow.

Vance measured the momentum flux for the purpose of determining the slip ratio (or the void fraction) and this is how he presents his data. This is not a valid method of determining the void fraction, however, as the many additional factors mentioned in Chapter II affect the momentum flux. This is the same error as made by Semenov and discussed in Chapter I.

4.4 Void Fraction Measurements

The void fraction measurements are presented in Appendix E and graphically in Figure 17. Two values are given in the appendix estimating the bounds of the range of reliability. The limiting values are connected by a line on Figure 17.

As can be seen from Figure 29 of Rose's data, the void fraction is essentially that of the homogeneous model at qualities approaching zero. As the quality increases the void fraction deviates toward the minimum momentum void value. By 30% quality the void is substantially the minimum momentum void value.

The momentum multiplier calculated by the two-velocity model from the measured void fraction data is shown on Figure 42. This line is substantially below the data, demonstrating, as did Rose's data, that factors in addition to the void fraction are important in determining the momentum flux. Attention is again called to Figures 18 and 19 which shown that large differences in the void fraction near the minimum possible momentum void fraction result in small changes in the momentum multiplier. Above 15% quality, the minimum possible momentum is essentially the same, with respect to the data, as that predicted by measured voids with the slip model. The void fraction deviation from the minimum momentum void plays only a small role in the deviation of the momentum multiplier from its minimum value at higher qualities.

The voids measured here essentially verify Martinelli's results.

4.5 Fluctuations

Two types of data on the fluctuations were reduced, data maximum fluctuation amplitudes as reduced from Brush recorder

traces and spectral density analysis performed on an analog computer from a taped signal.

4.5.1 Brush Recorder Samples of the Brush records are reproduced in Figure 44. Both the unfiltered and filtered signals were recorded (filter response shown in Figure 14). Figure 45 shows data on the maximum filtered amplitude as a percentage of the average force. The data on this figure represents all pressures and mixtures tested and thus is not intended to be an accurate plot. It is intended to indicate the region in which fluctuations play a major role.

The parameter of fluctuating amplitude divided by average amplitude is used in plotting the results of the fluctuating model. By comparing Figures 27 and 28 and 45, one can estimate values of γ in the fluctuation model.

4.5.2 Spectral Analysis Samples of spectral analysis made on an analog computer from a recorded signal can be seen in Figure 46. Also shown in the figure is an oscilloscope photograph of the raw signal during the analysis. The effect of the beam natural frequency is, of course, predominant. By comparison with the expected beam response with a white noise input, Figure 13, one can determine that the fluctuations are of interest in the lower frequency portion of the spectrum (0 - 10cps).

Very small amplitude fluctuations exist at frequencies higher than the beam natural frequencies due to droplet entrainment. This

can be tested empirically by holding one's hand in front of an expelling two-phase flow. These are difficult to detect with the beam arrangement and may well be impossible with a tee since the period of the fluctuations approaches the transit time in the tee. The fluctuations are still very small and they do not affect the validity of the large amplitude measurements at lower frequencies.

It is difficult to explain the fluctuating period of two seconds in a ten-foot long tube where the homogeneous velocity is perhaps 200 ft/sec. Yet Schlichting (13) reports the same sort of data in the velocity fluctuations in turbulent flow. In the two-phase flow it is suspected that the low frequencies are due to continuity type waves easily visible to investigators standing at a distance from a two-phase flow. Reasonable precautions have been taken to isolate the feed systems and the data is presently understood to be valid.

4.6 Choke Flow

A few of the data points taken approach the choke flow (choke flow predictions shown on the flow map of Figure 47 and on Figures 31, 32, 33, and 34). The momentum flux values are not the minimum possible momentum flux as is the assumption in the Fauske model. The Fauske model may predict the critical flow quite accurately, but it is clear from this investigation that the physical reasoning is incorrect.

Although it is inconceivable that the momentum flux would naturally arrive at its minimum possible value, some of the data in the 20-50% quality range indicates that the momentum multiplier drops as the critical flow is approached.

One may think of two-phase critical flow in the following way: as the pressure drops in a tube, the adiabatic momentum multiplier rises. However, if the pressure drops rapidly enough, the flow may not be able to redistribute itself rapidly enough, and the real momentum multiplier will lag behind the adiabatic value. Of course, it cannot lag too far behind because it runs into the continuity minimum -- but before that, some sort of realistic minimum momentum multiplier. When the flow reaches this condition it is unable to adjust more rapidly -- the critical flow model must incorporate the situation of maximum adjustment rate before continuing.

The factors influencing the maximum rate of adjustment are 1) thermodynamic metastability, 2) flow adjustment, and as a subtitle under adjustment, 3) fluctuations. The Fauske model assumes that the minimum possible momentum represents the maximum adjustment.

4.7 Non-Adiabatic Flow

In a heated tube, bubbles can be observed to occupy a large fraction of the flow channel although the average quality is known to be subcooled. This metastable effect obviously has an effect on

the momentum flux which is difficult to predict. Clearly in the case described, the momentum flux will be higher than that predicted on an average quality basis. Yet in a mist flow, the cool droplets might lag behind in the accelerating fluid stream and result in a lower momentum flux than predicted on an adiabatic basis. The answer to the question seems to be dependent upon the flow regime and the heating rate.

A condensing tube can be considered more generally. The metastable vapor can have no other effect than to make the momentum flux greater than that predicted on an adiabatic basis.

4.8 Discussion of Effects

The momentum multiplier deviates from the minimum possible for the reasons discussed in Chapter II. At this point it will be attempted to note where the various reasons predominate.

4.8.1 Void Fraction Deviation In the bubbly flow regime, the flow is almost homogeneous. The void fractions and momentum fluxes measured by Rose verify the homogeneous model as the single phase liquid is approached. The deviation of the void fraction from the minimum momentum flux value still plays a small role up to 10% quality, but is insignificant when the quality reaches 20%.

4.8.2 Velocity Distribution Velocity and density distribution are almost always important. This is the lion's share of the reason

that momentum multiplier is greater than the homogeneous model as single-phase liquid is approached. Investigators (6) (20) using velocity traverse probes have noted a significant, laminar like, velocity profile in the entrained annular flow region. As the single-phase gas is approached, the velocity profile approaches the same importance as in turbulent flow. The regime where the velocity profile plays the least role is in the annular flow without entrainment.

4.8.3 Entrainment Entrainment is important where there is droplet entrainment since the gas velocities are higher.

4.8.4 Fluctuations Slug flow momentum flux is predominantly fluctuation. As the void fraction influence tapers off, the fluctuation influence increases (the macroscopic void fraction fluctuation). Well into the slug-annular transition, the fluctuation plays a predominant role.

The continuity waves in the annular layer may be considered to be the same sort of fluctuation, but may also be considered to be axial velocity fluctuation similar to the turbulent flow fluctuation. This type of fluctuation is important even in the limiting single-phases if turbulence is present. This is experimentally demonstrated in the inability to calibrate totally on the basis of the universal velocity profiles.

4.9 Interpolation and Extrapolation

Much of the data is in regions where entrainment is expected. Furthermore, the forces causing entrainment are the same as those causing wavy films and some of the fluctuations. Thus it seemed reasonable to attempt to correlate on the basis of the entrainment.

Steen and Wallis (21) report that

$$\epsilon = f(V \rho_g^{(1-m)}) \quad (4-3)$$

where m is a constant between .52 and .85, the higher values at higher entrainments. They report that the entrainment is directly proportional to the velocity at lower entrainments and proportional to the square root of the density.

A more recent publication of Minh and Huyghe (22) reports that entrainment may be correlated on the basis of a homogeneous $V^2 \rho$ defined as

$$(V^2 \rho)_{\text{homogeneous}} = \frac{m_g^2}{\rho_g \alpha^2 A^4} \left(1 + \epsilon \frac{m_f}{m_g} \right) \quad (4-4)$$

This is very similar to that reported by Steen and Wallis, more concise but inconvenient as the entrainment correlation parameter itself includes entrainment.

The data reported in Appendices E and F give the homogeneous

velocity and an entrainment correlation parameter.

$$V_{\text{homogeneous}} \sqrt{\frac{\rho_g}{\rho_{\text{atm}}}} \quad (4-5)$$

It is recommended that the data be interpolated to intermediate pressure by means of this correlation parameter.

Appendices E and F give two factors

$$YK = \frac{\text{homogeneous MM} - \text{actual MM}}{\text{homogeneous MM} - \text{minimum MM}} \quad (4-6)$$

and

$$ZK = \frac{\text{actual MM}}{\text{minimum MM}} \quad (4-7)$$

The factor YK represents the location of the momentum multiplier with respect to the homogeneous and minimum values. It is suggested that this parameter remains relatively constant through pressure changes as the entrainment parameter remains constant. ZK is the ratio of the actual to the minimum momentum multiplier. As with the ratio of the homogeneous to the minimum, the values are expected to diverge with pressure change at lower qualities (see Figure 1). ZK serves as a convenient term when working with higher quality momentum fluxes where the difference between the homogeneous and minimum fluxes is only a small portion of the total value.

The difference between the homogeneous and minimum momentum

flux models is often proportionately a small part of the total flux. Thus the YK given in the appendices is in large error due to a small measuring error. It is recommended to make interpolation and extrapolations by the lines of constant velocity drawn on the data in Figures 31, 33, 35, 37 and 39.

The difference between the homogeneous and minimum fluxes becomes proportionately smaller as the pressure rises. It is considered safe then to extrapolate in that direction. Note that as the critical pressure is approached, the turbulent velocity fluctuation and velocity distribution become increasingly important.

CHAPTER V

SUMMARY

5.1 The Two-Velocity Slip Model

The two-velocity slip model results in the minimum possible momentum flux value for given flow rates of liquid and gas if the slip ratio is taken to be

$$\frac{V_g}{V_f} = \sqrt{\frac{U_g}{U_f}} \quad (5-1)$$

No rearrangement of the flow from that assumed in the model can result in a lower average momentum flux.

The two-velocity model results in a minimum momentum flux when a specific void fraction (or slip ratio) is established for that void fraction. No deviations from the steady, flat profile assumed in the model can further decrease the average momentum flux at that void fraction.

No criteria for an upper bound was found.

5.2 The Homogeneous Model

The homogeneous model correlates the experimental momentum flux data more closely than does the slip model. This does not mean that the flow is more homogeneous than like the two-velocity model, but merely that the disturbances from the minimum momentum flux slip

model drive the momentum flux toward a value corresponding to the homogeneous model. The flow cannot possibly achieve an absolute minimum momentum flux configuration nor a local minimum at a given void fraction.

5.3 Deviations from Minimum Momentum Flux

The momentum flux deviates from the minimum possible momentum flux for the following reasons:

a) The void fraction deviates from the void fraction for a minimum momentum flux. At extremely low qualities ($x < .003$), the flow is essentially homogeneous. The void fraction deviates considerably from the minimum momentum void fraction and the contribution to the real momentum is significant. However, by 15% quality the contribution of a non-minimum void fraction is small but detectible. Greater than 30% quality, the contribution is negligible.

b) The velocity profiles are not flat. Velocity profiles always play a significant role. They are especially important at high entrainments and least important when the flow is most nearly annular. The velocity profile effect remains of importance in determining the momentum flux even as the flow approaches single phase limits, either at the quality extremes or at the critical pressure.

c) phase distribution (entrainment).

and d) fluctuation. Two types of fluctuation are distinguished, both of which contribute to the momentum flux, turbulent fluctuation, and void fraction fluctuation. Turbulent like velocity variations are especially important in annular flow with waves. The turbulent fluctuation, like the velocity profile effect, is important even in the single-phase limits. Void fraction fluctuation is of great importance in slug and degenerating slug flows.

5.4 Implications

The implications of the investigation are threefold.

a) to replace the use of the slip model by the homogeneous model in predicting momentum flux values. More exact estimation of the fluxes can be made through direct reference to the data.

b) to reconsider critical flow and other momentum associated phenomena in the light of the data.

and c) to carefully investigate fluctuations. Two-phase flow has been considered for its average steady-state properties when it is basically an unsteady phenomenon where the unsteadinesses play a fundamental role.

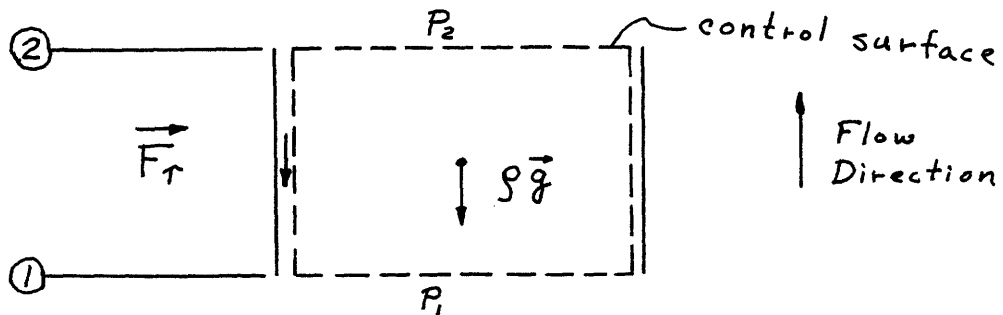
APPENDIX A
MOMENTUM EQUATION DERIVATIONS

Pressure Drop in a Pipe

The general momentum equation for a control volume can be written as (23)

$$\vec{F}_s + \iiint_{c.v.} \vec{B} \rho \, d\mathcal{V} = \oint_{c.s.} \vec{V} (\rho \vec{V} \cdot d\vec{A}) + \frac{d}{dt} \iiint_{c.v.} \vec{V} (\rho \, d\mathcal{V}) \quad (A-1)$$

In the case of upflow in a tube, the surface force is composed of pressure and shear forces while the body force is gravity.



Lumping the shear forces at the control surface into a single fractional term and writing the general momentum equation in the direction of flow, the only non-trivial principal direction, one arrives at an equation for pressure drop in a pipe.

$$F_r + \left[\int_A P dA \right]_0^2 + \iiint_{c.v.} \rho g dV = \left[\int_A \rho V^2 dA \right]_0^2 + \frac{\partial}{\partial t} \iiint_{c.v.} \rho V dV \quad (A-2)$$

Considering the pressure to be constant throughout a cross section perpendicular to the flow gives the more simplified relation

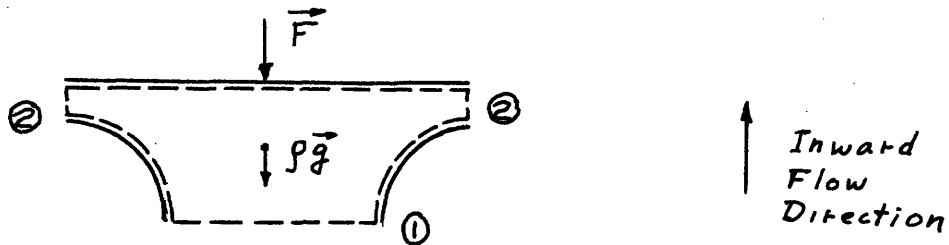
$$(P_1 - P_2)A = F_r + \iiint_{c.v.} \rho g dV + \left[\int_A \rho V^2 dA \right]_0^2 - \frac{\partial}{\partial t} \iiint_{c.v.} \rho V dV \quad (A-3)$$

(Note: The assumption of constant pressure throughout a cross section is excellent in vertical flow. It is also excellent at the homogeneous velocities tested for flow in any direction, losing validity as the flow begins to stratify due to large relative body forces.)

The pressure change is seen to be composed respectively of a frictional term, an hydrostatic consideration, momentum flux changes, and a transient effect.

Momentum Flux Measurement in a Tee

Writing the general momentum equation for the control volume in a tee which turns the flow through a right-angle bend, one arrives at



$$F + \iiint_{c.v.} \rho \vec{g} \, d\mathcal{V} = \iint_{\text{①}} \rho V^2 \, dA + \frac{d}{dt} \iiint_{c.v.} \rho V \, d\mathcal{V} \quad (\text{A-4})$$

in the direction of the inward flow, again the only non-trivial principal direction. In non-transient flow, the final term vanishes. The other control volume term can be made negligibly small as the size of the control volume is made small. In the case that the term cannot be made negligibly small, it can be estimated with sufficient accuracy to make the maximum possible error negligible. For experimental purposes the equation can be viewed as

$$F = \iint \rho V^2 \, dA \quad (\text{A-4})$$

The force on the tee is a direct measurement of the momentum flux entering the turning tee.

Since the measurements of momentum flux made with the tee are to be applied to sections other than exit sections, it is of importance to note a significant difference between exit and other sections. When the flow is reversing, the same fluid passing forward through

a section will return when the flow is reversed as it has been constrained in the pipe forward of the section. If, however, the section is at or near an exit, the forward flowing fluid may be dumped and replaced by the exit atmosphere fluid. The exit condition will persist as far into the tube as the exit fluid replaces the flowing fluid. The tee measurement therefore is inapplicable to measuring in-tube momentum fluxes with flow reversals. This region was avoided in experimentation.

APPENDIX B
CAUSES OF ZERO SHIFT

Thermal Expansion

Coefficients of thermal expansion are given (24) as

	$\frac{\Delta l}{l^{\circ}\text{C}}$
Stainless steel	17.3×10^{-6}
Steel	10.5×10^{-6}

The differential coefficient is thus

$$6.8 \times 10^{-6} \Delta l / l^{\circ}\text{C} \quad (\text{B-1})$$

Over fifteen inches, a 100°C temperature change gives a 0.01 inch which corresponds to a zero shift of 0.0714 volts. This is close to the observed zero shift of 0.077 volts.

Weight of Water

The strain area in the wall of the pressure vessel is

$$\pi (16 \text{ in.})(0.3125 \text{ in.}) = 15.7 \text{ in.}^2 \quad (\text{B-2})$$

The cross-sectional area of the tank is

$$\pi (8 \text{ in.})^2 \approx 200 \text{ in.}^2 \approx 1.4 \text{ ft.}^2 \quad (\text{B-3})$$

A one-inch change in the water level adds $.12 \text{ ft.}^3$ of water on 7.5 lbm of water.

$$\frac{7.5 \text{ lbm}}{15.7 \text{ in.}^2} = 30 \times 10^6 \text{ psi} \cdot \frac{\Delta l}{15 \text{ in.}} \quad (\text{B-4})$$

Therefore, using $E = 30 \times 10^6$ psi, the Δl over 15 inches is $.239 \times 10^{-6}$ inches. This is four orders of magnitude less than that observed in the thermal strains. It can be safely concluded that this effect cannot be detected since the maximum water level change is four inches.

Pressure Change

A 10 psi pressure change would cause a Δl change of $.637 \times 10^{-4}$ inches.

$$\frac{10 \text{ psi } 200 \text{ in.}^2}{15.7 \text{ in.}^2} = 30 \times 10^6 \text{ psi} \cdot \frac{\Delta l}{15 \text{ in.}} \quad (\text{B-5})$$

This is small, but detectible, $\sim .005$ volts for 100 psi pressure change.

APPENDIX C

FUNCTIONS TO FIT CURVES FOR DATA REDUCTION PROGRAM

To obtain water flow rate from the rotometer scale reading, the following equation is used:

$$\text{water flow rate (lbm/hr)} = 27.6 \times \text{scale reading} \quad (\text{C-1})$$

Temperature is obtained from Cu-Const. thermocouple millivolt reading by

$$\text{Temp (}^{\circ}\text{F)} = 32.0 + 46.2036R - 0.96412R^2 \quad (\text{C-2})$$

R = potentiometer reading in millivolts

when R = 4.5, and

$$\text{Temp (}^{\circ}\text{F)} = 40.655 + 41.9795R - 0.44641R^2 \quad (\text{C-3})$$

The orifice flow coefficients (16) are functions of Reynolds Number.

$$K = .5974 + \frac{26}{\text{Re} + 33.333} \quad (\text{C-4})$$

for the 0.4-inch orifice with a diameter ratio of .200, and

$$K = .6250 + \frac{126.884}{\text{Re} - 492.063} \quad (\text{C-5})$$

for the 1.0-inch orifice with a diameter ratio of .500.

Martinelli's void fraction versus quality curves were found to fit the form

$$X^{c_1} + (1 - \alpha)^{c_2} = 1 \quad (C-6)$$

quite well. Values of the coefficients for atmospheric and 60 psia steam-water data are

	c_1	c_2
atmospheric pressure	0.116	0.669
60 psia	0.153	0.660

For computational purposes, Rose's void fraction data was fit by

$$\alpha = 21.59 X^{0.574} \quad \text{for } x < .001$$

and by

$$\alpha = 4.07 X^{0.333} \quad \text{for } .001 < x < .004$$

APPENDIX D

EQUATION OF MOTION OF THE TEE

$$F = kx + c \frac{dx}{dt} + m \frac{d^2x}{dt^2} \quad (D-1)$$

$$F = k'e + c' \frac{de}{dt} + m \frac{d^2e}{dt^2} \quad (D-2)$$

where equation (D-2) is written in terms of the LVDT voltage output,

e. The relation between e and x is simply

$$x = 7.14 \left(\frac{\text{volts}}{\text{in.}} \right) e \quad (D-3)$$

Values of k and k' have been experimentally determined in static tests.

$$k = 208 \frac{\text{lb f}}{\text{in.}} \quad k' = 29.18 \frac{\text{lb f}}{\text{volt}} \quad (D-4, \text{ a\&b})$$

The natural frequency is 43.8 $\frac{\text{cycles}}{\text{sec}}$ or 275 $\frac{\text{radians}}{\text{sec}}$

$$\sqrt{\frac{k}{m}} = \sqrt{\frac{k'}{m'}} = 275 / \text{sec} \quad (D-5)$$

$$m = \frac{208 \frac{\text{lb f}}{\text{in.}}}{75625 / \text{sec}^2} \quad m' = \frac{29.18 \frac{\text{lb f}}{\text{volt}}}{75625 / \text{sec}^2}$$
$$= .275 \times 10^{-2} \frac{\text{lb f sec}^2}{\text{in.}} = .3855 \times 10^{-3} \frac{\text{lb f sec}^2}{\text{volt}} \quad (D-6, \text{ a\&b})$$

$$= 1.028 \text{ lb m.}$$

The measured mass of the tee was .84 lbm. The effective mass computed includes the pushrod mass and a contribution from the beam itself.

The decay constant β of the envelope was measured to be 0.4/sec.

$$\frac{c}{zm} = \frac{c'}{zm'} = 0.4/\text{sec.} \quad (\text{D-7})$$

$$c = 0.22 \times 10^{-2} \frac{\text{lb f sec}}{\text{in.}} \quad c' = 0.308 \times 10^{-3} \frac{\text{lb f sec}}{\text{volt}} \quad (\text{D-8, a\&b})$$

APPENDIX E

DATA

STEAM - WATER DATA

TEST NUMBER	MIXING WATER THERMOCOUPLE READING (millivolts)	ORIFICE MANOMETER READING (in.Hg.)	ROTOMETER READING (% SCALE)	LVDT VOLTAGE (volts)	ZERO VOLTAGE (volts)	MIXING WATER TEMPERATURE (°F)	MIXING WATER FLOW RATE (lbm/hr)	MIXING STEAM FLOW RATE (lbm/hr)	QUALITY	MASS VELOCITY (lbm/hr in ²)	FORCE ON TEE (lbf)	MOMENTUM MULTIPLIER (lbf hr ² in ² /lbm ²)	YK	ZK	ENTRAINMENT CORRELATION FACTOR (ft/sec)	HOMOGENEOUS VELOCITY (ft/sec)
D = 1.0640	1198.000000	14.70	2.280000													
TEMP = 212.00	PRESS = 14.70															
88	3.270	20.60	66.50	.2780	.0659	172.8	.1835E 04	.3664E 03	.1409	2476	6.178	.1133E-05	.1653	4.603	375	375
89	3.160	29.40	56.00	.3200	.0659	168.4	.1546E 04	.4338E 03	.1952	2227	7.402	.1678E-05	.0970	3.859	467	467
90	3.390	16.10	75.50	.2420	.0659	177.6	.2084E 04	.3251E 03	.1108	2709	5.130	.7860E-06	.2829	4.765	324	324
91	3.490	5.00	91.00	.1200	.0659	181.5	.2512E 04	.1827E 03	.0418	3030	1.576	.1930E-06	.5665	4.812	138	138
92	3.120	8.70	76.00	.1460	.0659	166.8	.2098E 04	.2403E 03	.0660	2629	2.333	.3795E-06	.4366	5.122	188	188
93	3.050	15.50	77.00	.2020	.0660	164.0	.2125E 04	.3191E 03	.0939	2749	3.962	.5896E-06	.3805	4.659	278	278
94	3.020	21.40	69.00	.2670	.0662	162.7	.1904E 04	.3732E 03	.1294	2562	5.849	.1003E-05	.2027	4.699	357	357
95	3.620	6.80	49.80	.1470	.0662	186.6	.1374E 04	.2128E 03	.1180	1785	2.354	.8306E-06	.2915	4.544	227	227
96	3.550	10.50	50.00	.1790	.0662	183.9	.1380E 04	.2637E 03	.1439	1849	3.286	.1081E-05	.2363	4.235	286	286
97	3.500	16.40	50.00	.2320	.0662	181.9	.1380E 04	.3280E 03	.1764	1921	4.538	.1283E-05	.1994	3.807	364	364
98	3.510	23.30	48.70	.2675	.0655	182.3	.1344E 04	.3889E 03	.2117	1949	5.884	.1142E-05	.1516	3.466	443	443
99	3.500	32.70	49.50	.3210	.0655	183.9	.1366E 04	.4574E 03	.2414	2051	7.442	.1790E-05	.1554	3.120	532	532
100	3.600	3.60	39.60	.1130	.0655	183.1	.1098E 04	.4574E 03	.1063	1410	1.384	.7827E-06	.2470	5.080	161	161
101	3.530	8.50	39.60	.1420	.0658	183.1	.1104E 04	.3130E 03	.1628	1496	2.228	.1119E-05	.3284	3.543	262	262
102	3.540	14.90	40.00	.1890	.0658	183.3	.1104E 04	.3130E 03	.2079	1594	3.589	.1589E-05	.2253	3.266	356	356
103	3.540	21.70	39.70	.2210	.0662	183.3	.1096E 04	.3738E 03	.2460	1655	4.800	.1971E-05	.1911	2.986	437	437
104	3.500	30.10	39.90	.2770	.0662	181.9	.1101E 04	.4397E 03	.2772	1733	6.140	.2299E-05	.1547	2.797	516	516
105	3.470	3.56	30.00	.0937	.0662	180.7	.8280E 03	.1544E 03	.1377	1105	.801	.7280E-06	.5193	3.117	164	164
106	3.420	9.10	30.00	.1310	.0662	178.7	.8280E 03	.2457E 03	.2136	1208	1.888	.1456E-05	.3576	2.849	277	277
107	3.450	17.10	30.00	.1750	.0662	179.9	.8280E 03	.3347E 03	.2785	1300	3.169	.2084E-05	.2837	2.514	391	391
108	3.490	22.10	29.90	.2030	.0662	181.5	.8252E 03	.3791E 03	.3087	1354	3.985	.2443E-05	.2251	2.333	449	449
109	3.590	28.70	29.50	.2310	.0662	185.4	.8142E 03	.4298E 03	.3445	1399	4.800	.2758E-05	.2219	2.235	517	517
110	3.380	6.30	20.00	.0980	.0662	177.2	.5220E 03	.2049E 03	.2578	851	.926	.1438E-05	.5702	1.998	236	236
111	3.460	10.70	19.90	.1260	.0662	180.3	.5492E 03	.2661E 03	.3204	917	1.742	.2330E-05	.3378	2.164	315	315
112	3.490	17.20	20.00	.1550	.0663	181.5	.5520E 03	.3387E 03	.3772	998	2.584	.2915E-05	.2851	1.992	404	404
113	3.510	23.10	19.80	.1825	.0664	182.3	.5465E 03	.3873E 03	.4172	1050	3.382	.3449E-05	.1987	1.946	470	470
114	3.500	32.00	20.00	.2170	.0665	181.9	.5520E 03	.4457E 03	.4557	1130	4.384	.3861E-05	.1692	1.840	552	552
115	3.550	32.00	30.00	.2550	.0666	183.9	.8280E 03	.4537E 03	.3521	1440	5.488	.2975E-05	.1454	2.315	544	544
116	3.580	32.00	40.00	.2910	.0668	185.1	.1104E 04	.4537E 03	.2854	1751	6.531	.2396E-05	.1402	2.761	536	536
117	3.350	32.00	50.00	.3190	.0700	176.0	.1380E 04	.4537E 03	.2312	2061	7.253	.1920E-05	.1441	3.257	512	512

Mixing
 Steam
 Enthalpy = 1198 BTU/lbm
 Specific
 Volume = 2.28 ft³/lbm

Pipe Diameter = 1.064 in.
 Pressure = 14.7 psia

AIR - WATER DATA

TEST NUMBER	ORIFICE MANOMETER READING (in. Hg)	ORIFICE AIR DENSITY (lbm/ft ³)	ROTOMETER READING (% scale)	LVDT VOLTAGE (volts)	ZERO VOLTAGE (volts)	WATER FLOW RATE (lbm/hr)	AIR FLOW RATE (lbm/hr)	QUALITY	MASS VELOCITY (lbm/hr in ²)	FORCE ON TEE (lbf)	MOMENTUM MULTIPLIER (lbf hr ² in ² / lbm ²)	YK	ZK	ENTRAINMENT CORRELATING FACTOR (ft/sec)	HOMOGENEOUS VELOCITY (ft/sec)
1	7.20	.2160	63.60	.0825	.0305	.17554E 04	.92680E C2	.0502	6024	1.515	.13607E-06	.4810	4.303	232.0	162.5
2	6.30	.2193	79.00	.0915	.0305	.12804E 04	.87428E 02	.0386	7392	1.777	.10800E-06	.4744	4.477	220.4	154.4
3	8.10	.2102	45.00	.0660	.0305	.12420E 04	.86897E C2	.0724	4364	1.034	.17697E-06	.6524	3.534	240.8	168.6
4	9.20	.2098	29.10	.0594	.0305	.80316E 03	.10307E C3	.1137	2934	.842	.31448E-06	.4859	3.879	254.6	178.8
5	10.00	.2030	15.00	.0485	.0305	.4140E 03	.10563E C3	.2033	1694	.524	.59574E-06	.4870	2.413	259.7	181.8
6	11.80	.2295	20.00	.0607	.0295	.5520E 03	.12180E C3	.1808	2196	.909	.61413E-06	.3385	3.037	299.7	209.8
7	10.30	.2365	40.00	.0720	.0295	.11040E 04	.11566E C3	.0948	3975	1.238	.25532E-06	.4970	3.492	286.3	200.6
8	8.90	.2396	61.00	.0880	.0295	.16836E 04	.10833E C3	.0605	5841	1.5704	.16281E-06	.4867	4.105	270.1	189.2
9	10.85	.2327	30.30	.0676	.0295	.83628E 03	.11770E C3	.1234	3109	1.110	.137413E-06	.4180	3.440	290.5	203.4
10	12.20	.2290	13.70	.0522	.0295	.37812E 03	.12368E C3	.2465	1656	.661	.180565E-06	.4079	2.332	303.7	212.7
11	12.65	.2290	8.80	.0442	.0295	.24288E 03	.12589E C3	.3414	1202	1.428	.19601E-06	.6301	1.554	308.7	216.2
12	15.50	.2677	8.80	.0516	.0292	.24288E 03	.13324E C3	.0623	1282	.652	.12949E-05	.4559	1.691	368.5	258.0
13	14.20	.2677	22.00	.0735	.0292	.60720E 03	.14401E C3	.1917	2449	1.290	.170155E-06	.2655	3.141	354.2	248.0
14	13.20	.2708	39.10	.0896	.0292	.10792E 04	.13970E C3	.1147	3973	1.759	.36930E-06	.3782	3.742	345.2	241.7
15	11.80	.2770	58.00	.1180	.0292	.16008E 04	.13324E C3	.0771	5654	2.1587	.26375E-06	.3041	4.831	332.1	232.6
16	11.15	.2870	74.00	.1170	.0292	.20424E 04	.13244E C3	.0609	7089	2.1587	.16589E-06	.4789	4.145	330.2	231.2
17	15.20	.2690	13.00	.0594	.0292	.35880E 03	.14922E C3	.2937	1656	1.880	.110457E-05	.3370	2.812	366.2	258.4
18	13.90	.2940	52.00	.1050	.0305	.14352E 04	.14934E C3	.1524	5165	2.170	.126517E-06	.4651	3.660	359.7	258.9
19	14.60	.2940	39.50	.1000	.0305	.10902E 04	.15297E C3	.1230	4052	2.1024	.440189E-06	.3547	3.711	377.5	264.4
20	14.80	.2880	30.70	.0923	.0305	.84732E 03	.15241E C3	.1524	3259	1.800	.55259E-06	.2645	3.625	375.4	262.9
21	15.65	.2860	21.70	.0819	.0305	.59892E 03	.15607E C3	.2067	2461	1.497	.180588E-06	.1985	3.171	383.7	288.7
22	16.20	.2835	14.60	.0702	.0305	.40286E 03	.15803E C3	.2817	1829	1.156	.11273E-05	.1836	2.572	387.9	271.6
23	17.20	.2870	8.60	.0570	.0305	.23736E 03	.16370E C3	.4082	1307	.772	.114723E-05	.3871	1.701	401.2	281.0
24	16.40	.2910	18.00	.0750	.0305	.49680E 03	.16106E C3	.2448	2144	1.329	.191890E-06	.2537	2.892	395.6	277.0
25	18.55	.3125	12.00	.0707	.0305	.33120E 03	.17720E C3	.3485	1657	1.171	.13899E-05	.8079	2.153	434.5	304.3
26	17.35	.3115	23.00	.0931	.0307	.63480E 03	.17126E C3	.2125	2627	1.1818	.85828E-06	.1571	3.821	420.9	294.7
27	16.80	.3140	30.80	.1040	.0309	.85008E 03	.16927E C3	.1661	3323	2.1129	.628070E-06	.2272	3.583	416.7	291.8
28	16.05	.3230	40.50	.1110	.0311	.11178E 04	.16790E C3	.1306	4191	1.8327	.143196E-06	.3458	3.634	414.2	290.0
29	16.00	.3560	55.50	.1300	.0313	.15318E 04	.17599E C3	.1031	5567	2.875	.30243E-06	.4364	3.660	435.2	304.7
30	18.30	.3060	16.00	.0810	.0315	.44160E 03	.17420E C3	.12829	2007	1.442	.11666E-06	.1432	2.642	427.5	299.4
31	18.90	.3040	8.00	.0608	.0315	.22080E 03	.17637E C3	.4441	1255	1.853	.18600E-05	.3566	1.638	432.2	302.6

Pipe Diameter = 0.625 in.

$\rho_{water} = 62.2 \text{ lbm/ft}^3$

$\rho_{air} = 0.076 \text{ lbm/ft}^3$

VOID FRACTION DATA

TEST NUMBER	ORIFICE MANOMETER READING (in. Hg.)	ORIFICE AIR DENSITY (lbm/ft ³)	ROTOMETER READING (% SCALE)	LENGTH FILLED WITH WATER (cm.)	WATER FLOW RATE (lbm/hr)	AIR FLOW RATE (lbm/hr)	MASS VELOCITY (lbm/hr in ²)	QUALITY	a MINIMUM POSSIBLE	a MAXIMUM POSSIBLE
1	5.40	.1620	25.10	6.70	.69274E 03	.69662E 02	1726	.0914	.9107	.9219
2	4.43	.1630	40.00	8.60	.11746E 04	.64757E 02	2646	.0554	.8853	.8959
3	4.30	.1670	50.00	9.90	.13100E 04	.63189E 02	3267	.0438	.8680	.8781
4	3.85	.1685	58.50	9.70	.16144E 04	.60091E 02	3791	.0359	.8707	.8808
5	3.50	.1720	75.00	12.20	.20700E 04	.57910E 02	4817	.0272	.8373	.8466
6	2.90	.1740	91.30	13.70	.25195E 04	.53062E 02	5824	.0206	.8173	.8260
7	2.70	.1750	98.00	15.50	.27148E 04	.51361E 02	6239	.0186	.7937	.8014
8	2.70	.1580	19.90	4.90	.54124E 03	.70663E 02	1403	.1140	.9347	.9466
9	6.10	.1570	10.00	4.40	.27600E 03	.72839E 02	790	.2088	.9413	.9534
10	5.70	.1570	20.00	5.90	.55200E 03	.70439E 02	1409	.1132	.9213	.9329
11	5.25	.1628	30.00	6.70	.82800E 03	.68867E 02	2030	.0768	.9107	.9219
12	8.40	.2080	28.30	4.20	.78108E 03	.98132E 02	1990	.1116	.9440	.9562
13	7.95	.2175	41.20	5.20	.11371E 04	.97657E 02	2795	.0791	.9307	.9425
14	7.10	.2179	50.00	6.70	.13800E 04	.92445E 02	3333	.0628	.9107	.9219
15	6.90	.2225	60.50	7.90	.16698E 04	.92105E 02	3988	.0523	.8947	.9055
16	6.68	.2180	60.70	7.70	.16753E 04	.89725E 02	3395	.0508	.8973	.9082
17	6.60	.2278	70.00	7.50	.19330E 04	.91170E 02	4580	.0451	.9000	.9110
18	6.05	.2255	79.90	8.70	.22012E 04	.86894E 02	5188	.0379	.8840	.8945
19	5.90	.2310	94.00	9.80	.25914E 04	.86860E 02	6069	.0324	.8693	.8795
20	5.70	.2295	94.00	9.60	.25914E 04	.85115E 02	6065	.0318	.8720	.8822
21	8.50	.2065	26.00	3.80	.71713E 03	.98350E 02	1847	.1205	.9493	.9616
22	12.25	.2640	27.50	3.50	.75911E 03	.13304E 03	2019	.1491	.9533	.9658
23	11.80	.2715	40.00	4.40	.11011E 04	.13246E 03	2799	.1071	.9413	.9534
24	10.55	.2690	50.00	5.40	.13813E 04	.12480E 03	3406	.0829	.9280	.9397
25	10.35	.2760	60.80	6.30	.16711E 04	.12523E 03	4082	.0694	.9160	.9274
26	9.43	.2735	71.00	6.90	.19596E 04	.11908E 03	4705	.0573	.9080	.9192
27	9.15	.2810	84.50	8.00	.23322E 04	.11893E 03	5548	.0485	.8933	.9041
28	8.50	.2830	95.50	7.50	.26381E 04	.11509E 03	6227	.0418	.9000	.9110
29	10.70	.3100	88.00	7.00	.24218E 04	.13489E 03	5803	.0526	.9067	.9178
30	11.00	.2970	66.00	5.60	.18216E 04	.13384E 03	4426	.0684	.9253	.9370
31	1.36	.1447	99.90	26.80	.27572E 04	.33260E 02	6316	.0119	.6427	.6466
32	1.74	.1428	80.00	19.50	.22080E 04	.37334E 02	5082	.0166	.7400	.7466
33	2.32	.1398	58.00	14.20	.16008E 04	.42604E 02	3720	.0259	.8107	.8192
34	1.17	.1202	61.00	19.20	.16836E 04	.28154E 02	3875	.0164	.7440	.7507
35	.83	.1212	79.00	22.20	.21804E 04	.23851E 02	4989	.0108	.7040	.7096
36	.55	.1248	97.30	27.00	.26855E 04	.19742E 02	6123	.0073	.6400	.6438

APPENDIX F

DATA OF VANCE

VANCE'S DATA, STEAM-WATER

TEST NUMBER	WATER SPECIFIC VOLUME (ft ³ /lbm)	STEAM SPECIFIC VOLUME (ft ³ /lbm)	MASS VELOCITY (lbm/hr ft ²)	FORCE (lbf)	QUALITY	MOMENTUM MULTIPLIER (lbf hr ² in ² /lbm ²)	MINIMUM MOMENTUM MULTIPLIER	HOMOGENEOUS MOMENTUM MULTIPLIER	YK	ZK	HOMOGENEOUS VELOCITY/25 (ft/sec)	ENTRAINMENT CORRELATING FACTOR/25(ft/sec)
1	.0176	5.4720	293.4100	10.5443	.5246	.9803E-06	.5748E-06	.9942E-06	.3306E-01	.1706E 01	.3379E 02	.7472E 02
2	.0176	5.4720	295.6900	6.8220	.3979	.6245E-06	.3527E-06	.7555E-06	.3525E 00	.1771E 01	.2588E 02	.5726E 02
3	.0176	5.3370	297.3400	7.44810	.4168	.6773E-06	.3866E-06	.8006E-06	.2979E 00	.1752E 01	.2757E 02	.6066E 02
4	.0176	5.4720	290.4400	5.4530	.3244	.5174E-06	.2486E-06	.6172E-06	.2708E 00	.2081E 01	.2076E 02	.4595E 02
5	.0176	9.0250	295.0000	19.4030	.4416	.1785E-05	.1347E-05	.2002E-05	.3317E 00	.1325E 01	.6841E 02	.1179E 03
6	.0173	8.6780	297.3800	15.6000	.3357	.1472E-05	.9277E-06	.1608E-05	.2884E 00	.1522E 01	.5539E 02	.9734E 02
7	.0173	8.5150	196.1500	10.7400	.431	.2235E-05	.1675E-05	.2187E-05	.2380E-05	.1335E 01	.4667E 02	.8812E 02
8	.0173	8.5150	199.3400	12.2000	.4090	.2478E-05	.1966E-05	.2187E-05	.1668E 00	.1500E 01	.5495E 02	.9749E 02
9	.0173	8.5150	297.3800	12.1300	.4287	.1098E-05	.6073E-06	.1264E-05	.2300E 00	.1608E 01	.4354E 02	.7724E 02
10	.0173	8.5150	294.9900	8.3880	.3311	.7715E-06	.3837E-06	.9776E-06	.3470E 00	.2011E 01	.3340E 02	.5926E 02
11	.0171	10.7500	293.7300	14.6400	.3353	.1358E-05	.7822E-06	.1619E-05	.3105E 00	.1745E 01	.5207E 02	.8699E 02
12	.0173	8.5150	197.3800	5.5360	.3377	.1138E-05	.6306E-06	.1291E-05	.2308E 00	.1805E 01	.2949E 02	.5232E 02
13	.0173	8.3590	398.1800	20.2240	.4246	.1021E-05	.5822E-06	.1330E-05	.1739E 00	.1739E 01	.5672E 02	.1016E 03
14	.0172	8.8480	416.3900	26.7500	.4422	.1235E-05	.6658E-06	.1354E-05	.1335E 00	.1855E 01	.6532E 02	.1137E 03
15	.0174	7.1750	289.7600	10.3970	.4440	.9911E-06	.5506E-06	.1104E-05	.2034E 00	.1800E 01	.3704E 02	.5178E 02
16	.0175	3.8160	298.6100	8.5900	.4209	.7711E-06	.2790E-06	.5582E-06	.1778E-05	.1883E 00	.2763E 01	.1931E 02
17	.0168	23.0000	287.9000	7.3090	.3262	.8989E-06	.5249E-06	.1883E-06	.1788E-05	.5950E 00	.1712E 01	.6277E 02
18	.0170	16.4030	287.9000	14.5460	.2273	.7287E-06	.3257E-06	.1156E-05	.5897E 00	.2046E 01	.4261E 02	.5463E 02
19	.0171	11.8940	321.6300	24.4580	.4150	.1892E-05	.1548E-05	.2401E-05	.5961E 00	.1223E 01	.8944E 02	.1255E 03
20	.0169	16.3030	234.1400	23.6840	.3300	.3406E-05	.3930E-05	.4617E-05	.1634E 01	.8799E 00	.1268E 02	.1378E 03
21	.0173	8.5150	301.5700	4.9250	.4229	.1062E-05	.5926E-06	.1247E-05	.2827E 00	.1792E 01	.4303E 02	.7634E 02
22	.0173	8.5150	302.5800	11.7750	.4061	.4245E-06	.1791E-06	.6260E-06	.4171E 00	.2454E 01	.2187E 02	.3879E 02
23	.0173	8.5150	297.8900	7.7200	.4113	.4396E-06	.1791E-06	.6260E-06	.4171E 00	.2454E 01	.2187E 02	.3879E 02
24	.0173	8.5150	399.0700	11.1370	.4157	.3619E-06	.1853E-06	.6389E-06	.1610E 00	.1954E 01	.2953E 02	.5239E 02
25	.0173	8.3590	499.8800	18.0730	.4129	.3568E-06	.1785E-06	.6192E-06	.5955E 00	.1979E 01	.3585E 02	.6419E 02
26	.0173	8.5150	496.4600	5.0060	.4209	.9020E-06	.5875E-06	.1241E-05	.5188E 00	.1535E 01	.5757E 02	.1021E 03
27	.0173	8.5150	496.4600	4.3890	.4044	.1626E-06	.8983E-07	.3128E-06	.5983E 00	.2634E 01	.1799E 02	.3191E 02
28	.0170	13.7460	399.0500	4.3890	.4046	.1626E-06	.8983E-07	.5090E-06	.6880E 00	.2456E 01	.2353E 02	.3285E 02
29	.0170	13.7460	398.2300	3.5910	.4496	.8031E-07	.3270E-07	.2408E-06	.7112E 00	.2456E 01	.1669E 02	.2309E 02
30	.0172	10.2580	699.2300	3.7680	.4488	.6160E-07	.2701E-07	.1771E-06	.7695E 00	.2281E 01	.1635E 02	.2319E 02
31	.0173	8.5150	497.6500	2.7680	.4580	.7370E-07	.2967E-07	.1763E-06	.6996E 00	.2484E 01	.1016E 02	.1802E 02
32	.0173	8.5150	396.2100	1.4400	.4611	.7136E-07	.3141E-07	.4152E-06	.7401E 00	.2722E 01	.8498E 01	.1508E 02
33	.0173	8.5150	397.4200	5.1460	.4503	.6432E-07	.2474E-07	.1335E-06	.6676E 00	.2575E 01	.2272E 02	.2272E 02
34	.0173	8.5150	397.4200	3.5900	.4512	.1821E-06	.6617E-07	.3355E-06	.5738E 00	.6711E 01	.1444E 02	.2738E 02
35	.0173	8.3590	797.6600	11.7310	.4061	.1476E-06	.6220E-07	.3118E-06	.6880E 00	.2372E 01	.2880E 02	.5157E 02
36	.0173	8.4000	297.6200	2.0990	.4215	.1889E-06	.7096E-07	.3427E-06	.5662E 00	.2661E 01	.1181E 02	.2110E 02
37	.0170	13.3000	298.9700	7.7390	.4215	.6495E-06	.2894E-06	.1037E-05	.5484E 00	.2400E 01	.3591E 02	.5059E 02
38	.0170	13.3000	402.5900	12.4300	.4188	.6138E-06	.2801E-06	.1012E-05	.5438E 00	.2191E 01	.4717E 02	.6689E 02
39	.0170	13.7000	400.1800	3.6100	.4603	.1085E-06	.4128E-06	.9208E-06	.7308E 00	.2627E 01	.1349E 02	.1895E 02
40	.0176	5.4720	296.6400	3.6100	.4210	.3828E-06	.1429E-06	.4224E-06	.3248E 00	.2471E 01	.1451E 02	.3122E 02
41	.0173	8.5150	398.1300	7.0900	.4212	.3253E-07	.1553E-07	.6818E-07	.5900E 00	.2812E 01	.3144E 02	.5578E 02
42	.0173	8.4000	798.8000	1.7300	.4120	.2176E-07	.9360E-08	.4068E-07	.16059E 00	.2319E 01	.3764E 01	.6722E 01

Pipe Diameter = 0.5045 in.

REFERENCES

- 1) Martinelli, R.C., and D.B. Nelson, "Prediction of Pressure Drop During Forced Circulation Boiling of Water," Trans. Am. Soc. Mech. Engrs., 70, 695, 1948.
- 1a) Martinelli, R. C., L.M.K. Boelter, T.H.M. Taylor, E.G. Thomson, and E.H. Morrin, "Isothermal Pressure Drop for Two-Phase, Two-Component Flow in a Horizontal Pipe," Trans. Am. Soc. Mech. Engrs., 66, 139, 1944.
- 1b) Lockhart, R.W., and R. C. Martinelli, "Proposed Correlation of Data for Isothermal, Two-Phase, Two-Component Flow in Pipes," Chem. Eng. Prog., 45, 39, 1949.
- 2) Thom, J.R.S., "Prediction of Pressure Drop During Forced Circulation of Boiling of Water," International Journal of Heat and Mass Transfer, 7, 709, 1964.
- 3) Magiros, P.G. and A.E. Dukler, "Entrainment and Pressure Drop in Concurrent Gas-Liquid Flow II. Liquid Property and Momentum Effects," Developments in Mechanics, Vol. I, Plenum Press, New York, 1961.
- 4) Bankoff, S.G., "A Variable Density Single-Fluid Model for Two-Phase Flow with Particular Reference to Steam-Water Flow," Trans. Am. Soc. Mech. Engrs., Series C, 84, 265, 1960.
- 5) Anderson, G.H., and B.C. Mantzoranis, "Two-Phase (gas-liquid) Flow Phenomena - Part I," Chem. Eng. Sci., 12, 109, 1960.
- 6) Silvestri, M., et al., "A Research Program in Two-Phase Flow," Centro Informazioni Studi Esperienze, EURATOM Contract No. 002-59-11, ROI (CAN-1), January, 1963.

- 7) Linning, D.L., "The Adiabatic Flow of Evaporating Fluids in Pipes of Uniform Bore," Proc. Inst. Mech. Engrs., London, 1B 2, 64, 1952.
- 8) Semenov, N.I., "Pressure Pulsations During the Flow of Gas-Liquid Mixtures in Pipes," Heat Power Engineering Part I, U.S.A.E.C., Division of Technical Information, AEC-tr-4496, Dec. 1961, translated.
- 9) Vance, W.H., "A Study of Slip Ratios for the Flow of Steam-Water Mixtures at High Void Fractions," Ph.D. thesis, University of Washington, 1962.
- 10) Rose, S., "Some Hydrodynamic Characteristics of Bubbly Mixtures Flowing Vertically Upward in Tubes," Sc.D. thesis, Massachusetts Institute of Technology, 1964.
- 11) Fauske, H.K., "Two-Phase Critical Flow," Two-Phase Gas-Liquid Flow, ed. by P. Griffith and S. W. Gouse, Jr., Special Summer Program, MIT, Cambridge, Mass., 1964.
- 12) Zivi, S.M., "Estimation of Steady-State Steam Void-Fraction by Means of the Principle of Minimum Entropy Production," Trans. Am. Soc. Mech. Engrs., Series C, 86, 247, 1964.
- 13) Schlichting, H., Boundary Layer Theory, McGraw-Hill, New York, 1960.
- 14) Von Karman, T., "Mechanische Ahnlichkeit und Turbalenz," Proc. 3rd Intern. Congress Appl. Mech., Stockholm, 1930.
- 15) Pai, Fluid Dynamics of Jets, D. Van Nostrand, New York, 1954.
- 16) ASME Power Test Codes; Chapter 4, Flow Measurement; Part 5, Measurement of Quantity of Materials, PTC 19.5, 4-1959, New York.
- 17) Radiotron Designers' Handbook, F. Langford-Smith, Amalgomated Wireless Valve Company Ptg, Ltd., Sidney, Australia, 1953.

- 18) Electronic Designers' Handbook, R. W. Landee, D. C. Davis, and A. P. Alvrecht, McGraw Hill, New York, 1957.
- 19) Griffin, E. and T. F. Crang, "Steam Flow in Nozzles: Velocity Coefficient at Low Steam Speeds," Proc. of Inst. of Mech. Eng., 155, 83, 1946.
- 20) Gill, L.E., G.F. Hewitt, and P.M.C. Lacey, "Sampling Probe Studies of the Gas Core in Annular Two-Phase Flow, Part III, Studies of the Effect of Phase Flow Rates on Phase and Velocity Distributions," AERE-R3955, Harwell, England, 1963.
- 21) Wallis, G.B., D. S. Steen, S.N. Brenner, and J.M. Turner, Thayer School of Engineering, Dartmouth College, Hanover, New Hampshire, Report NYO 10, 489, 1964.
- 22) Minh, Q.T. and J.D. Huyghe, "Mesure et Correlation de la Fraction D'Entrainement en Ecoulement Diphasé a Deux Composants en Regime Annulaire Dispersé," Centre D'Etudes Nucléaires de Grenoble, Commissariat a l'Energie Atomique, Grenoble, France, Rapport TT No. 52, 1965.
- 23) Shames, I.H., Mechanics of Fluids, McGraw-Hill, New York, 1962.
- 24) Handbook of Chemistry and Physics, 35th edition, C. D. Hodgman, Chemical Rubber Publishing Co., Cleveland, 1953.

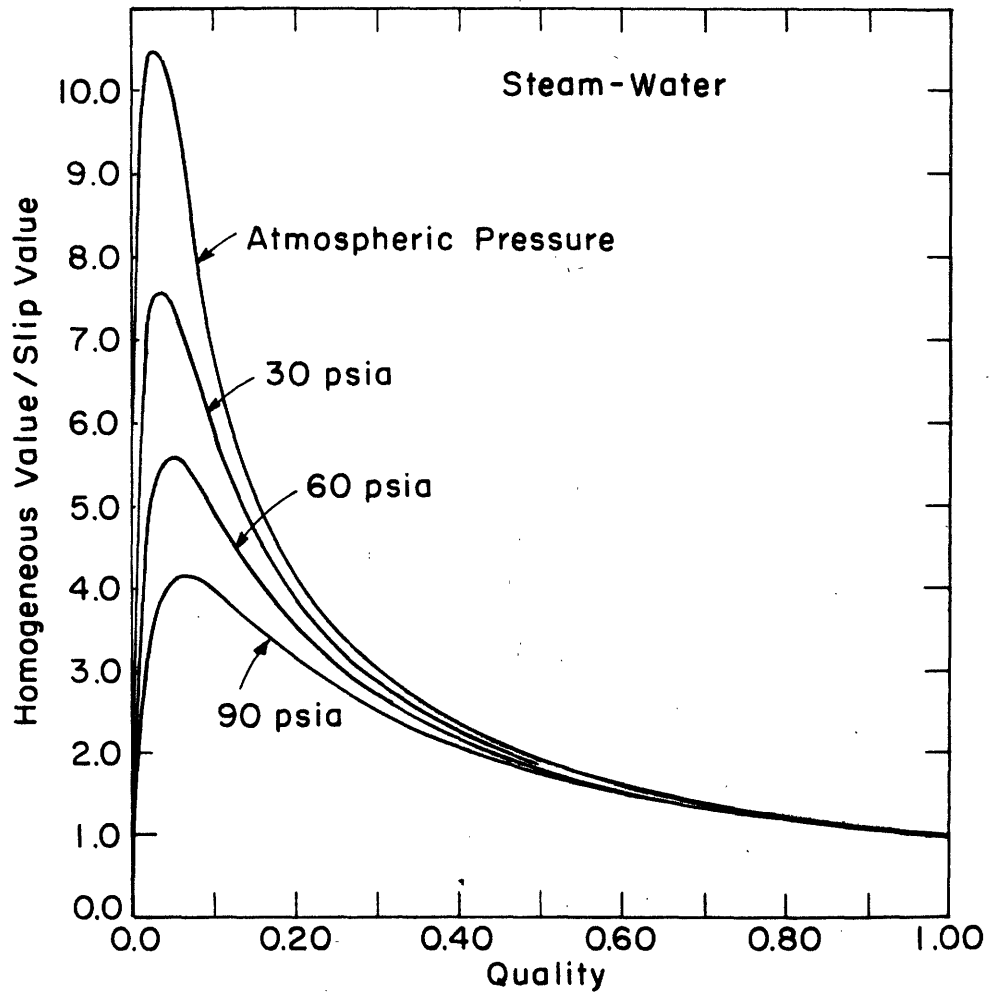
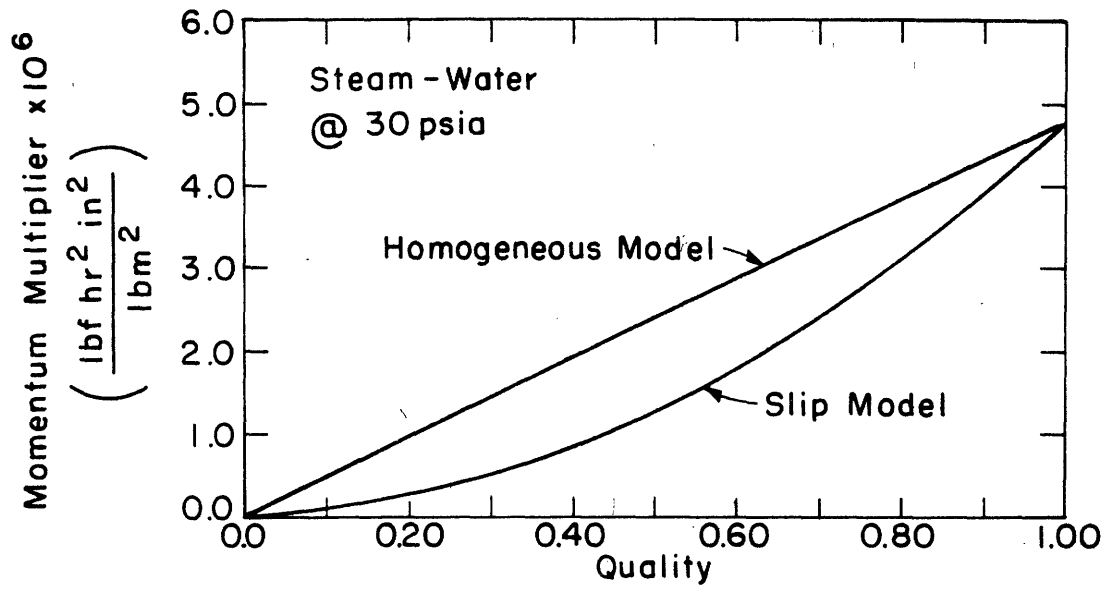


FIGURE 1. COMPARISON BETWEEN HOMOGENEOUS AND SLIP MODELS

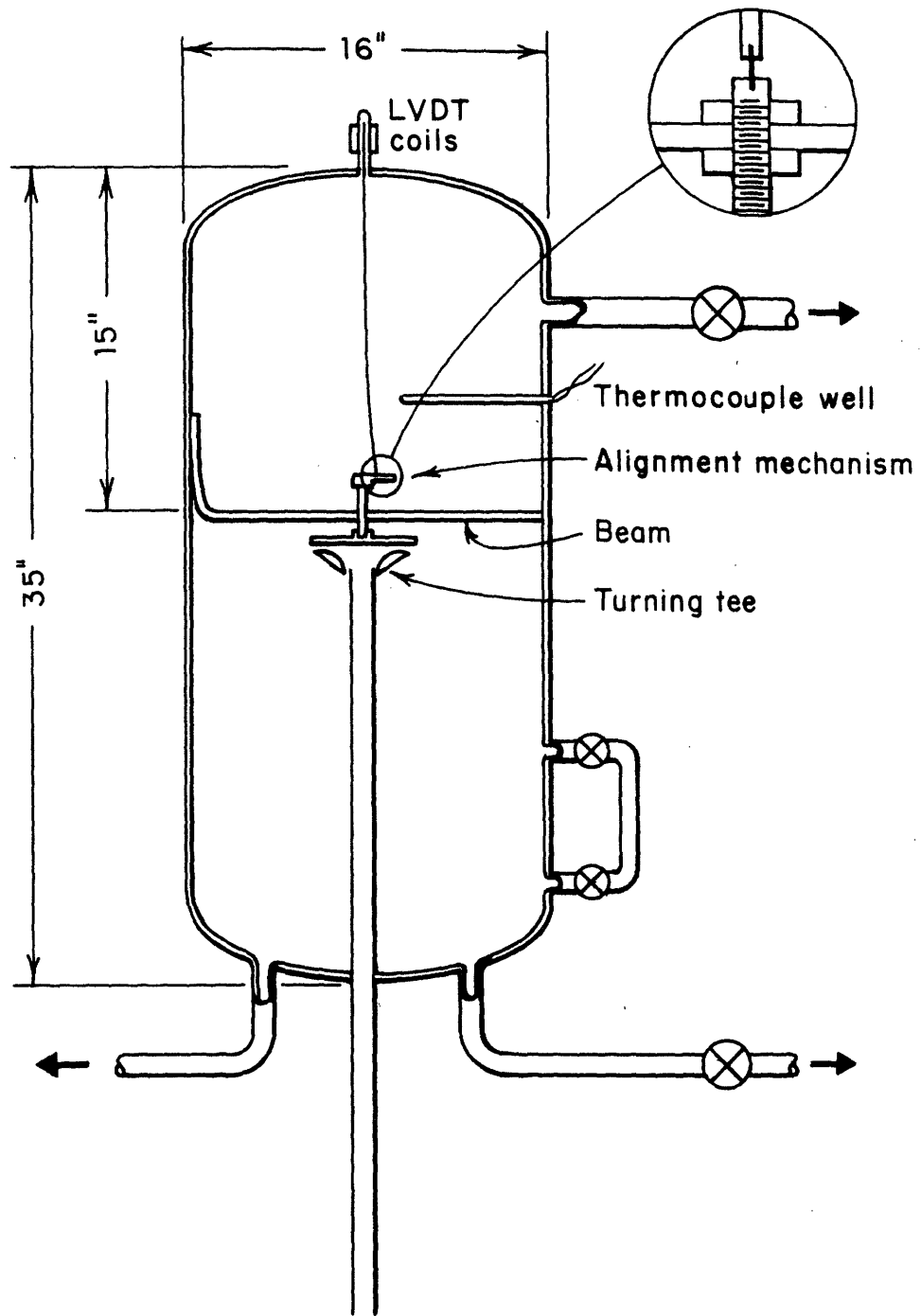


FIGURE 2. CROSS SECTION OF PRESSURE VESSEL
 SHOWING INTERNALS

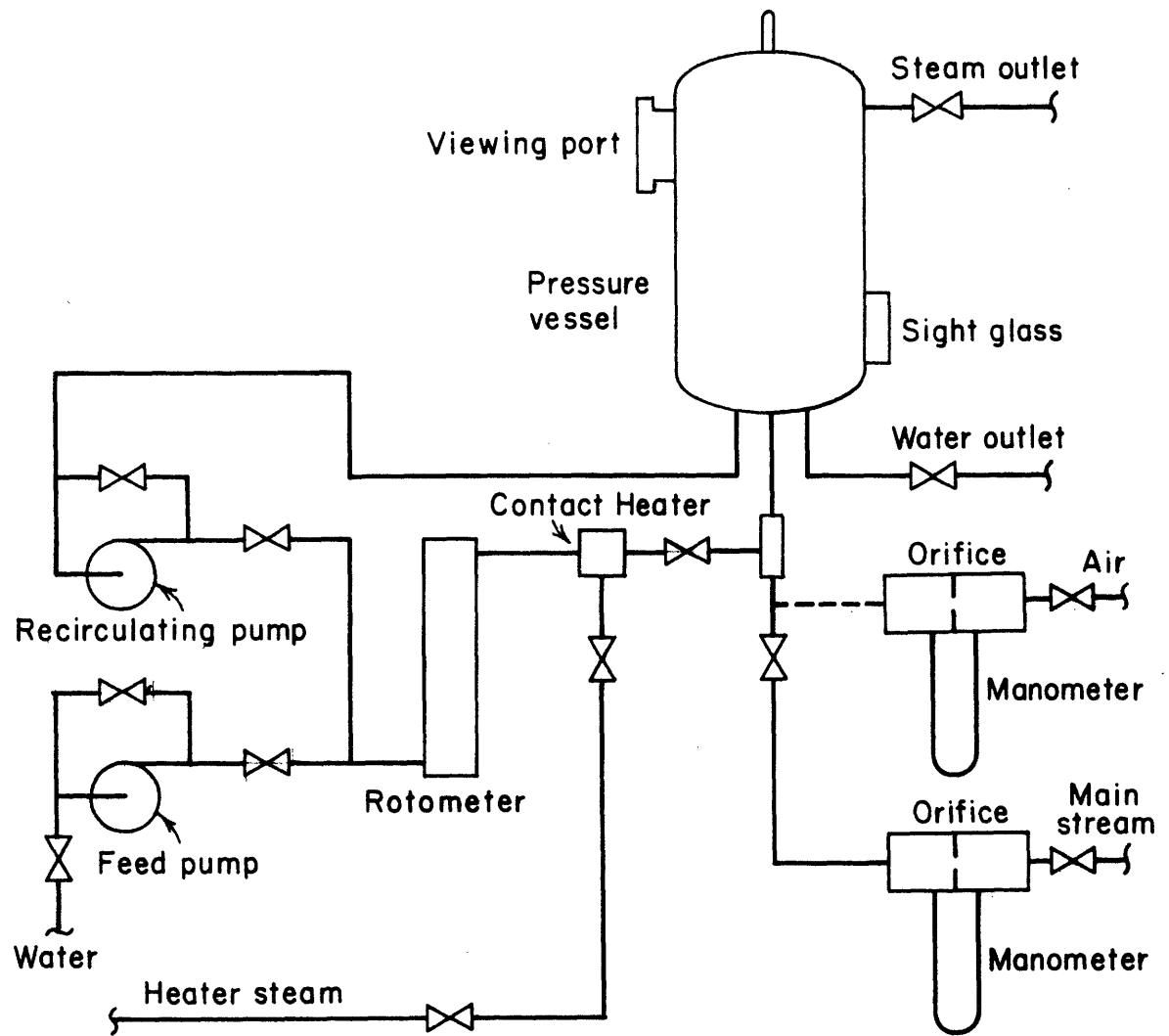


FIGURE 3. SCHEMATIC OF TEST APPARATUS

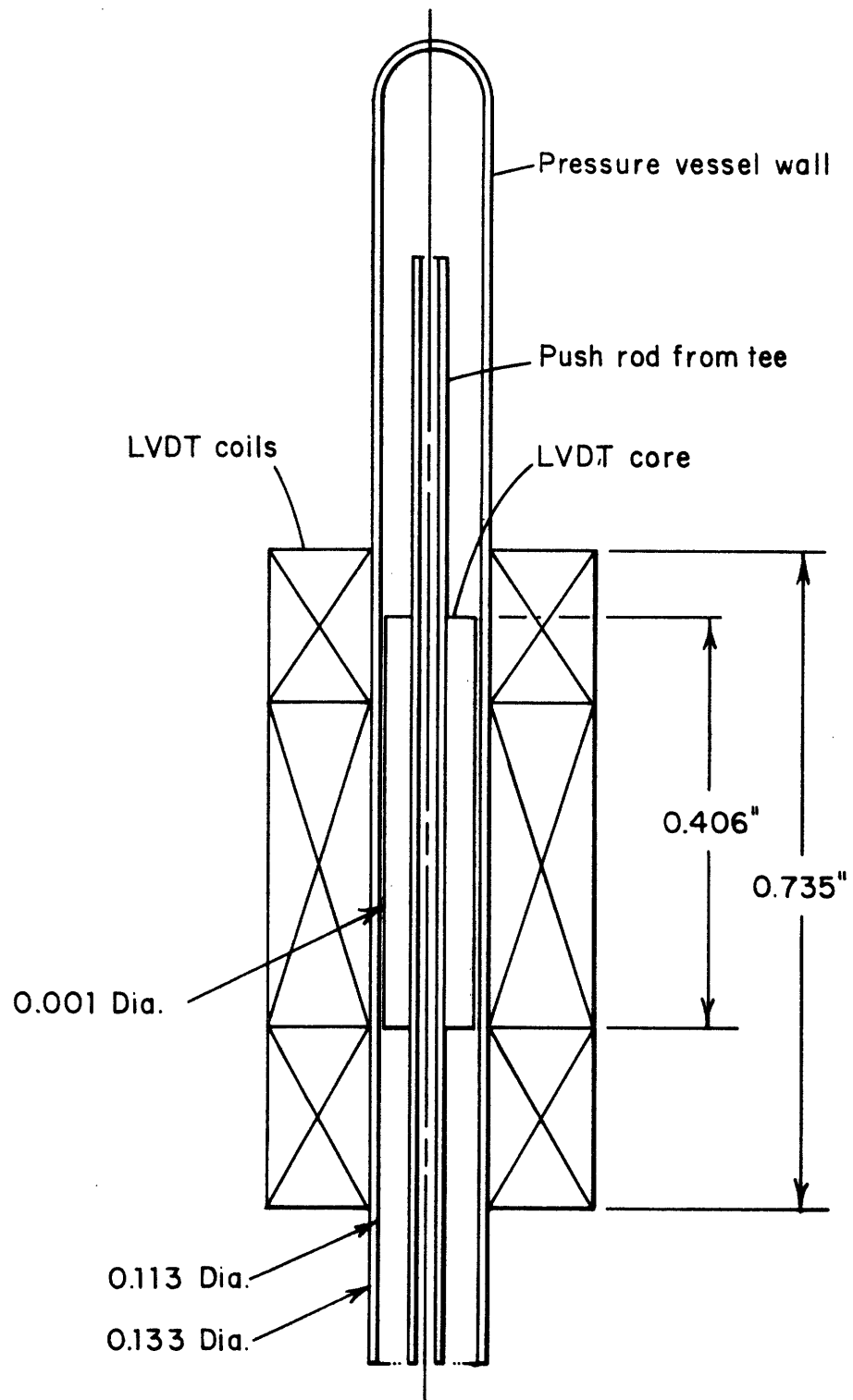
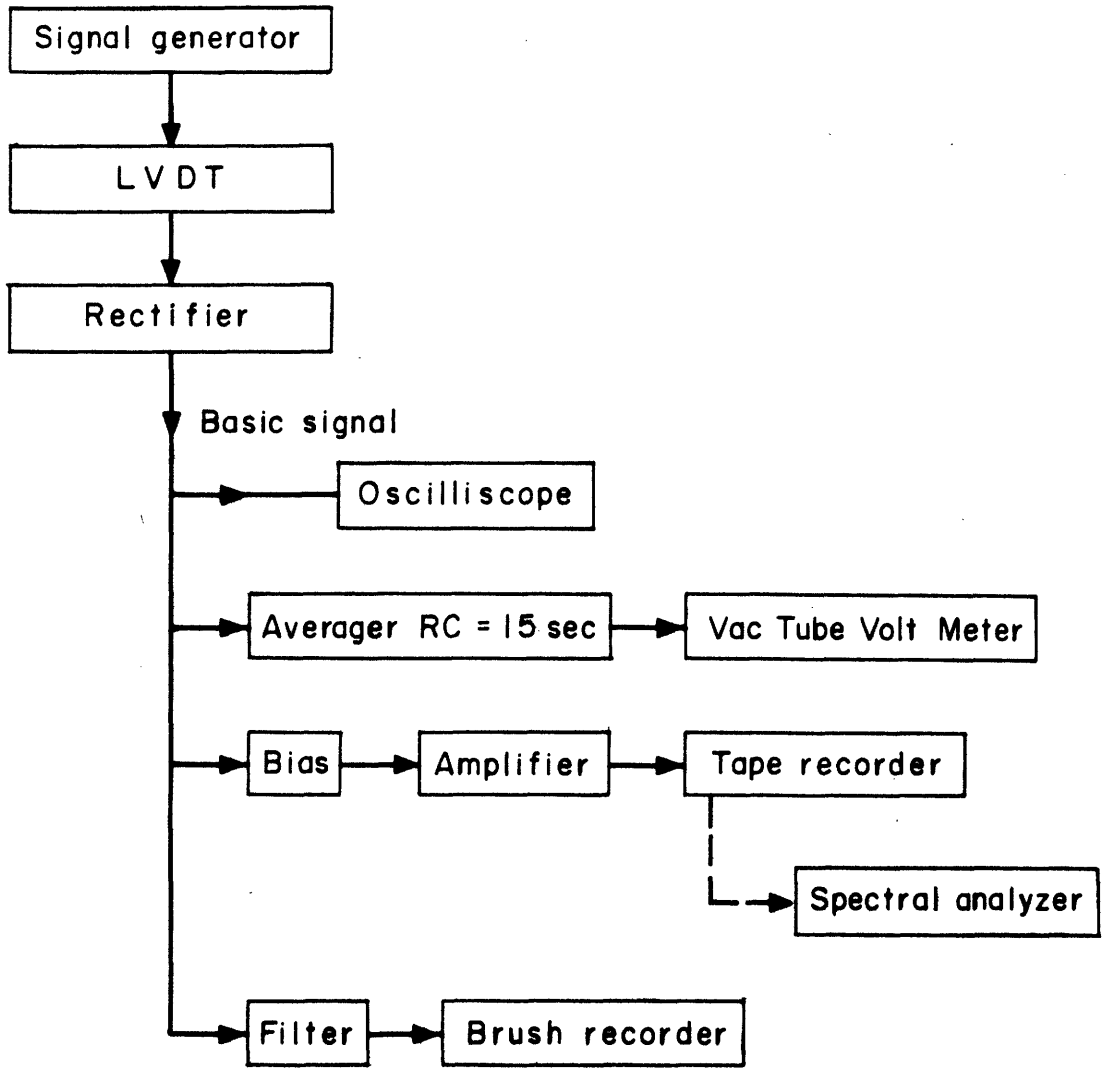


FIGURE 4. LVDT ARRANGEMENT



ELECTRICAL APPARATUS

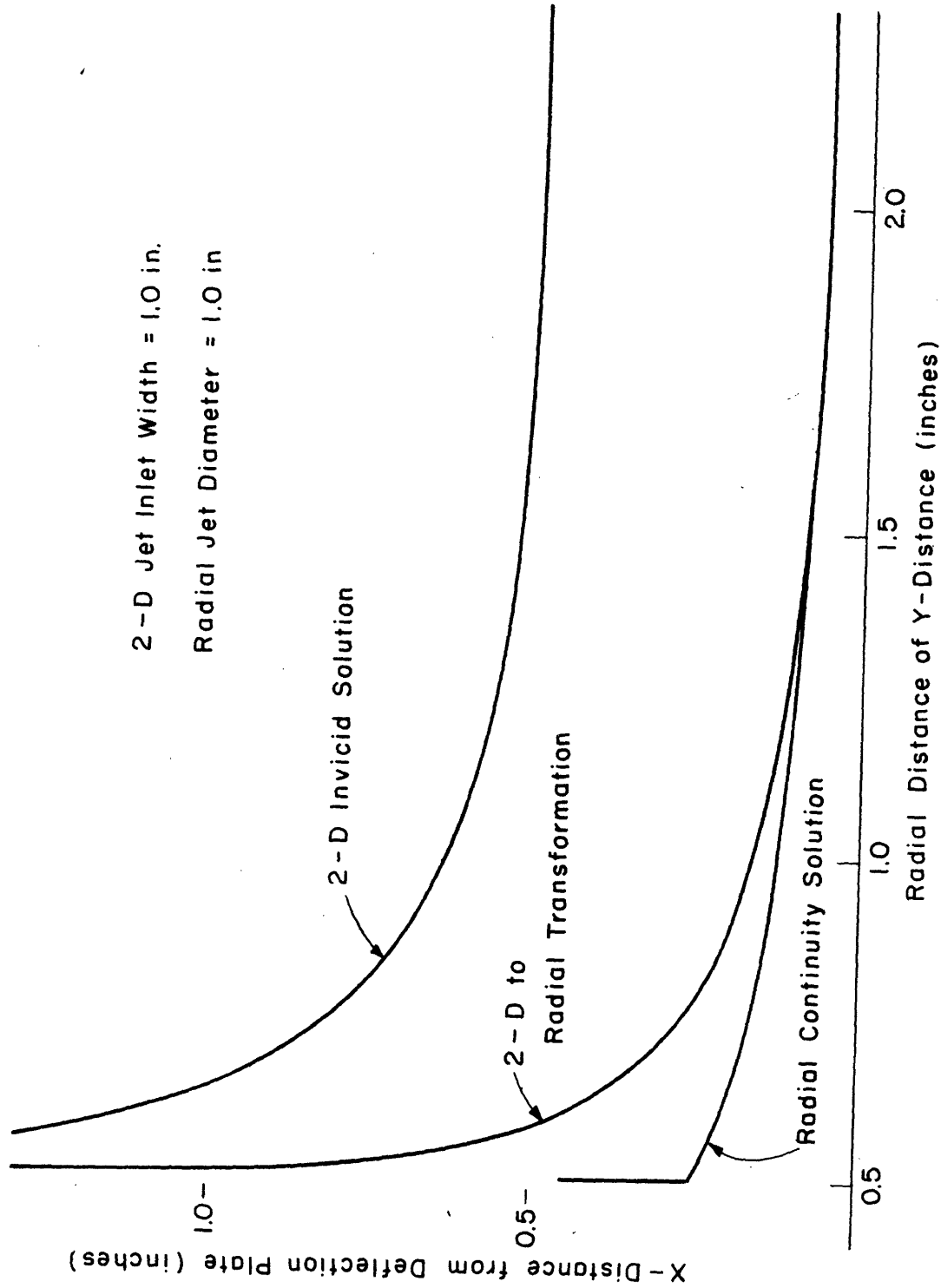
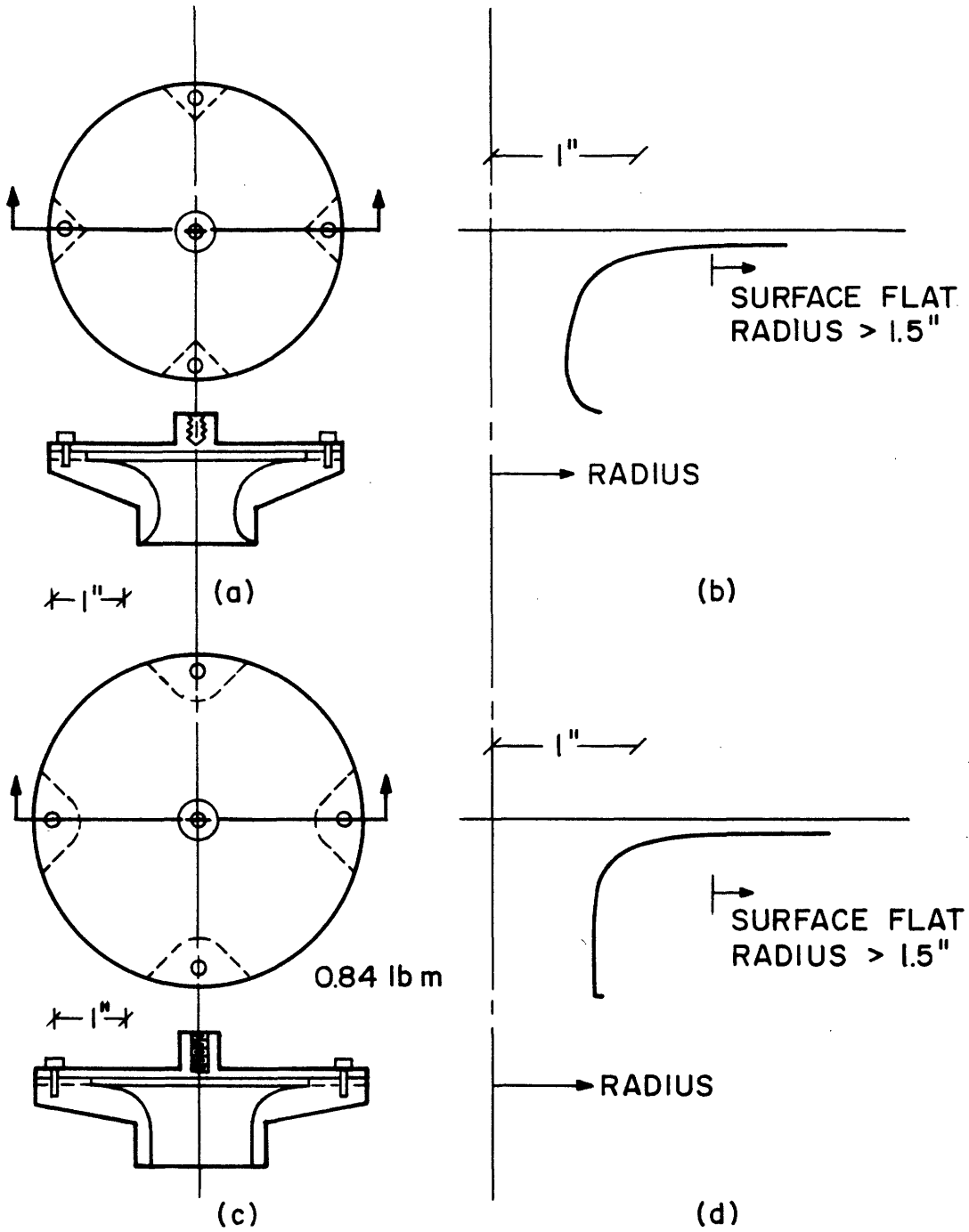


FIGURE 6. JET SURFACE PROFILES



FIRST DESIGN ABOVE
FINAL DESIGN BELOW

PROFILES SHOWN TO
LARGER SCALE

All Aluminum

FIGURE 7. TURNING TEE DESIGNS

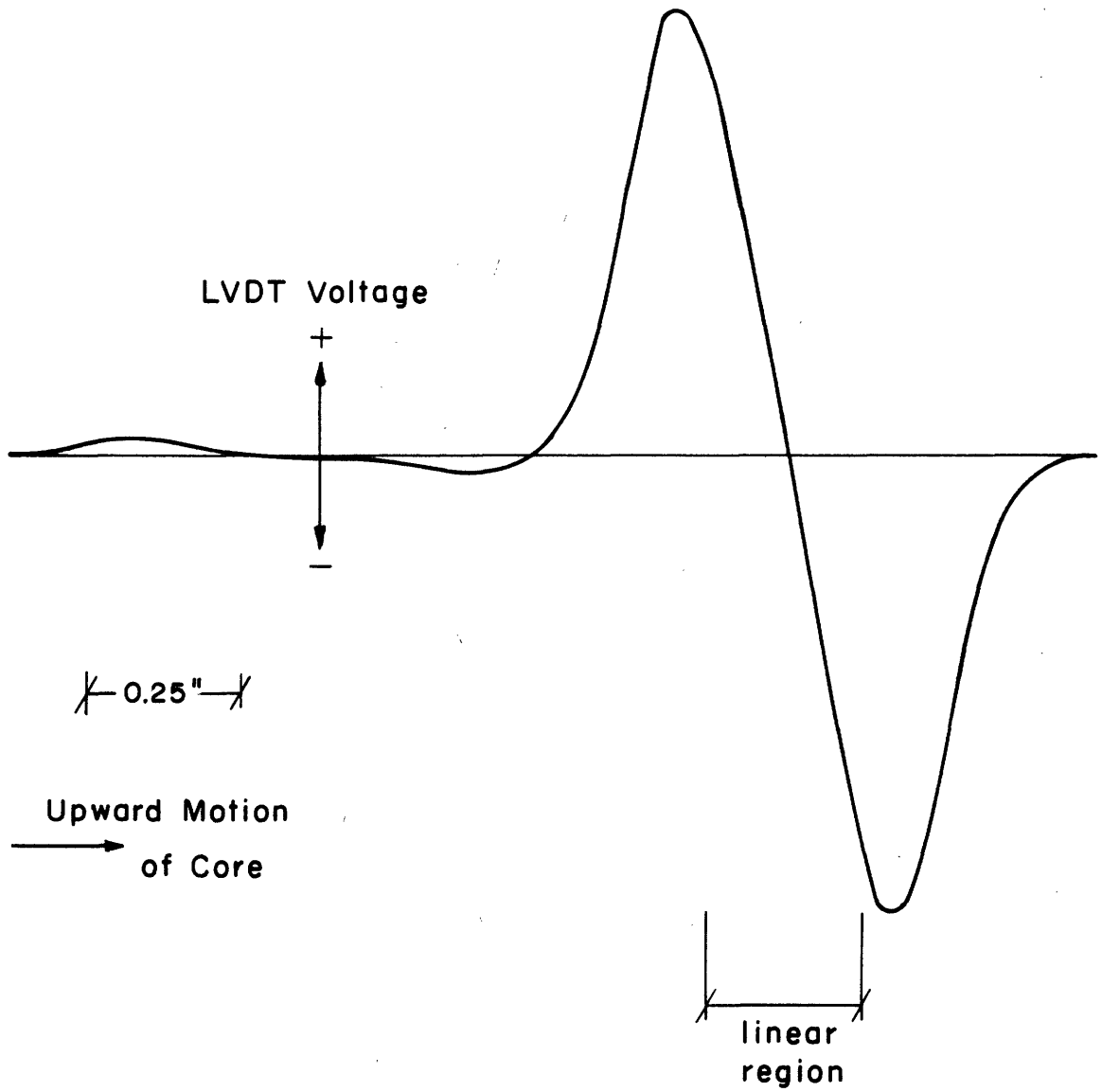


FIGURE 8.

CORE TRAVERSE

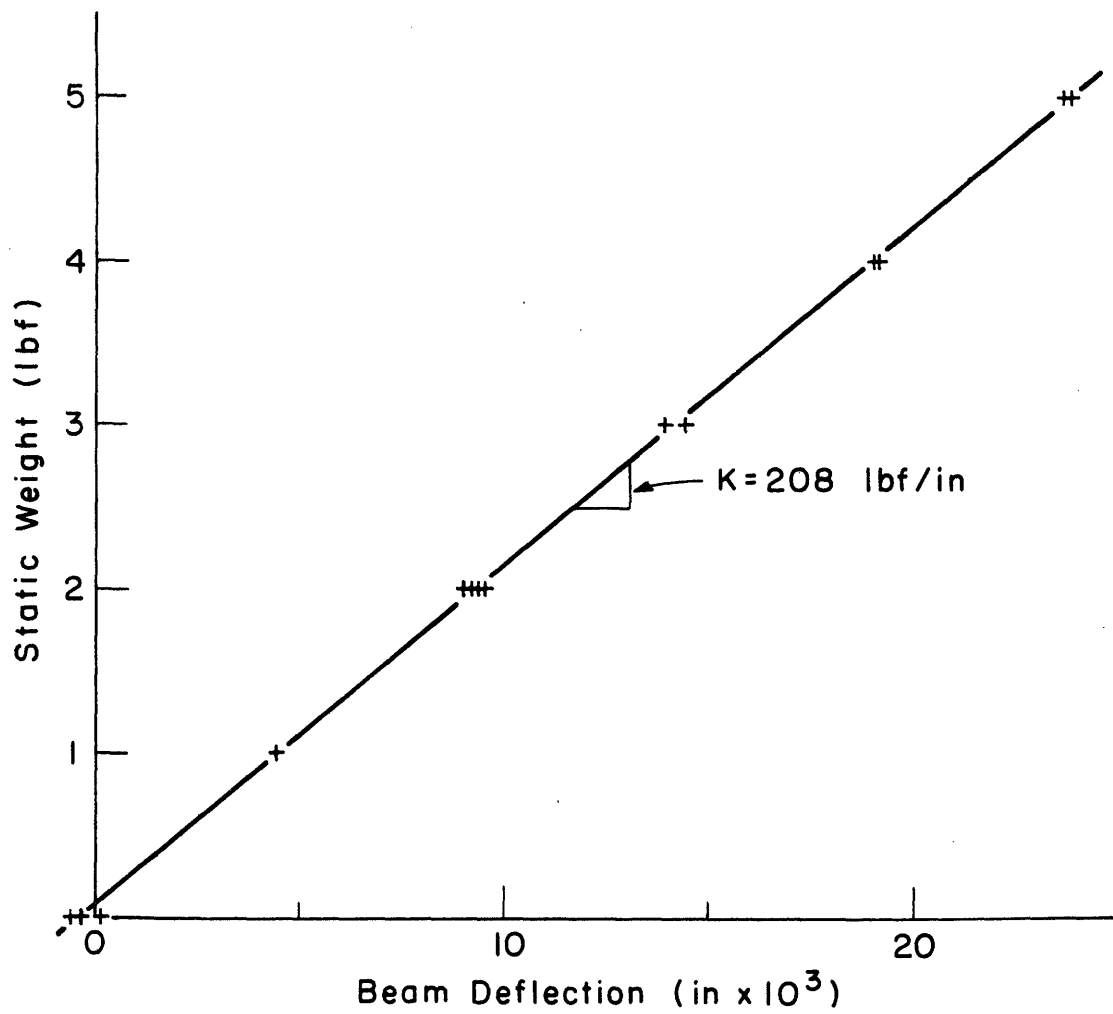


FIGURE 9.

BEAM CONSTANT

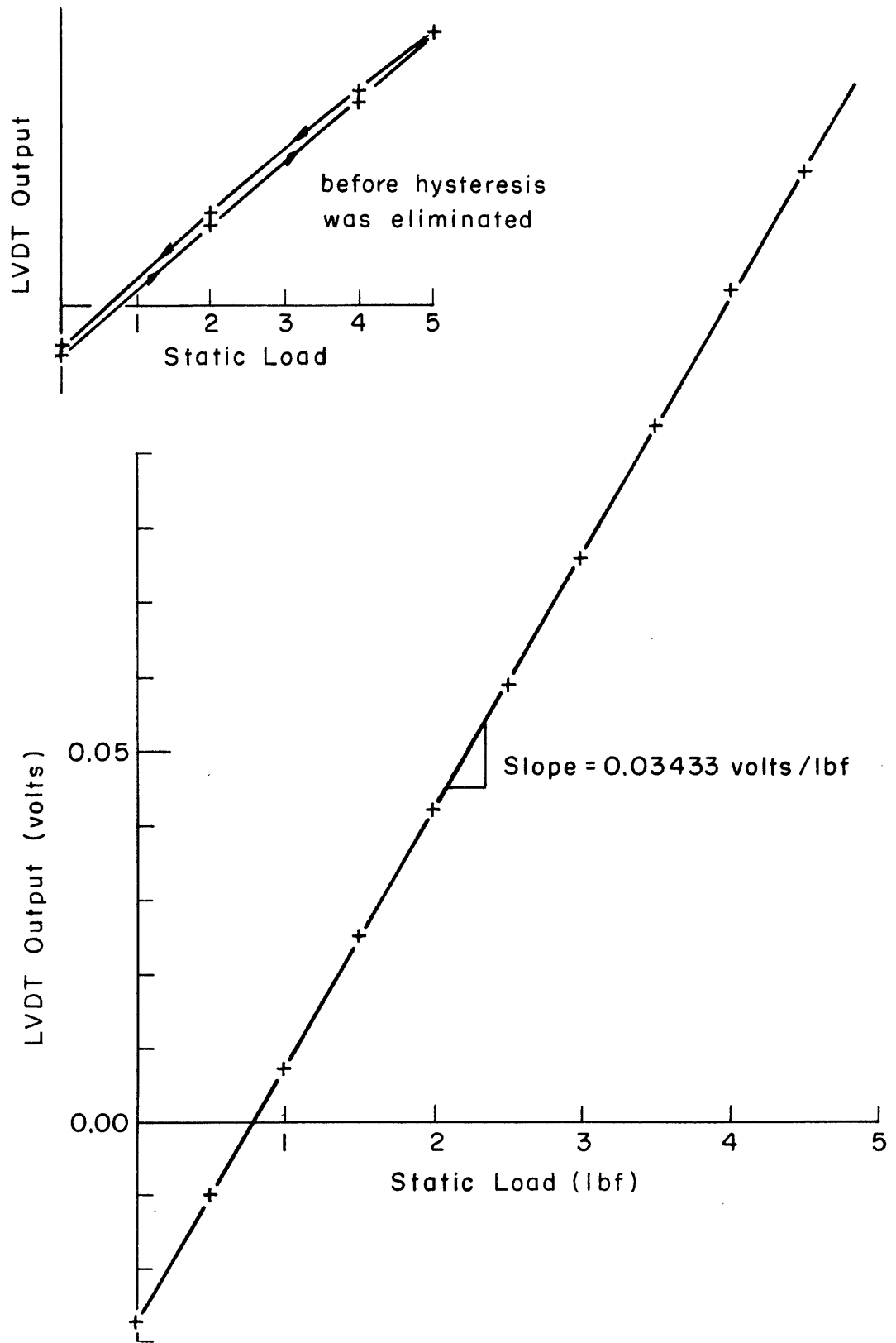


FIGURE 10. STATIC TEST

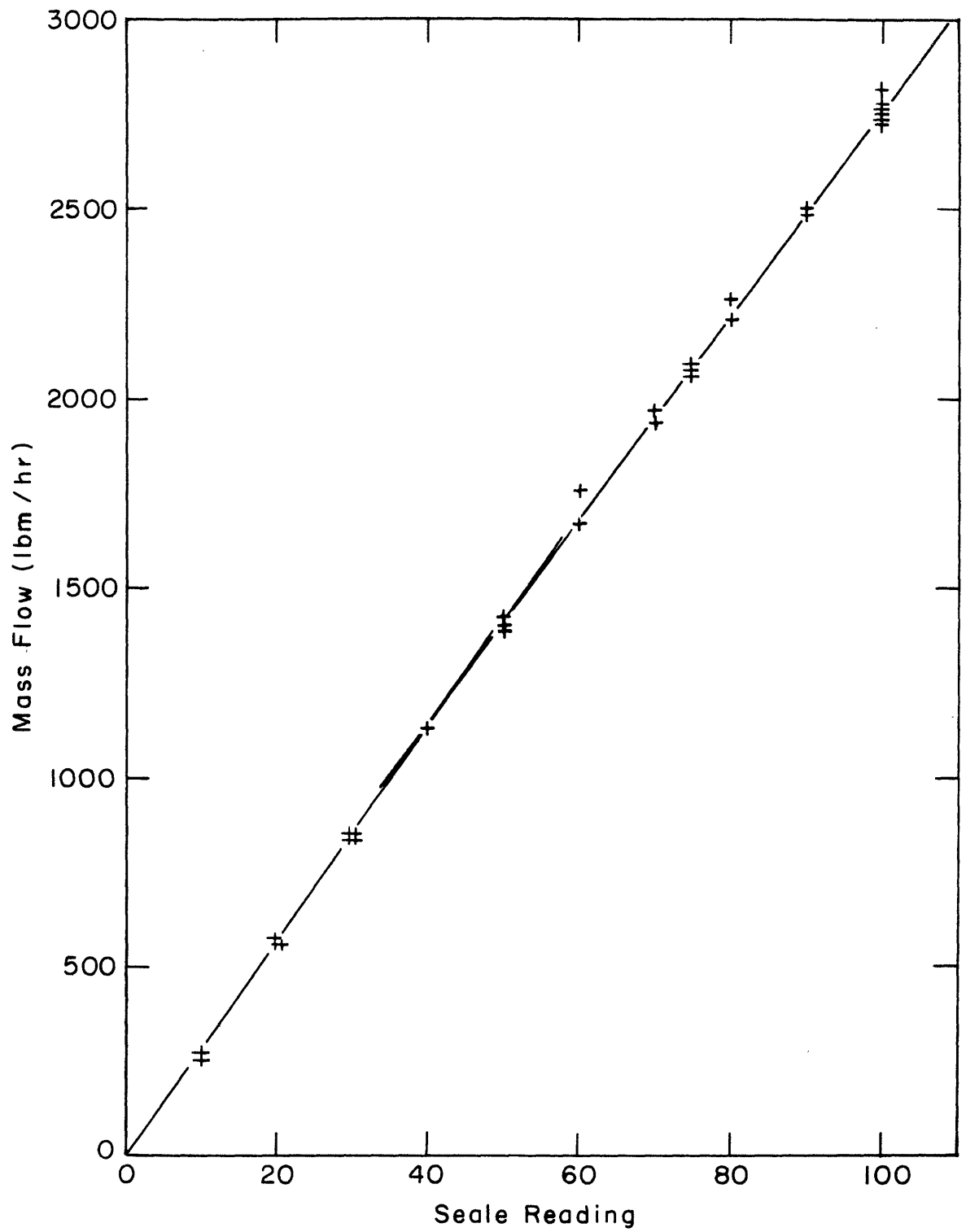


FIGURE II. WEIGH TANK CALIBRATION

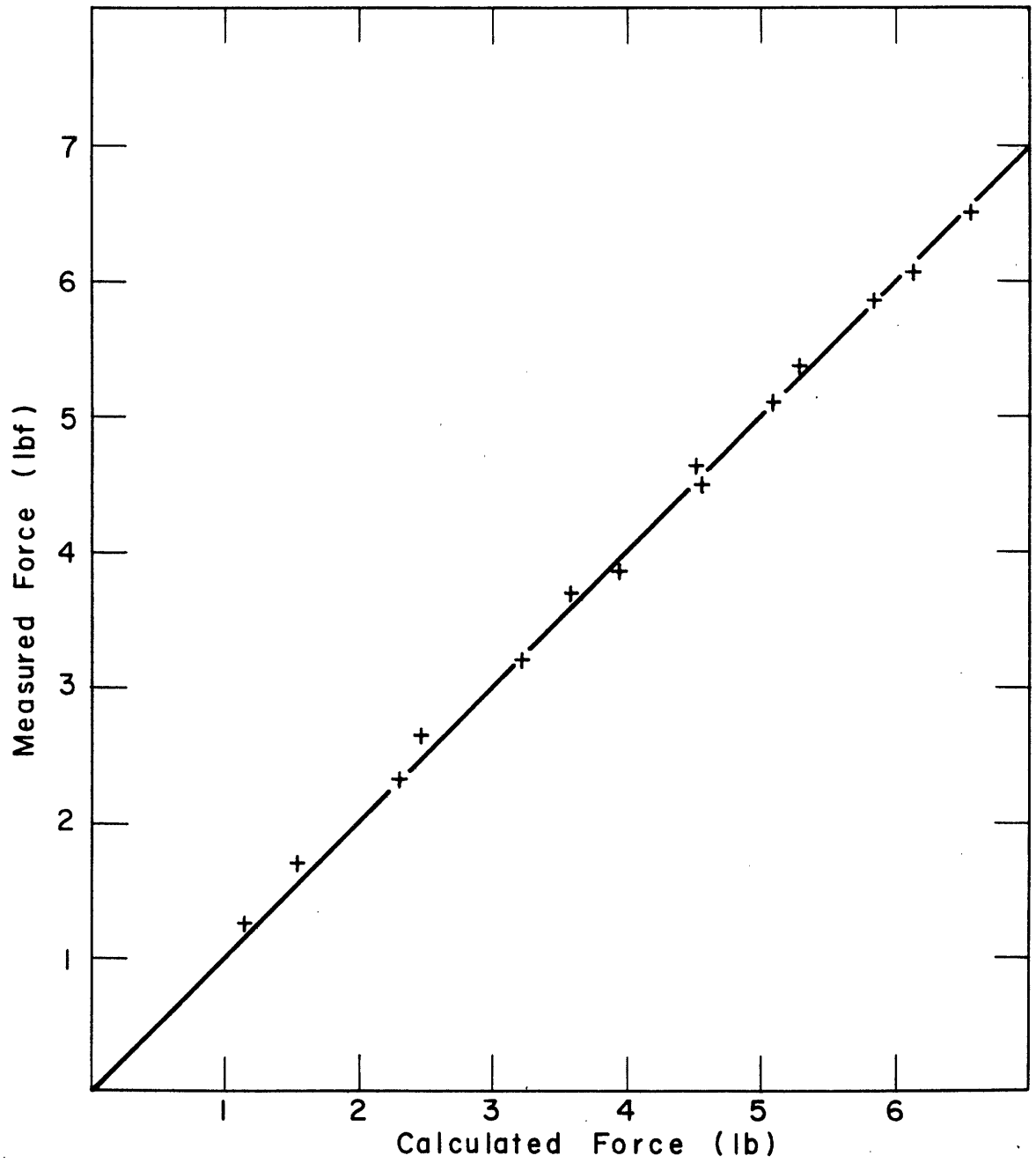


FIGURE 12. STEAM CALIBRATION TEST

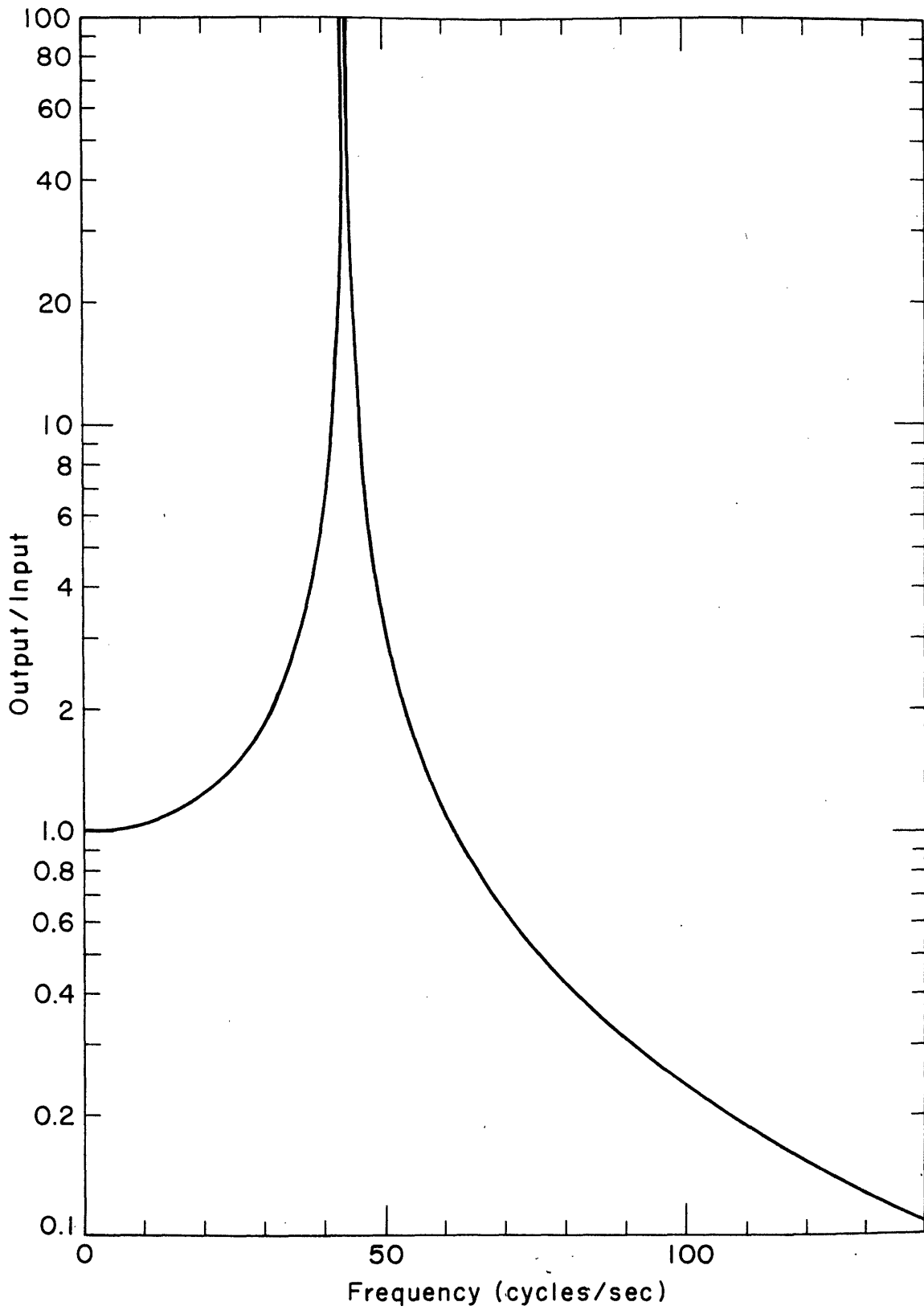


FIGURE 13. BEAM RESPONSE

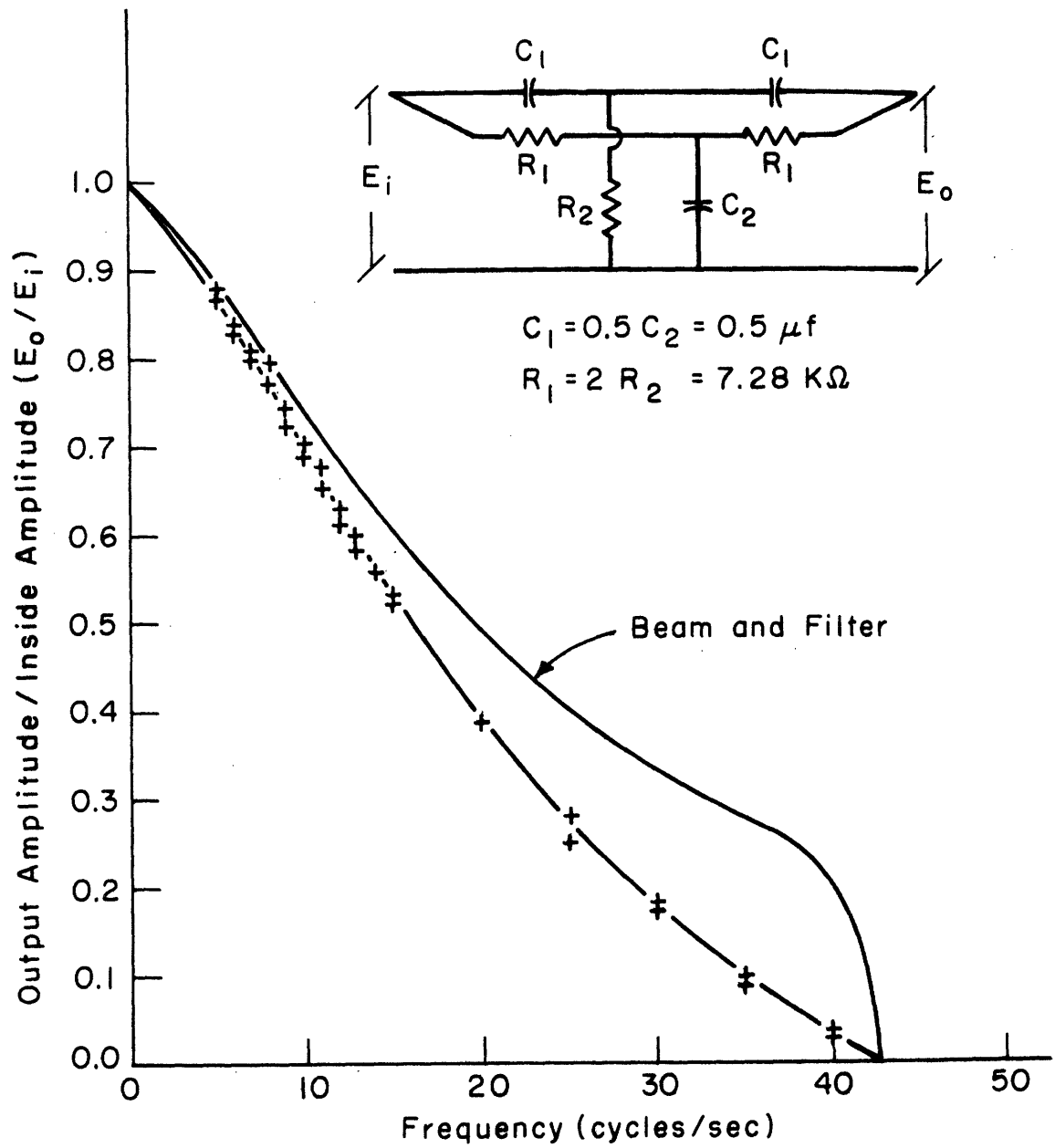
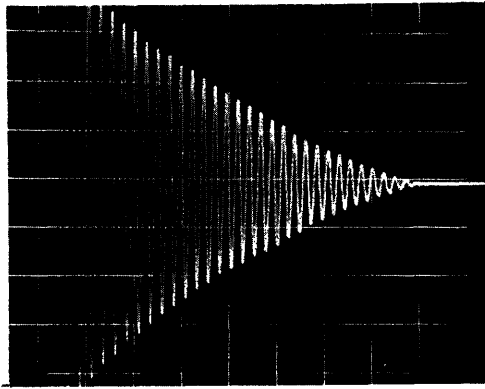
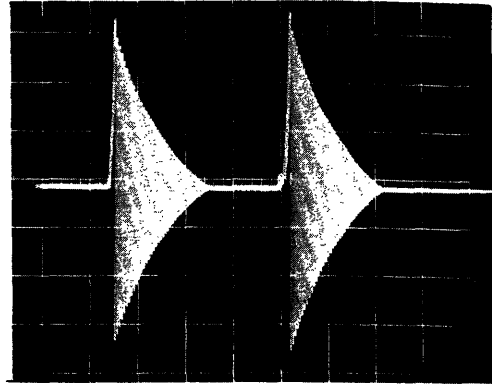


FIGURE 14. FILTER PERFORMANCE

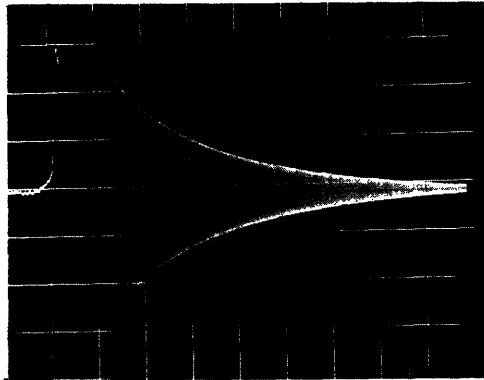


(b) Horiz. Scale 0.1 sec/unit
Vert. Scale 0.05 volts/units

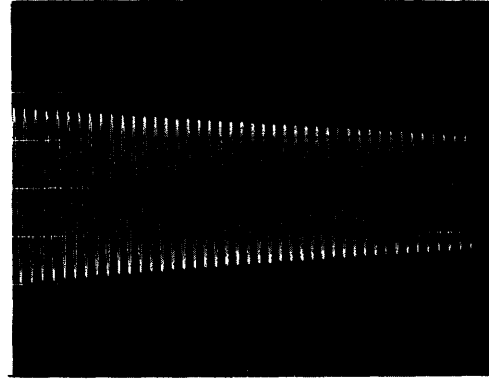


(b) Horiz. Scale 0.5 sec/unit
Vert. Scale 0.1 volts/units

with frictional damping

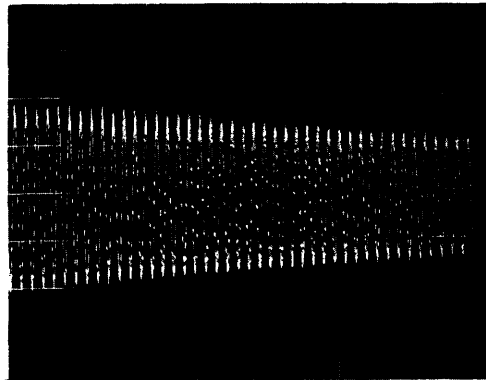


(c) Horiz. Scale 1.0 sec/unit
Vert. Scale 0.02 volts/units



(d) Horiz. Scale 0.1 sec/unit
Vert. Scale 0.02 volt/units

frictional damping eliminated



(e) Horiz. Scale 0.1 sec/unit
Vert. Scale 0.5 volts/units

as playback from tape deck

FIGURE 15. PLUCK TESTS

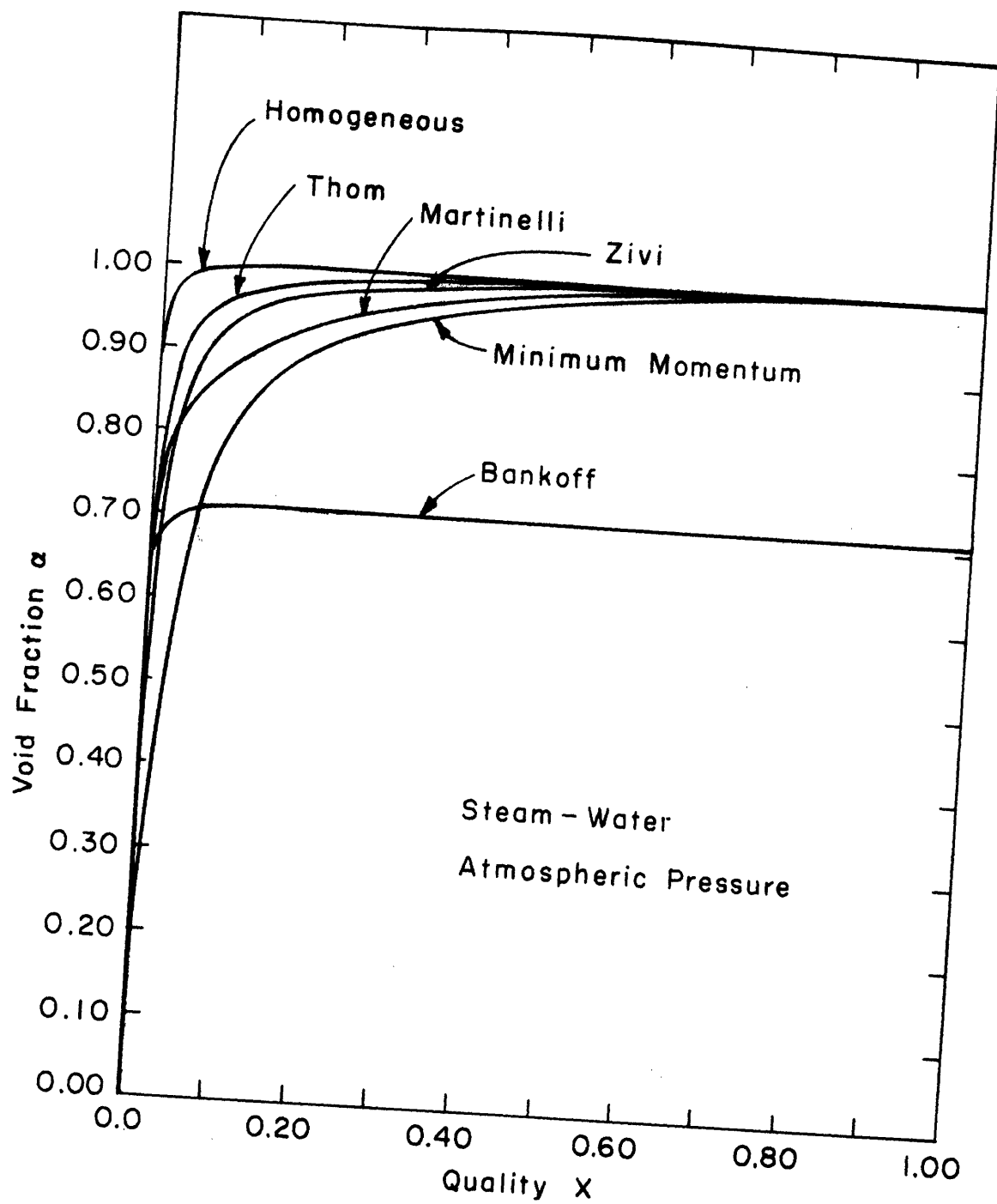


FIGURE 16. QUALITY-VOID FRACTION RELATIONSHIP

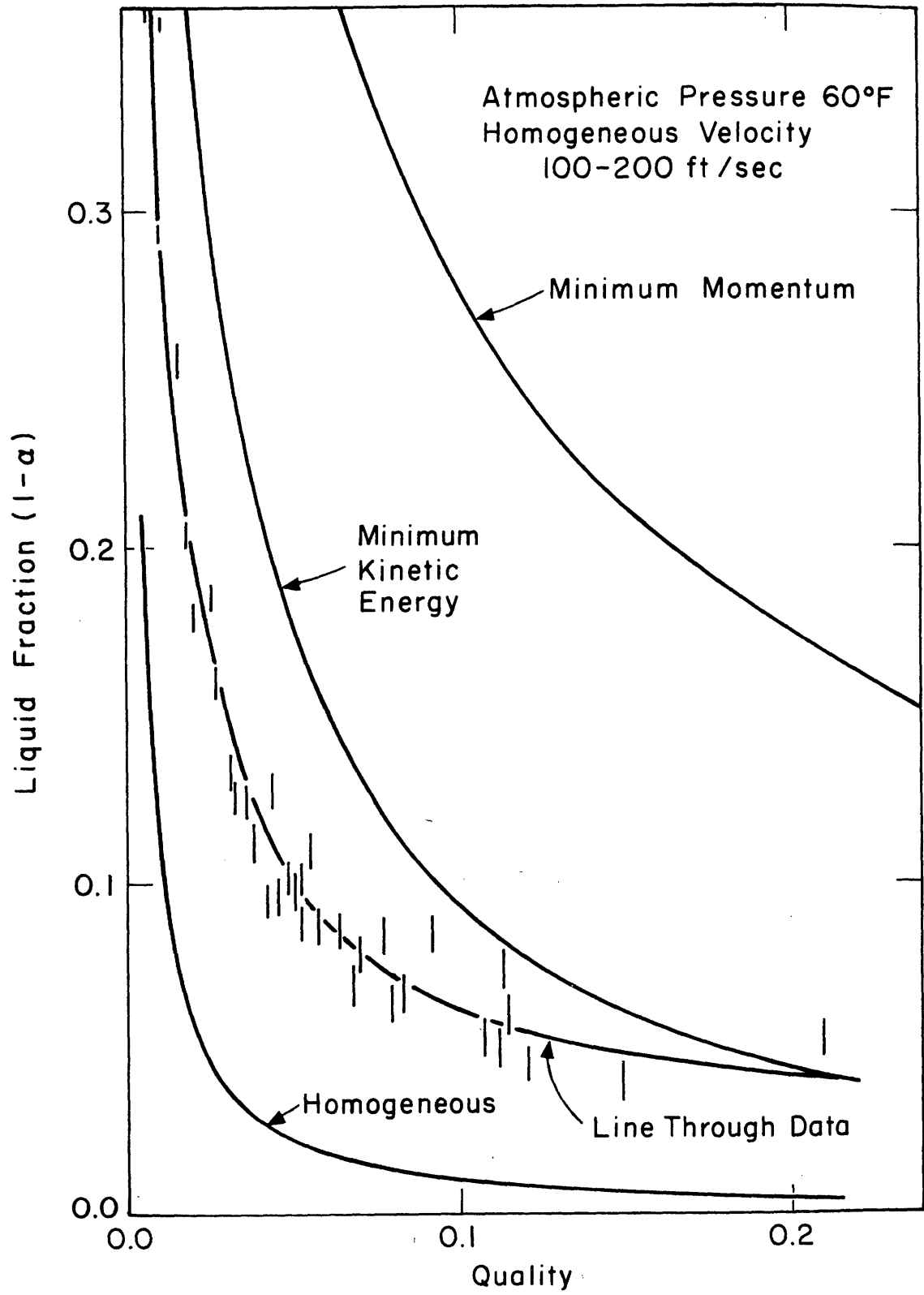


FIGURE 17. AIR-WATER LIQUID FRACTION

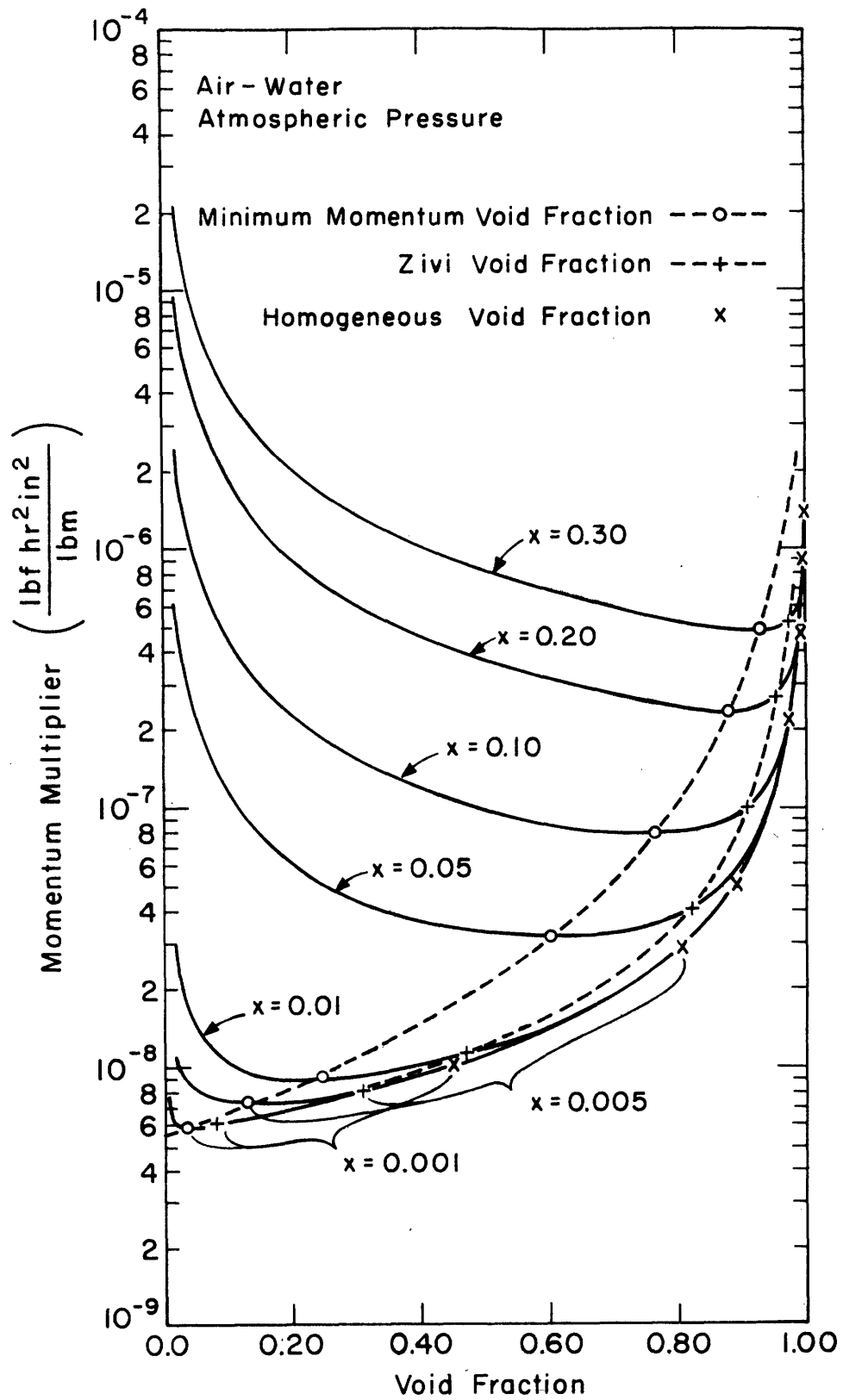


FIGURE 18. EFFECT OF VOID FRACTION ON SLIP MODEL MOMENTUM AMPLIFIER

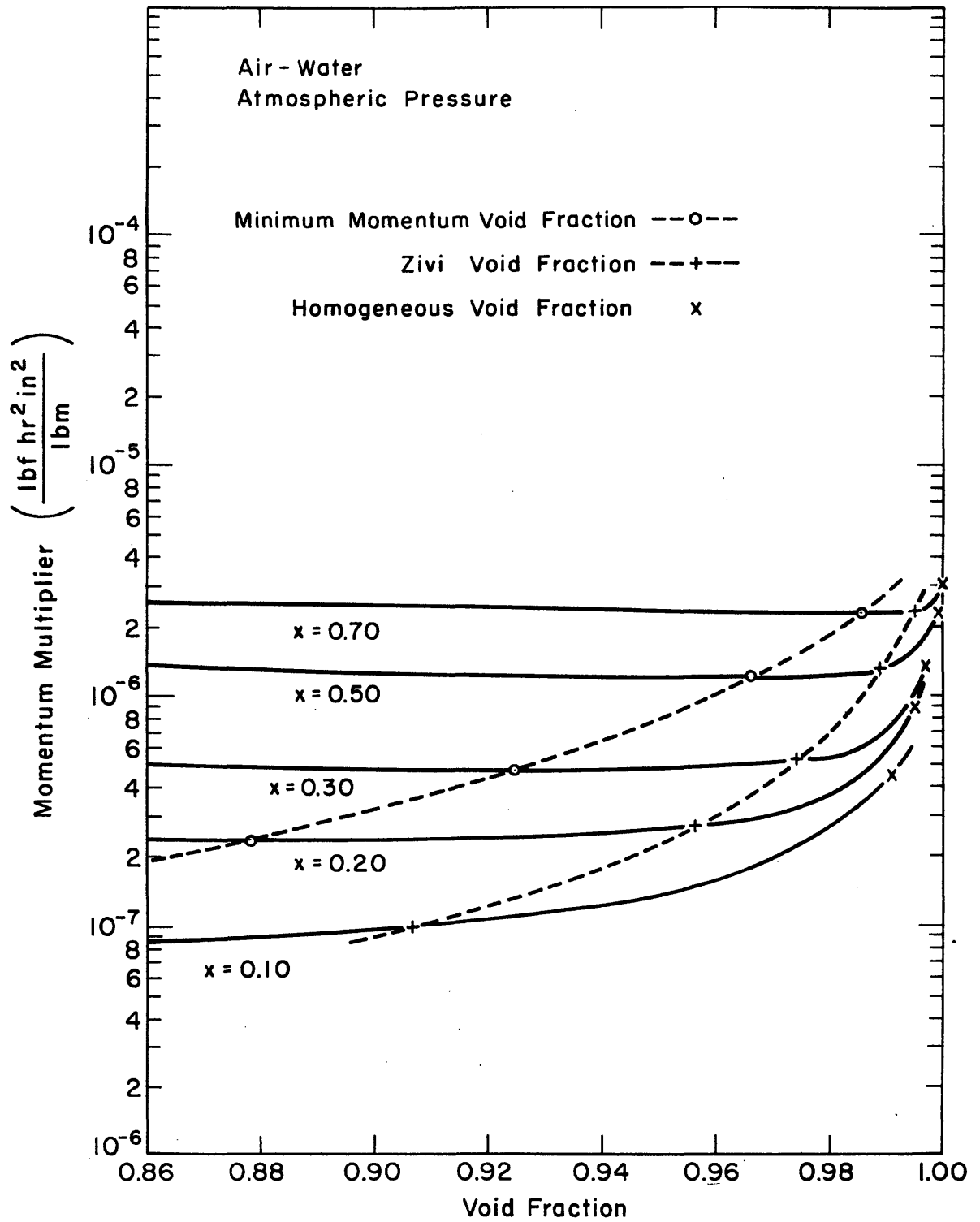


FIGURE 19. EFFECT OF VOID FRACTION ON SLIP MODEL MOMENTUM MULTIPLIER

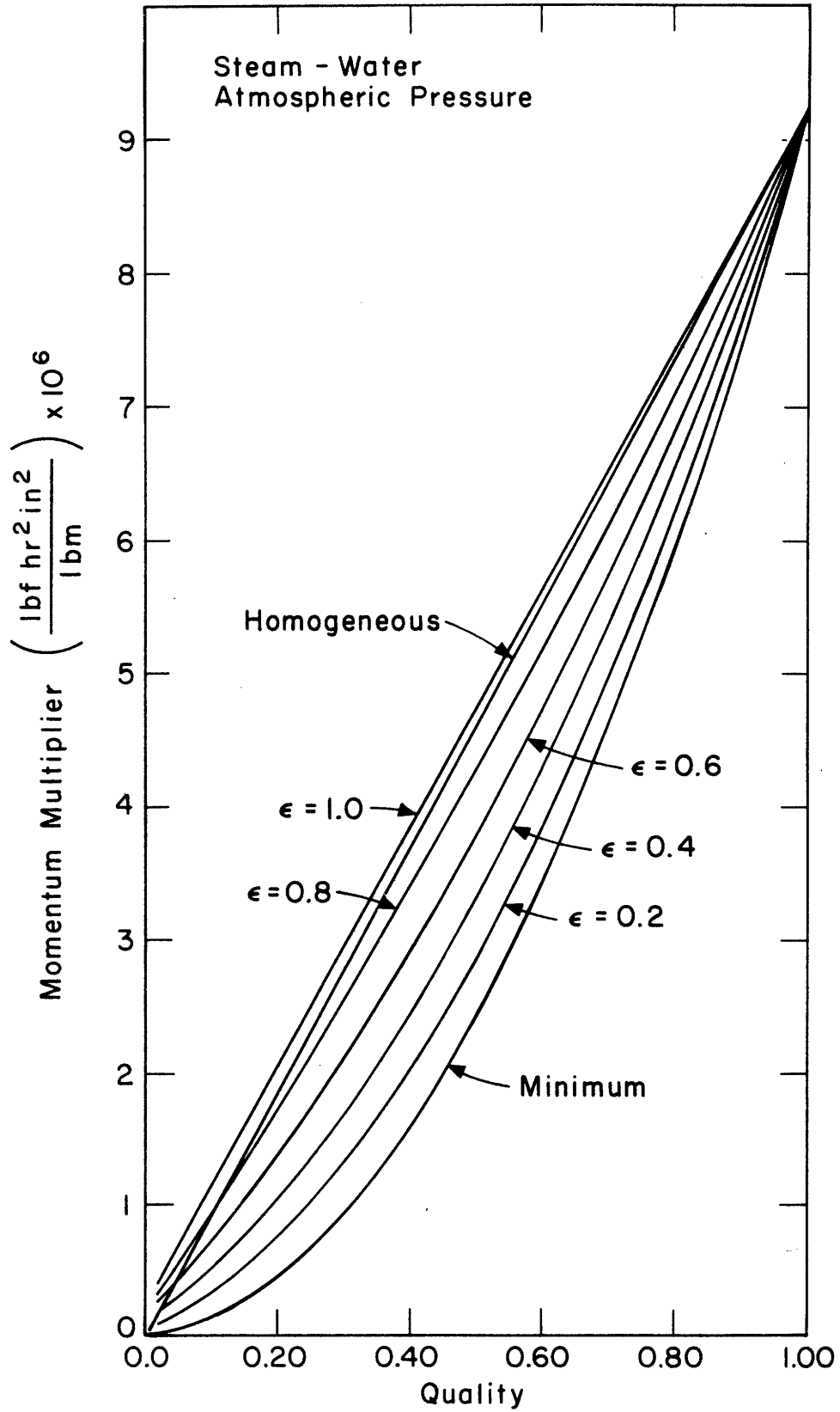


FIGURE 20. ENTRAINMENT MODEL

PAGES (S) MISSING FROM ORIGINAL

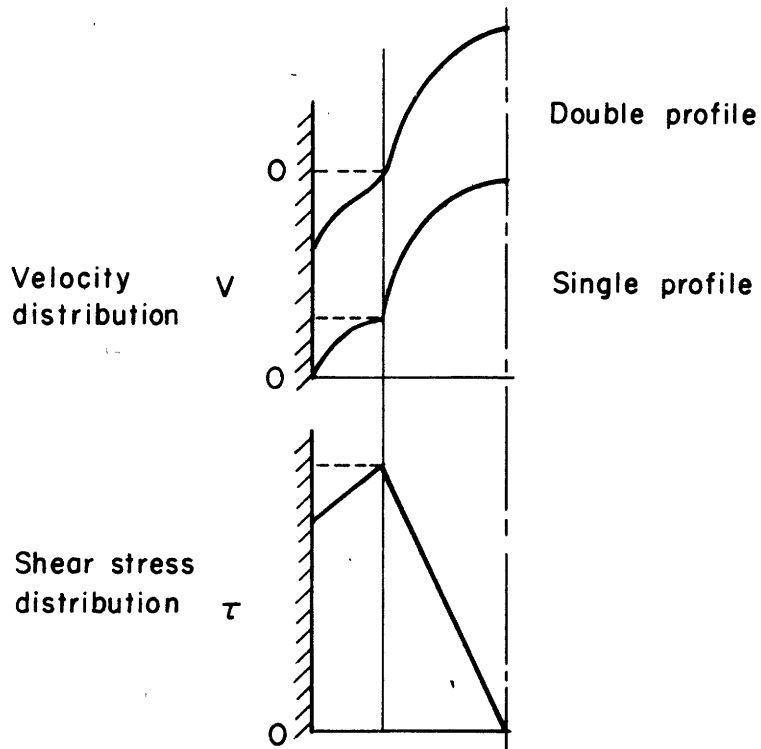


FIGURE 21. ANDERSON AND MANTZOURANIS MODEL

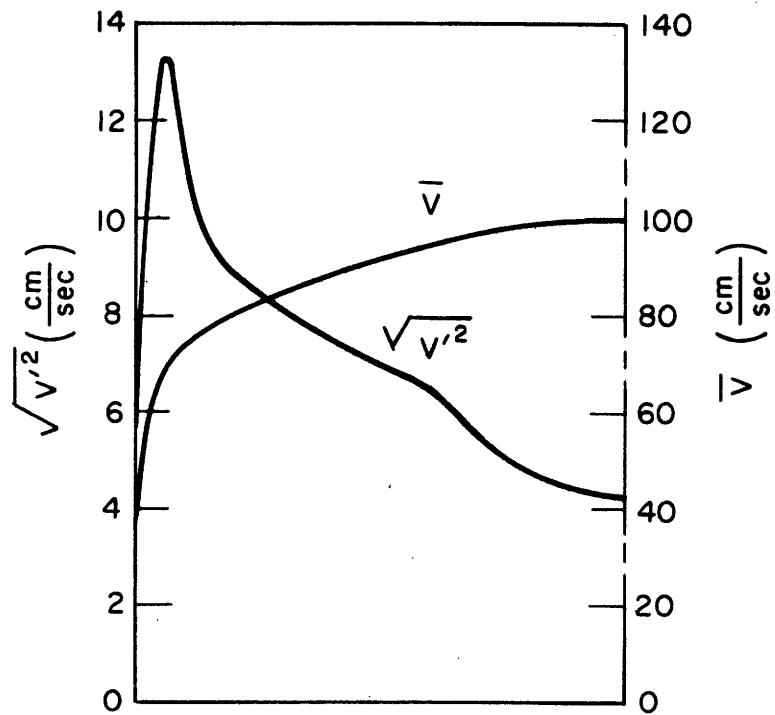


FIGURE 22. REICHARDT'S HOT-WIRE DATA

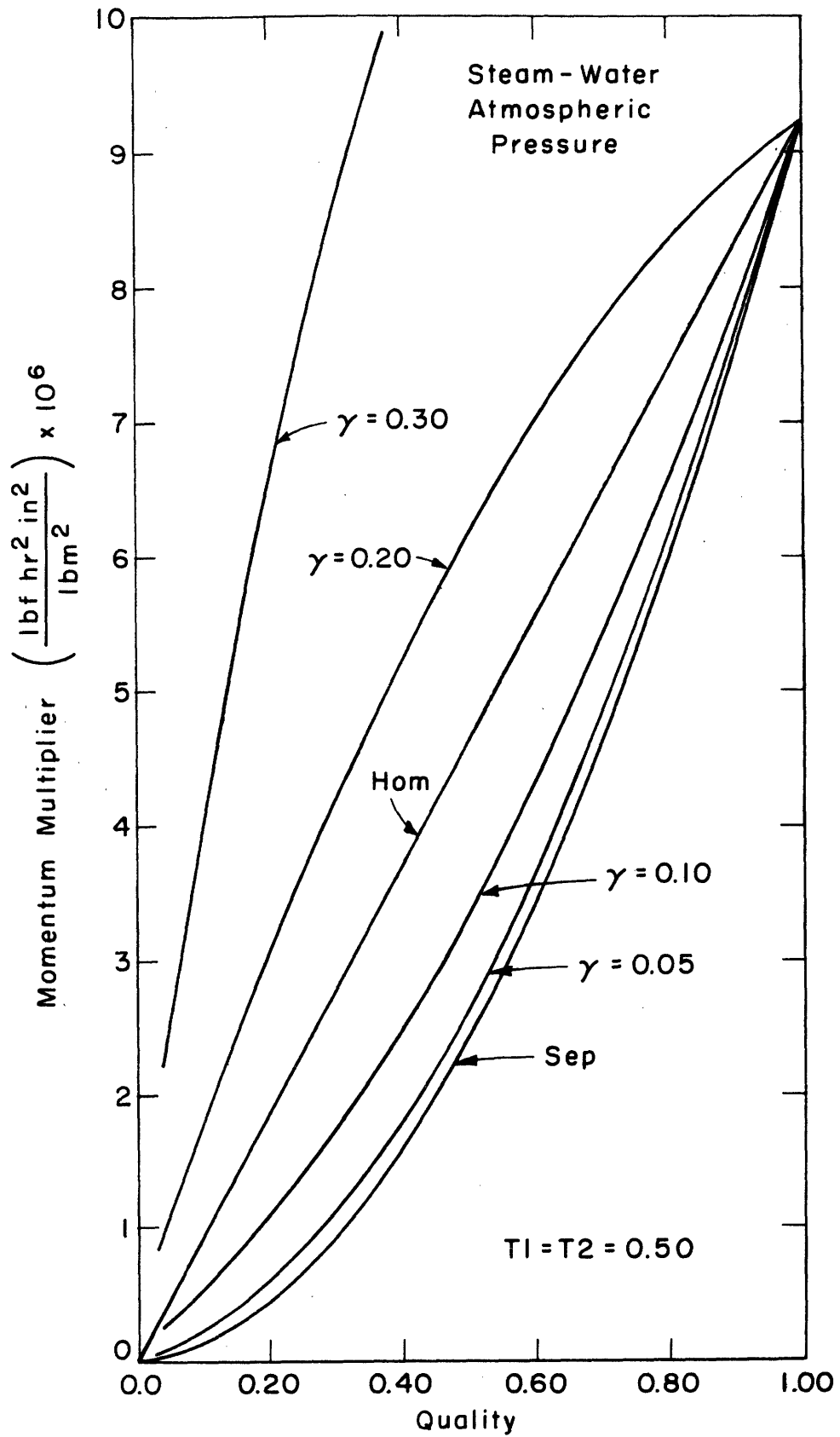


FIGURE 23. FLUCTUATING MODEL

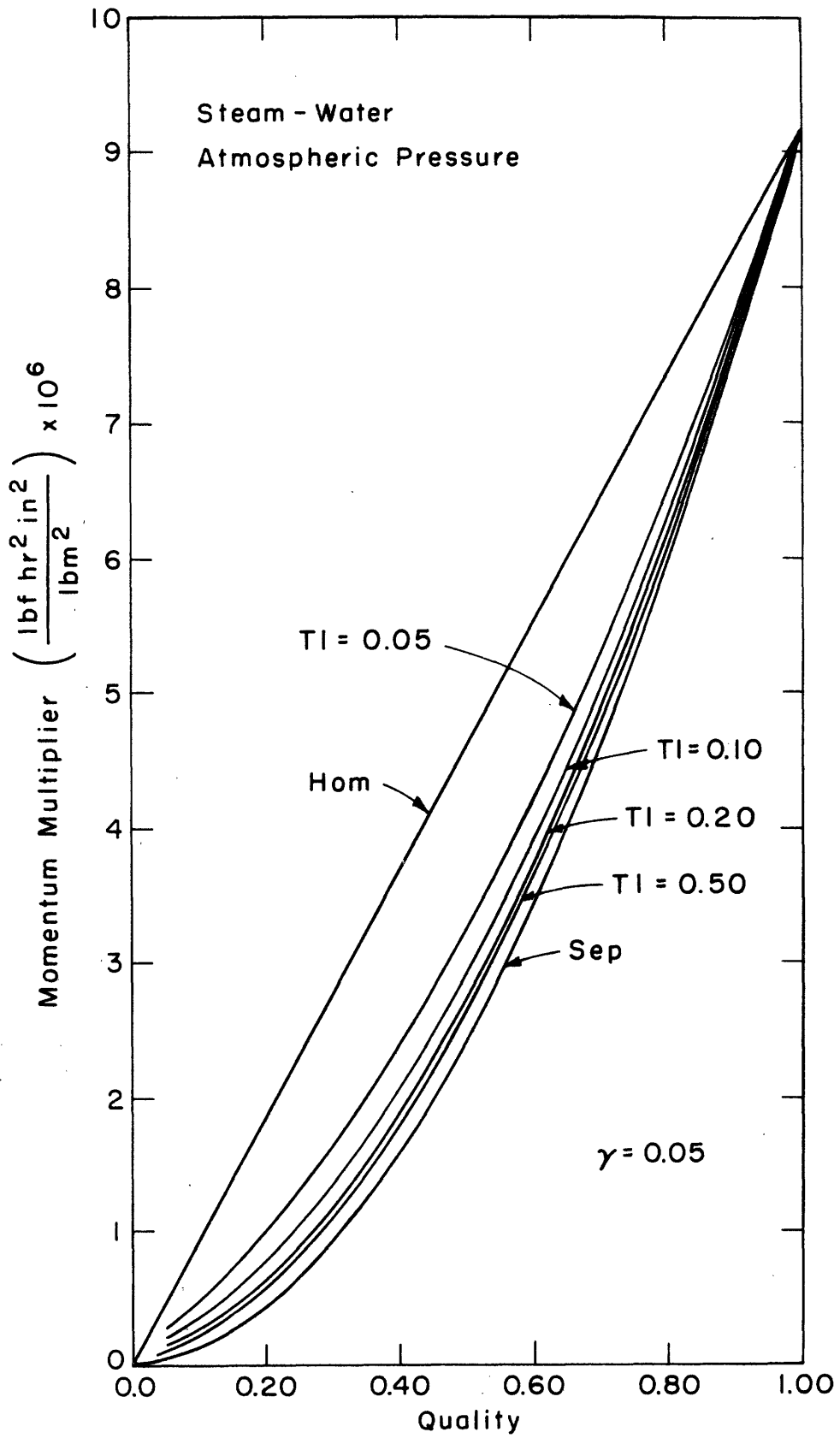


FIGURE 24. FLUCTUATING MODEL

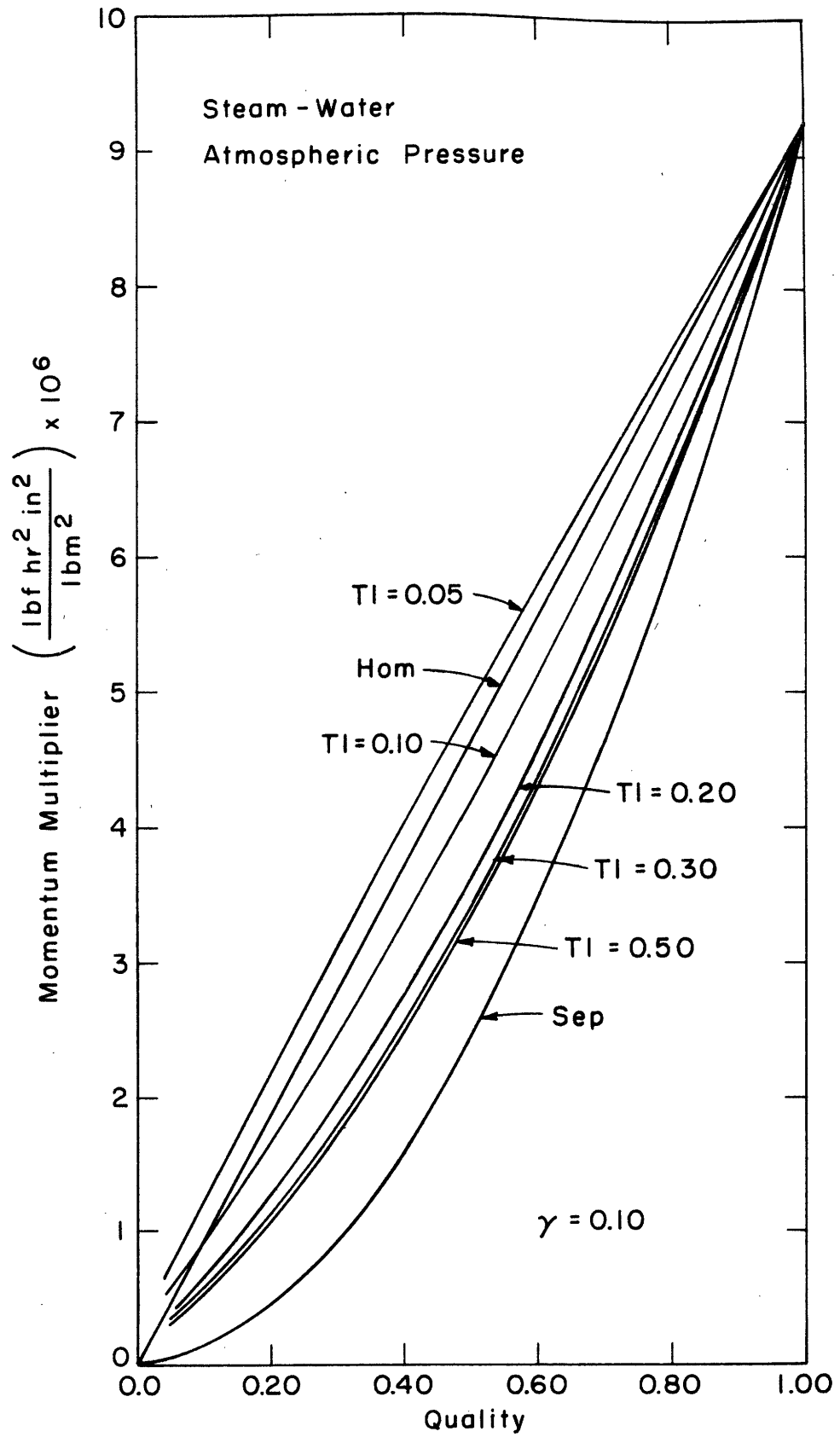


FIGURE 25. FLUCTUATING MODEL

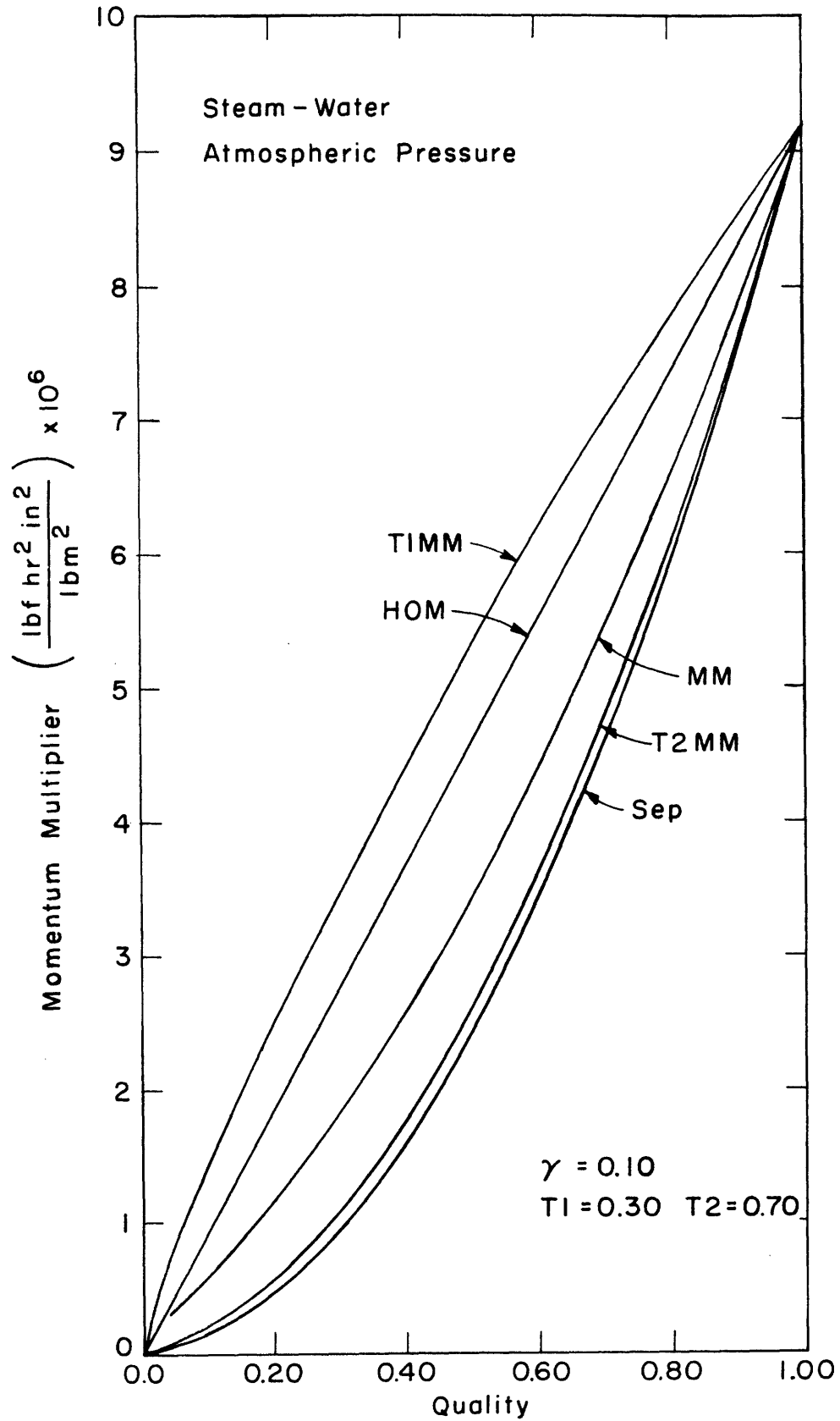


FIGURE 26.

FLUCTUATING MODEL

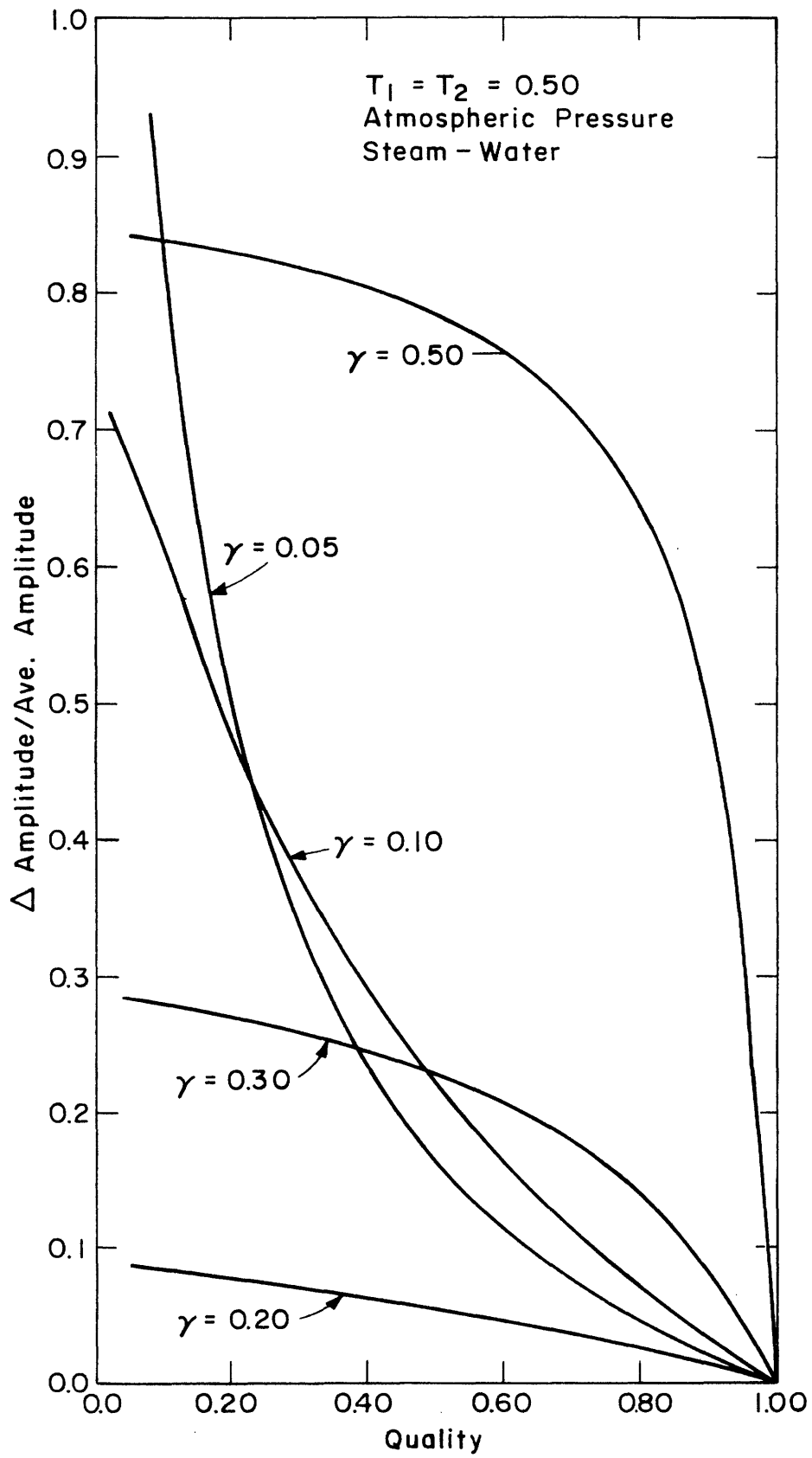


FIGURE 27. FLUCTUATION MODEL

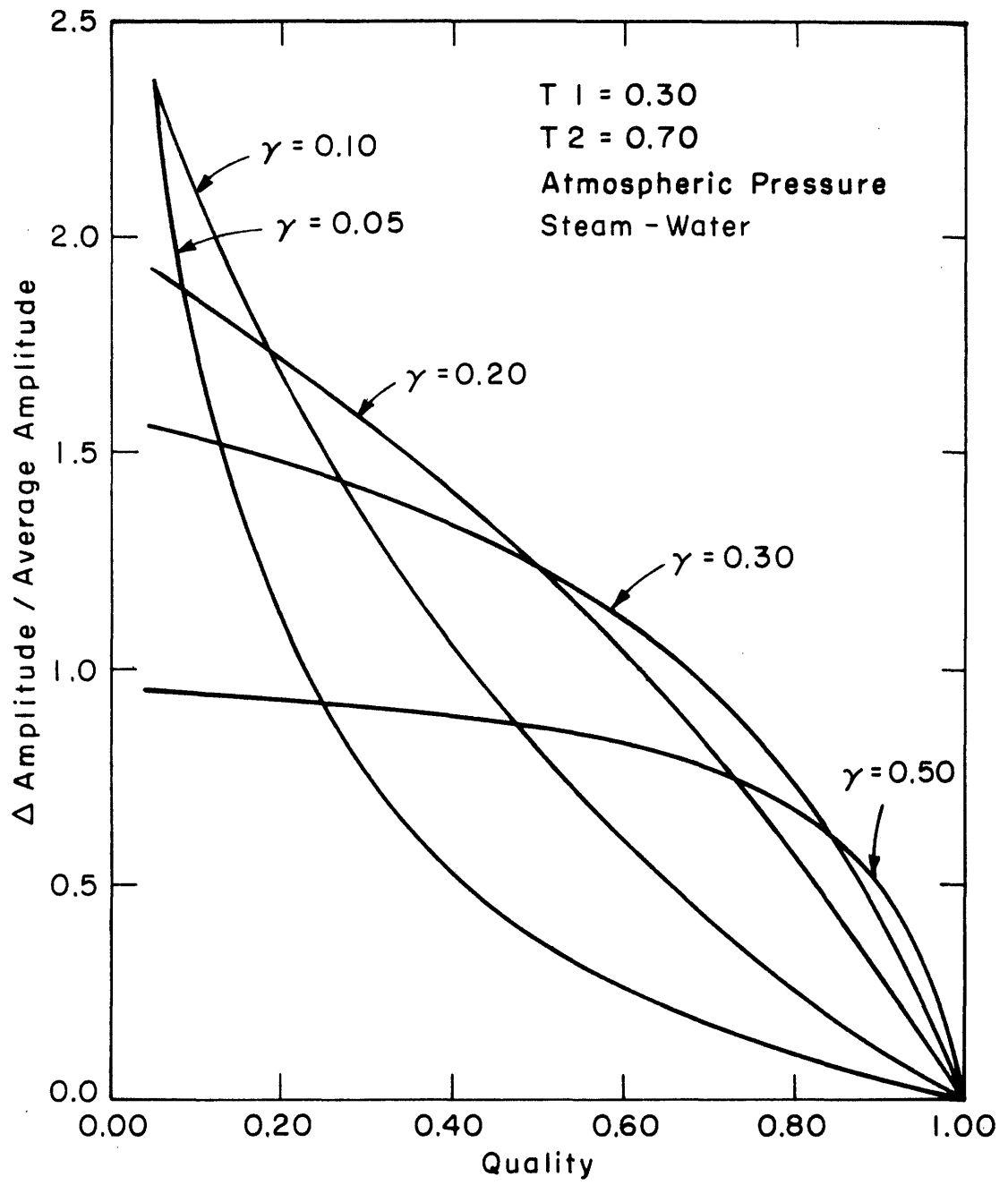


FIGURE 28. FLUCTUATION MODEL

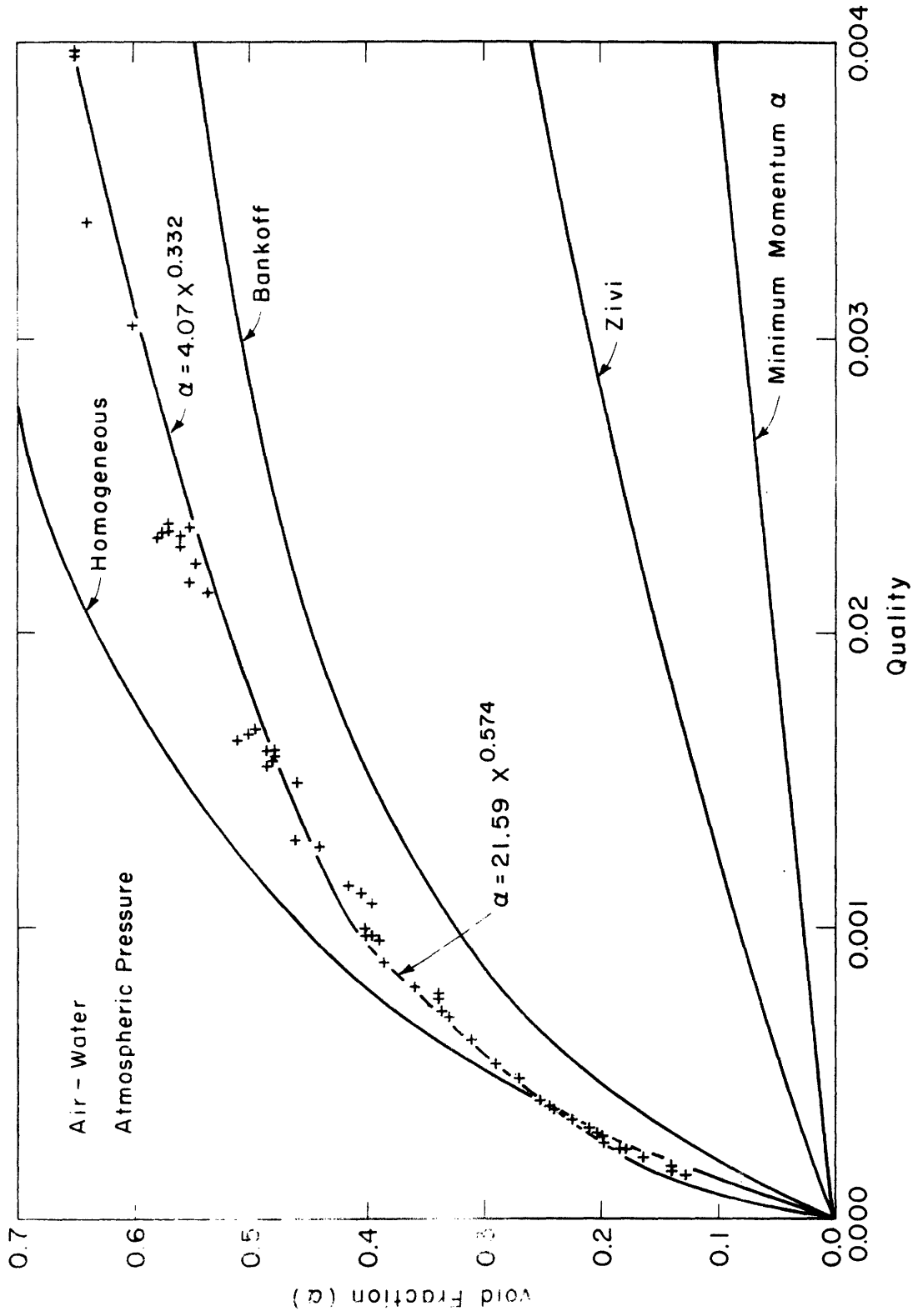


FIGURE 29. ROSE'S VOID FRACTION DATA

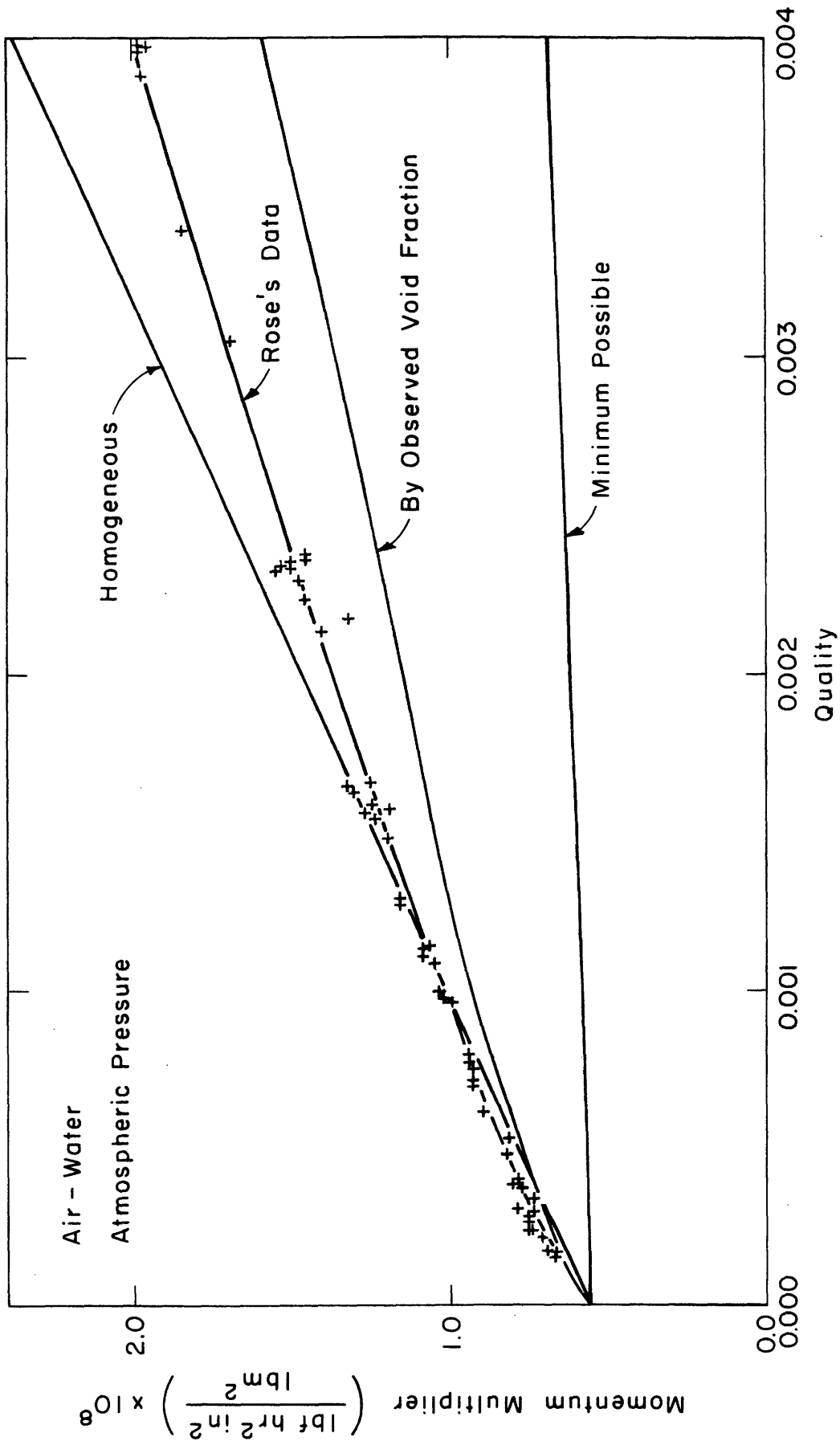


FIGURE 30. ROSE'S MOMENTUM FLUX DATA

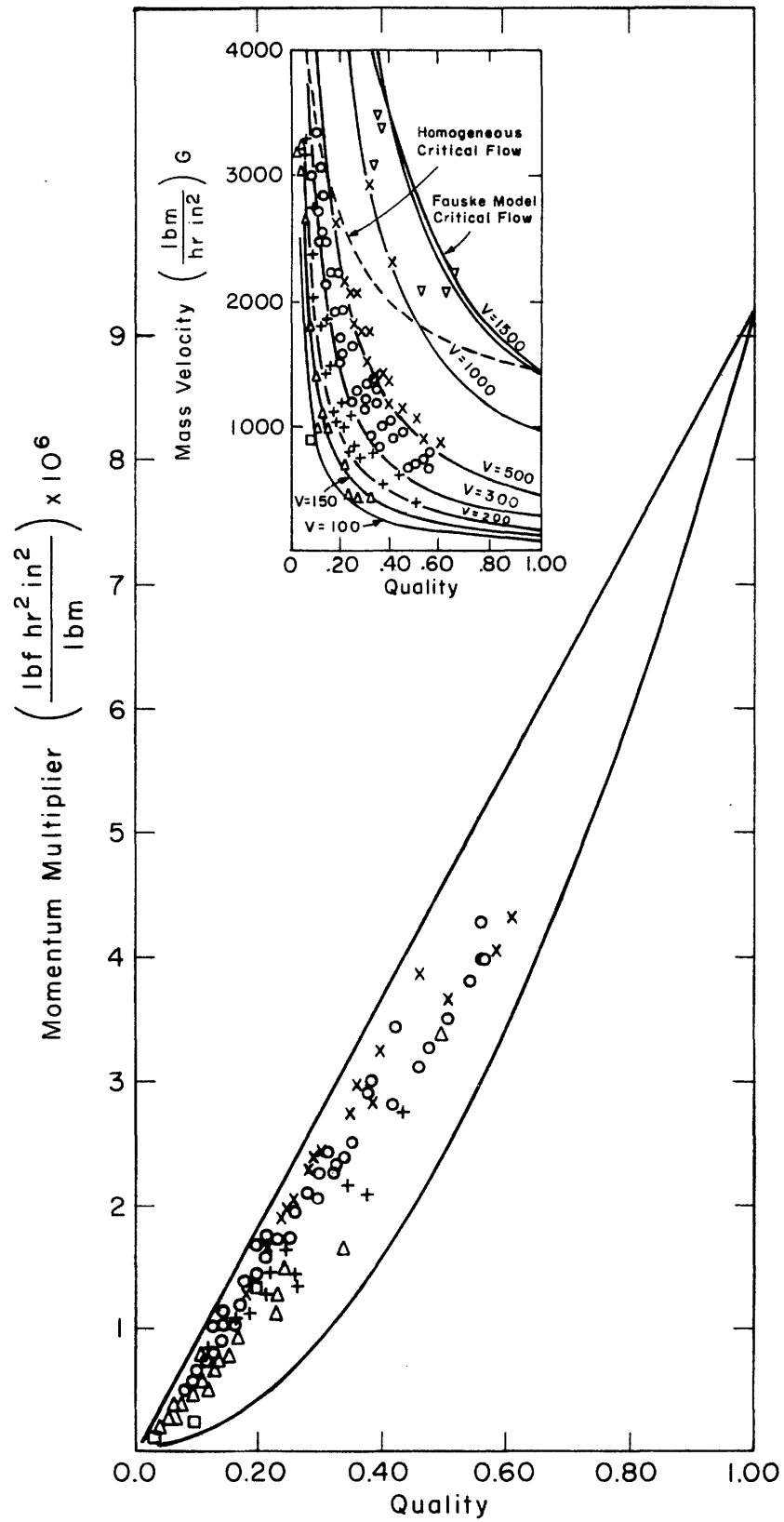


FIGURE 31. ATMOSPHERIC PRESSURE
ONE INCH PIPE

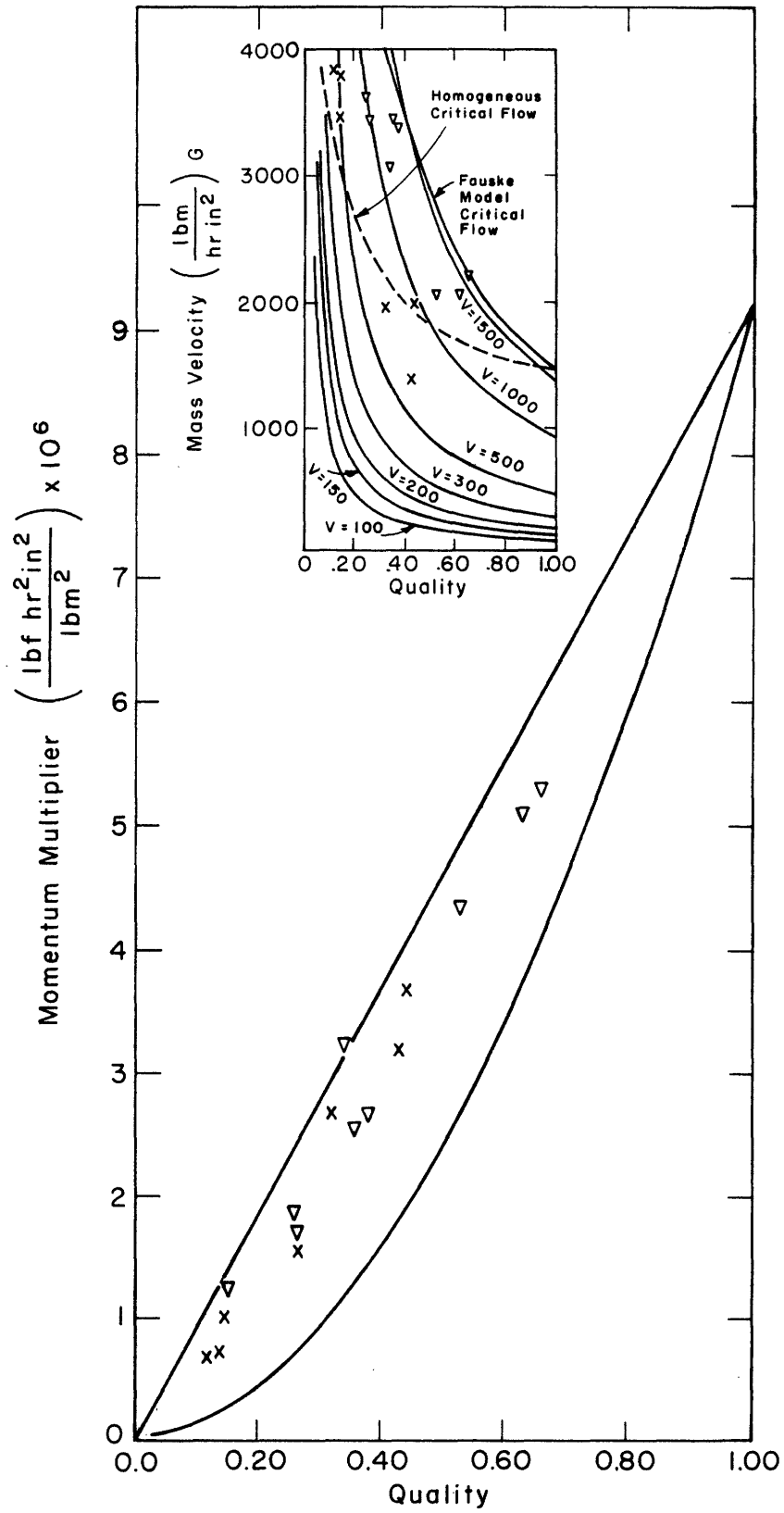


FIGURE 32. ATMOSPHERIC PRESSURE ONE-HALF INCH PIPE

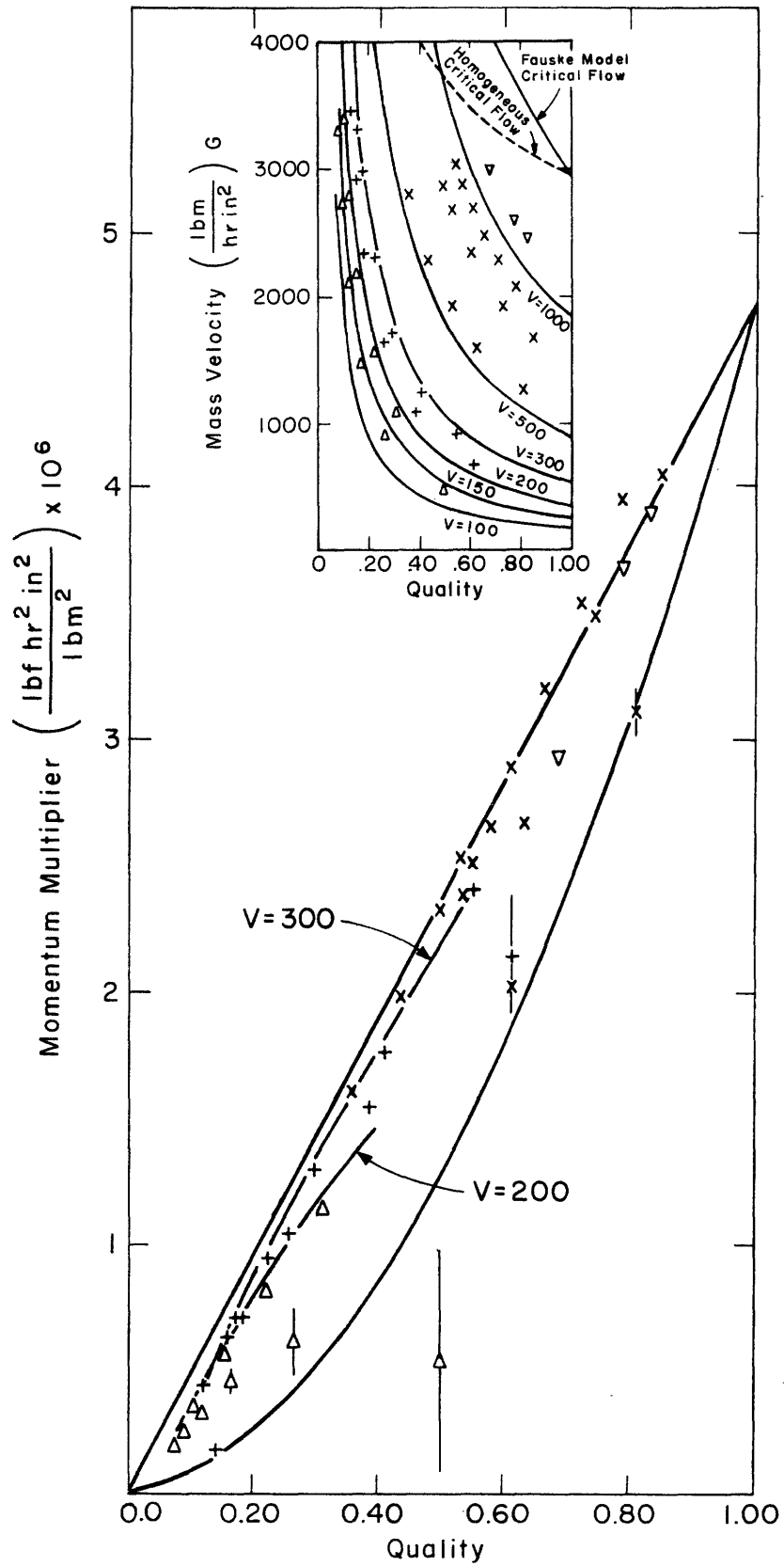


FIGURE 33. 30 PSIA ONE INCH PIPE

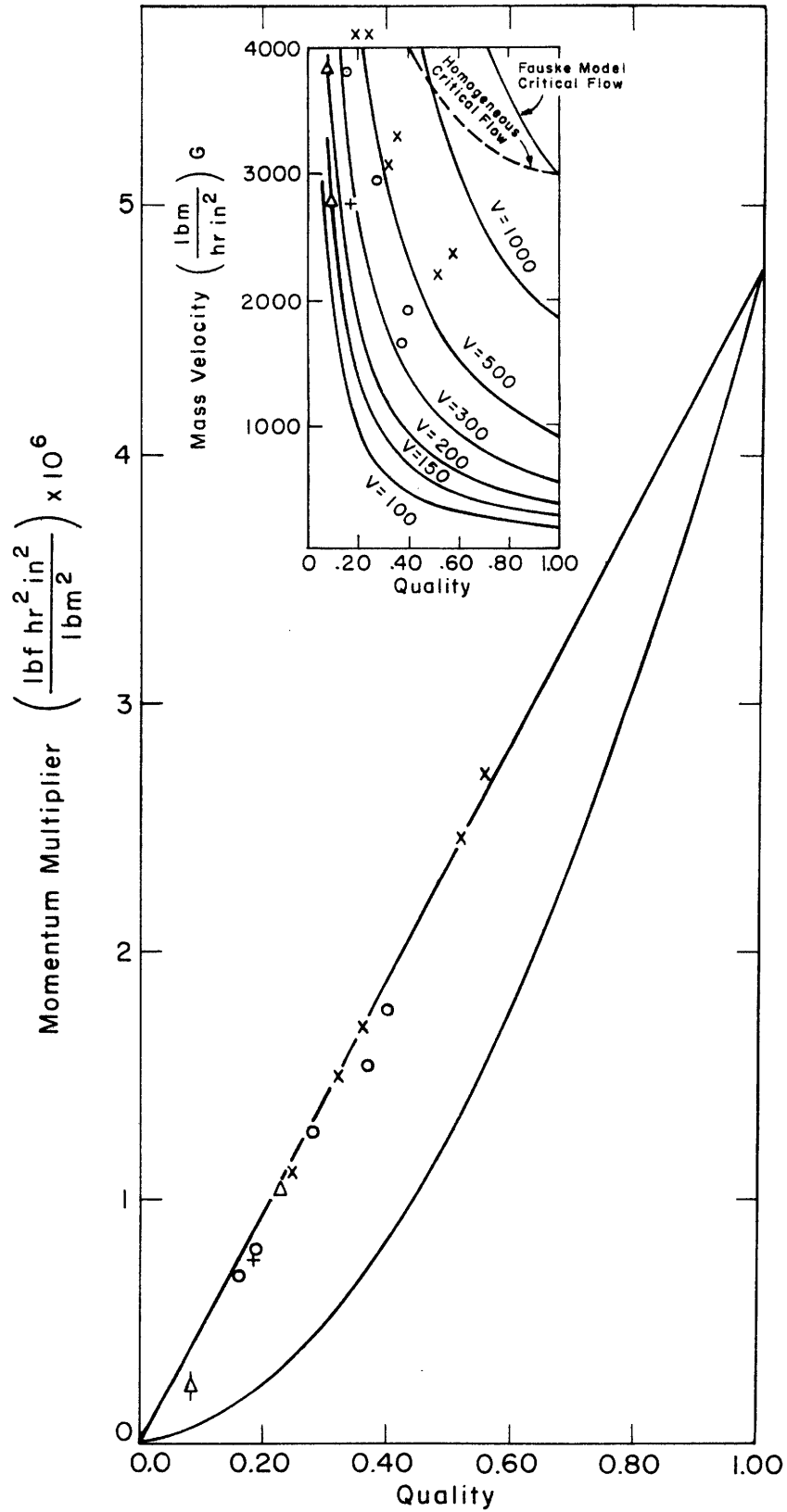


FIGURE 34. 30 PSIA ONE-HALF INCH PIPE

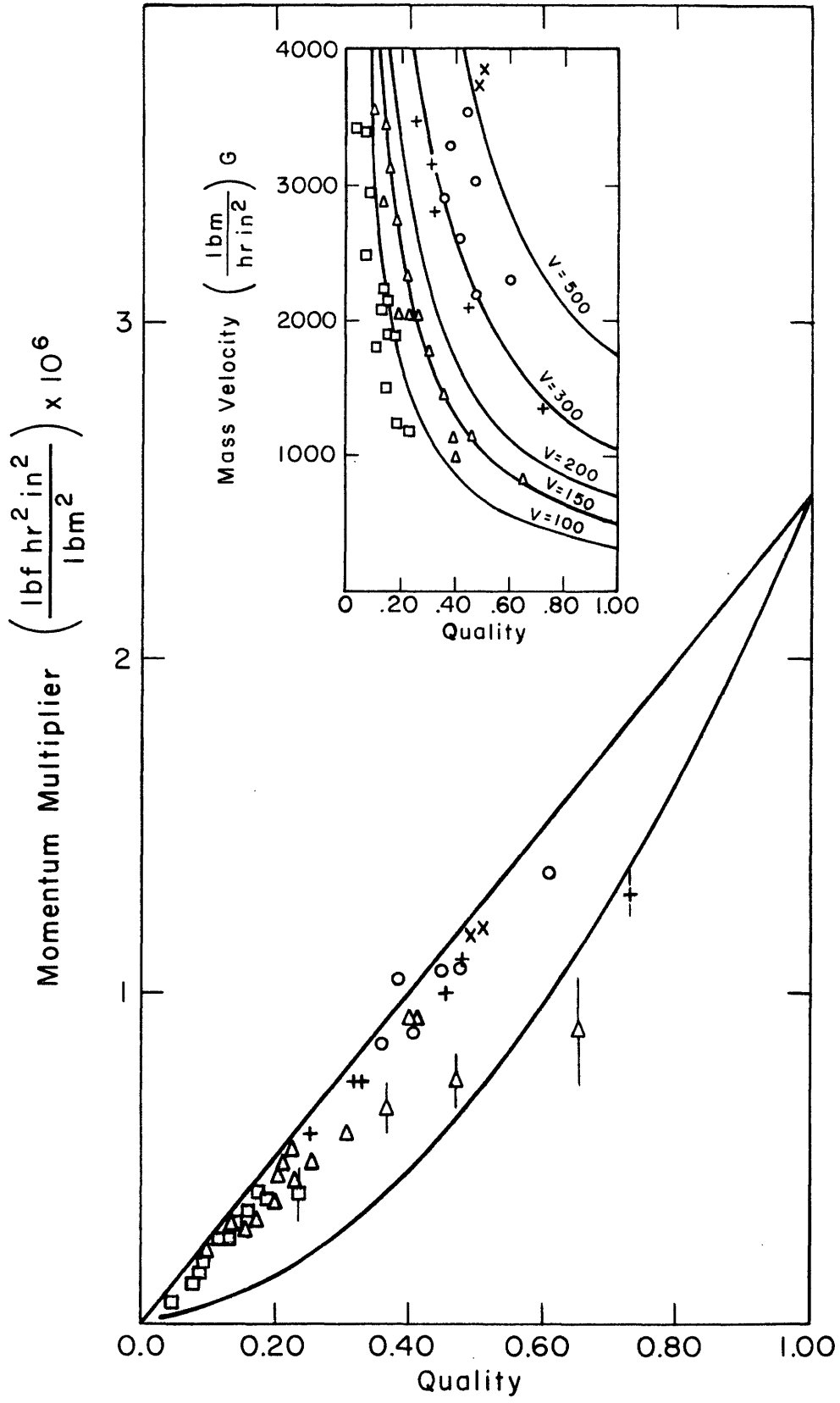


FIGURE 35. 60 PSIA ONE INCH PIPE

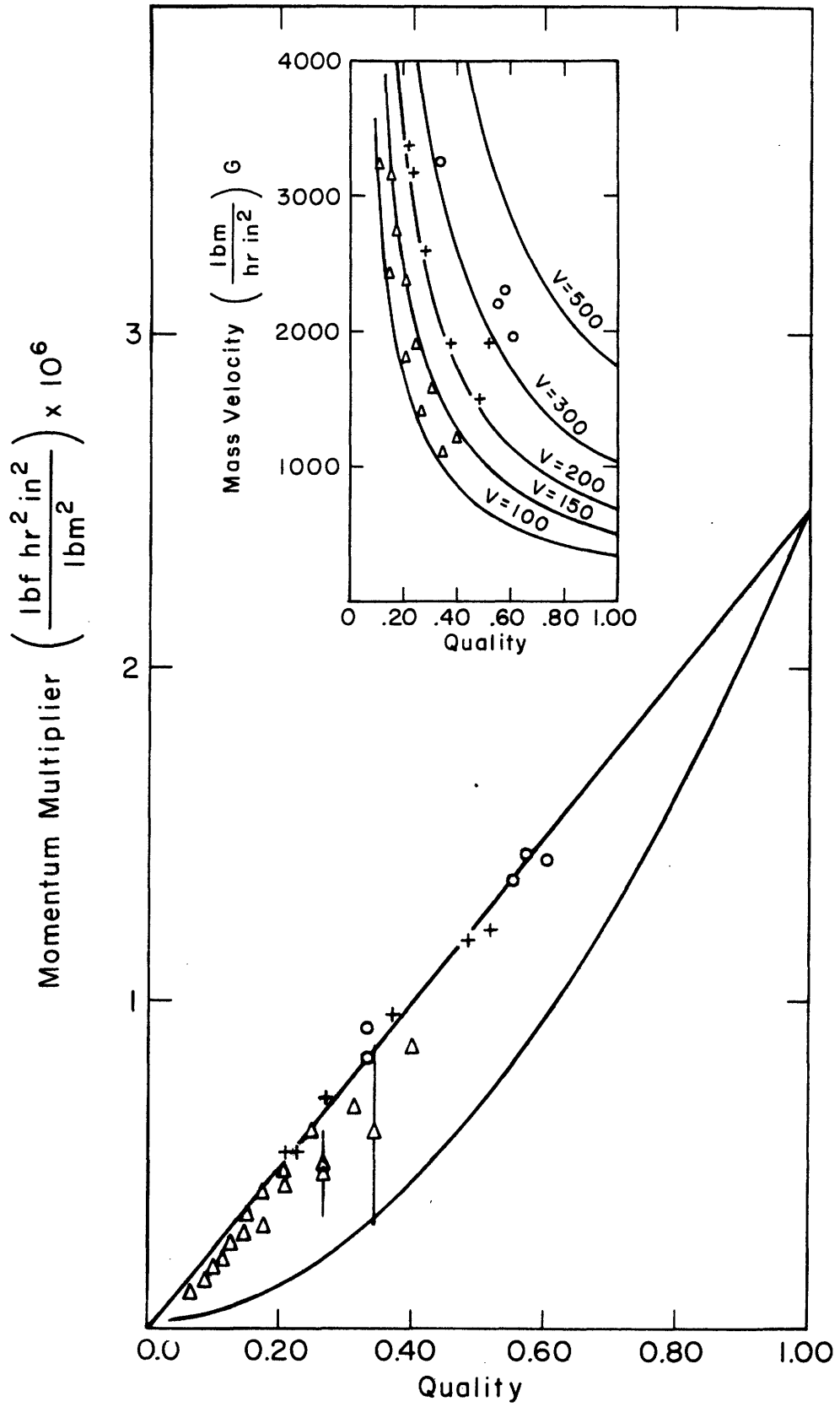


FIGURE 36. 60PSIA ONE-HALF INCH PIPE

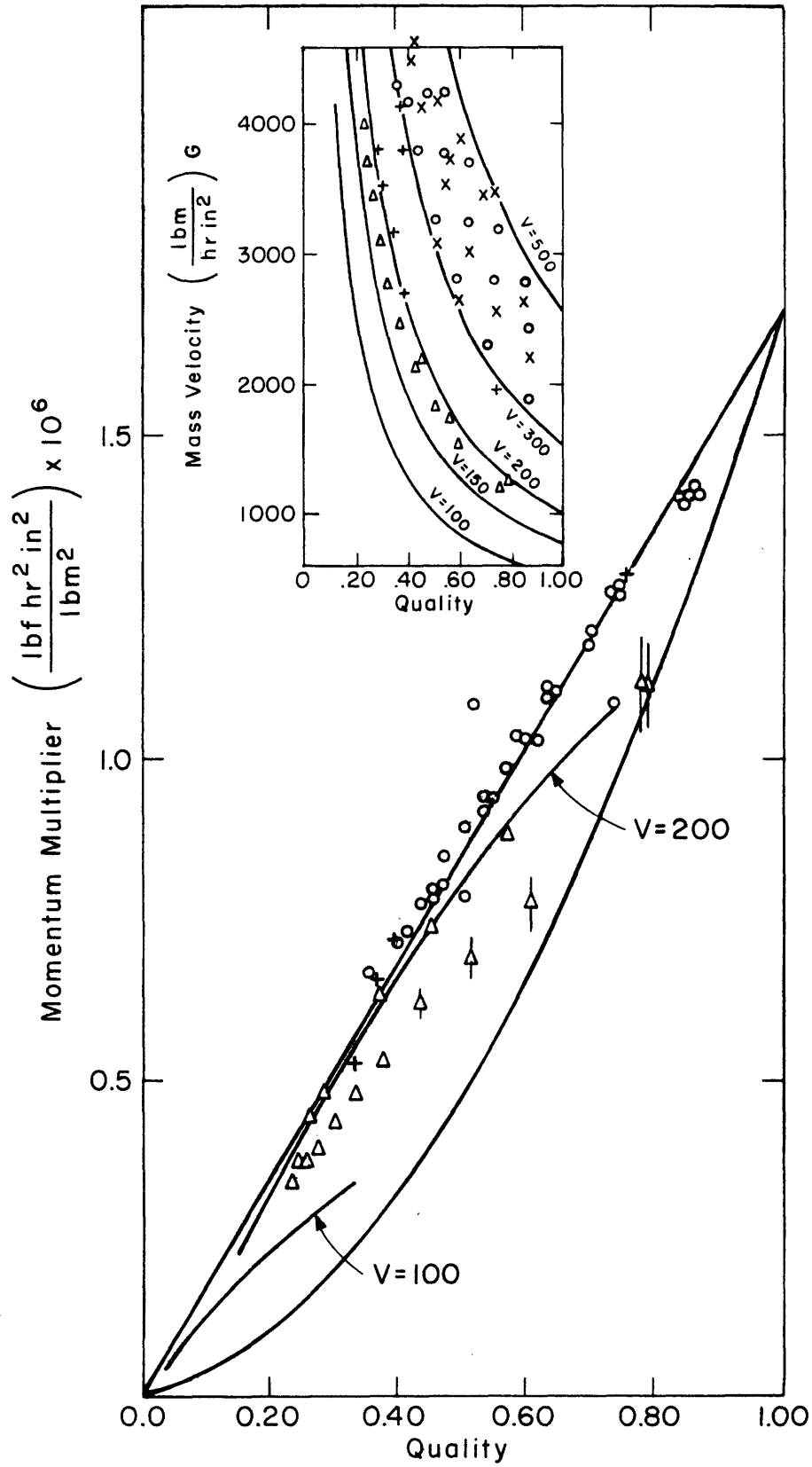


FIGURE 37. 90 PSIA ONE INCH PIPE

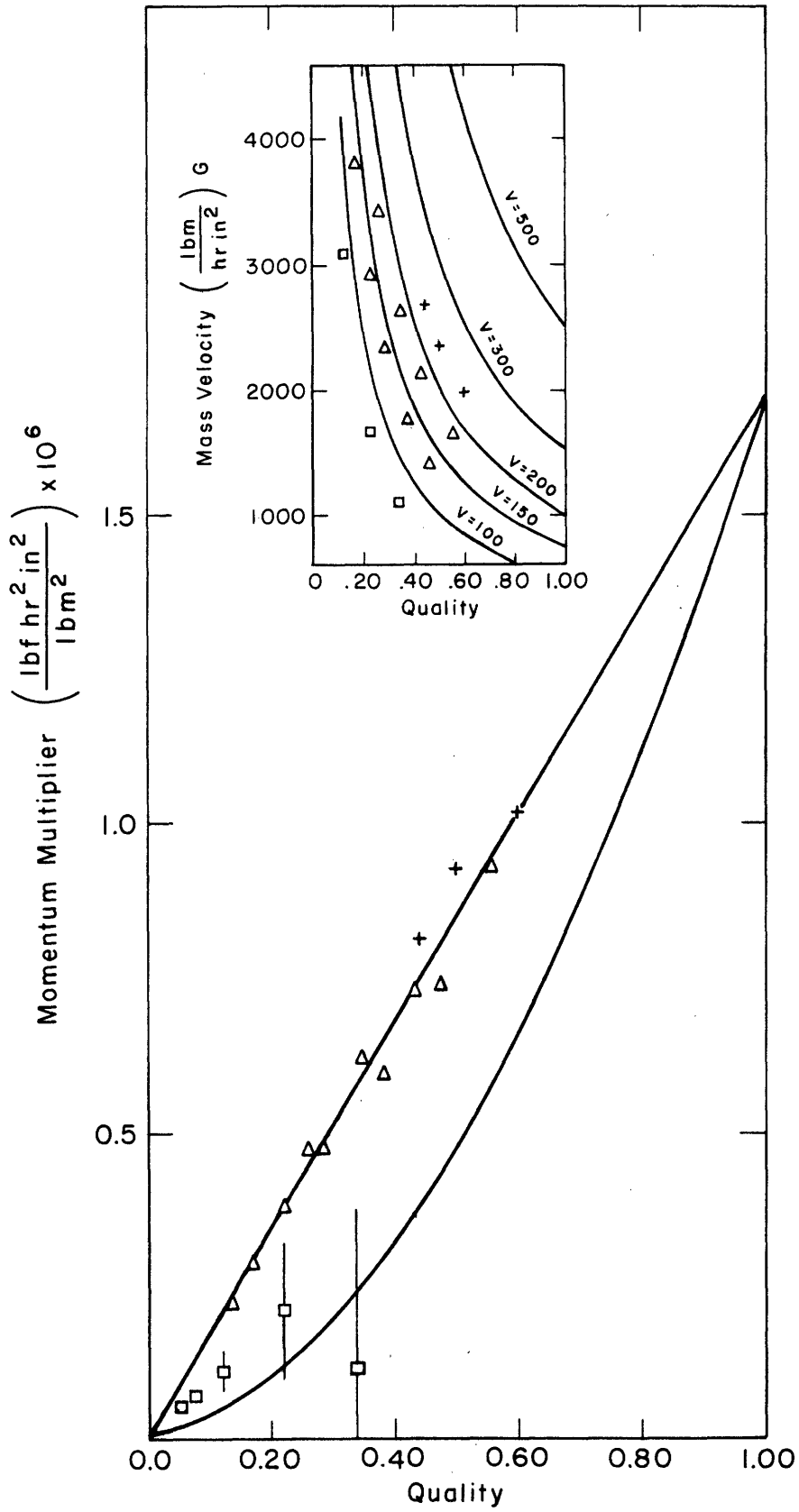


FIGURE 38. 90 PSIA ONE-HALF INCH PIPE

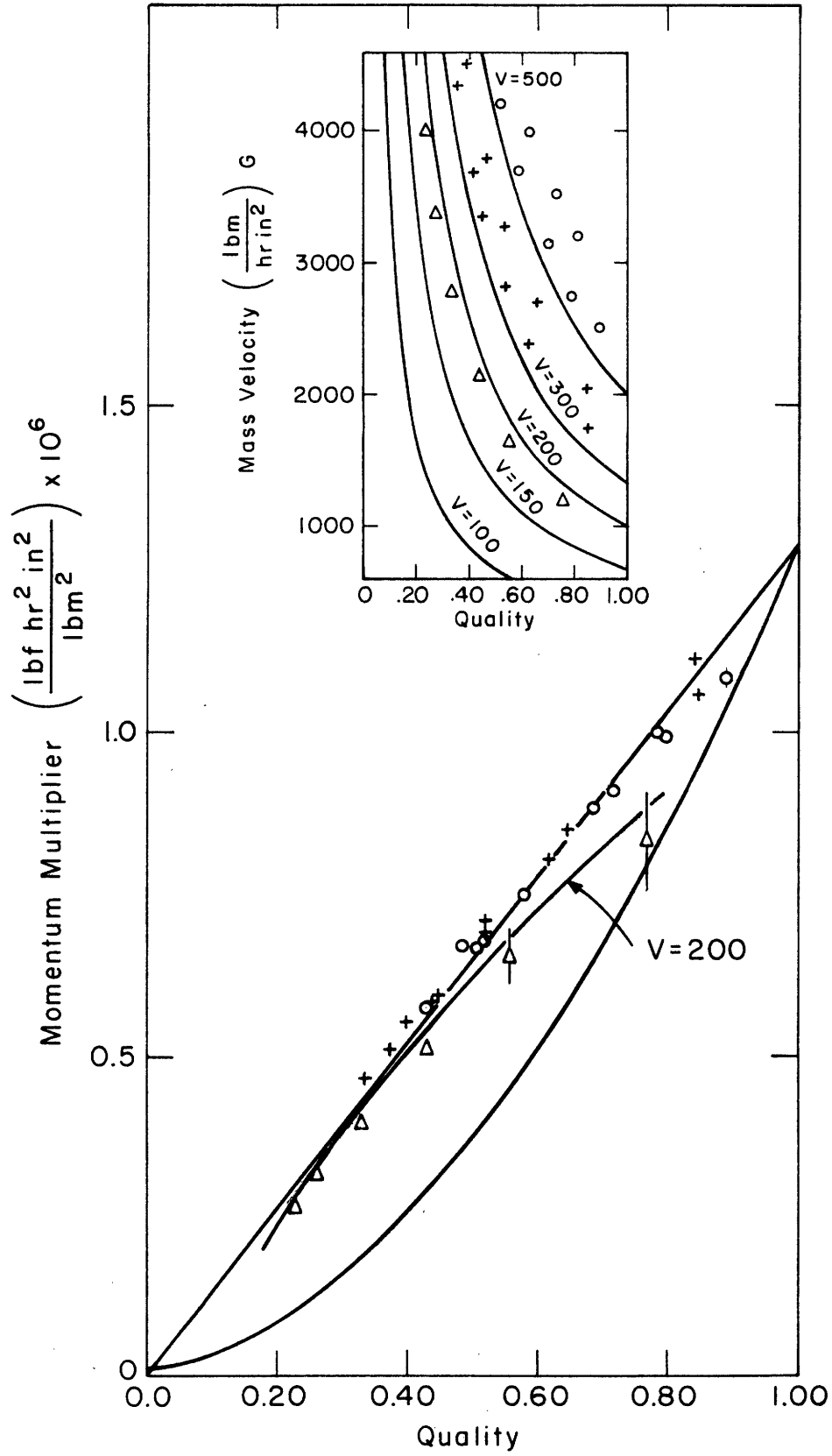


FIGURE 39. 120 PSIA ONE INCH PIPE

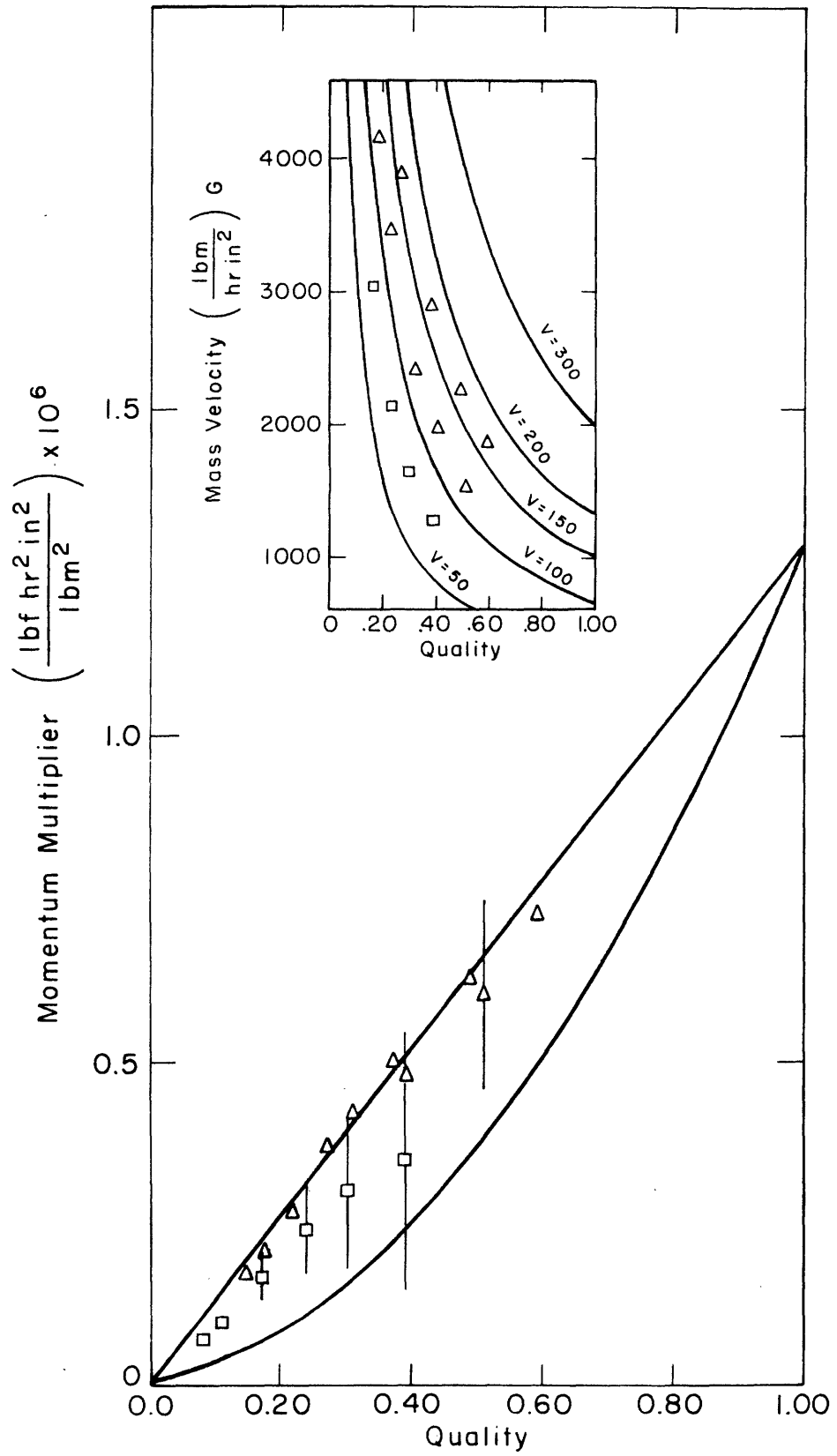


FIGURE 40. 120 PSIA ONE-HALF INCH PIPE

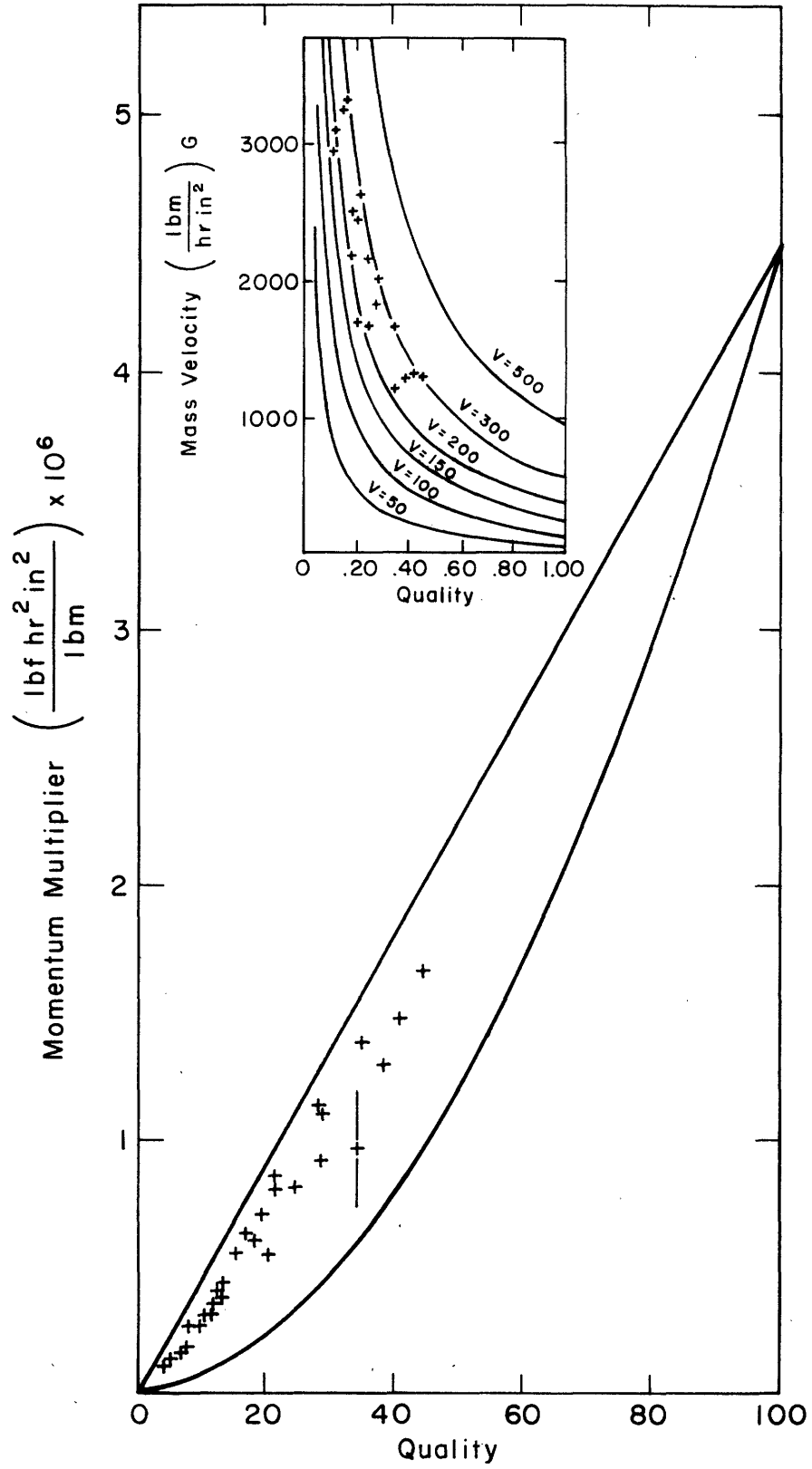


FIGURE 41.

AIR - WATER 65°F

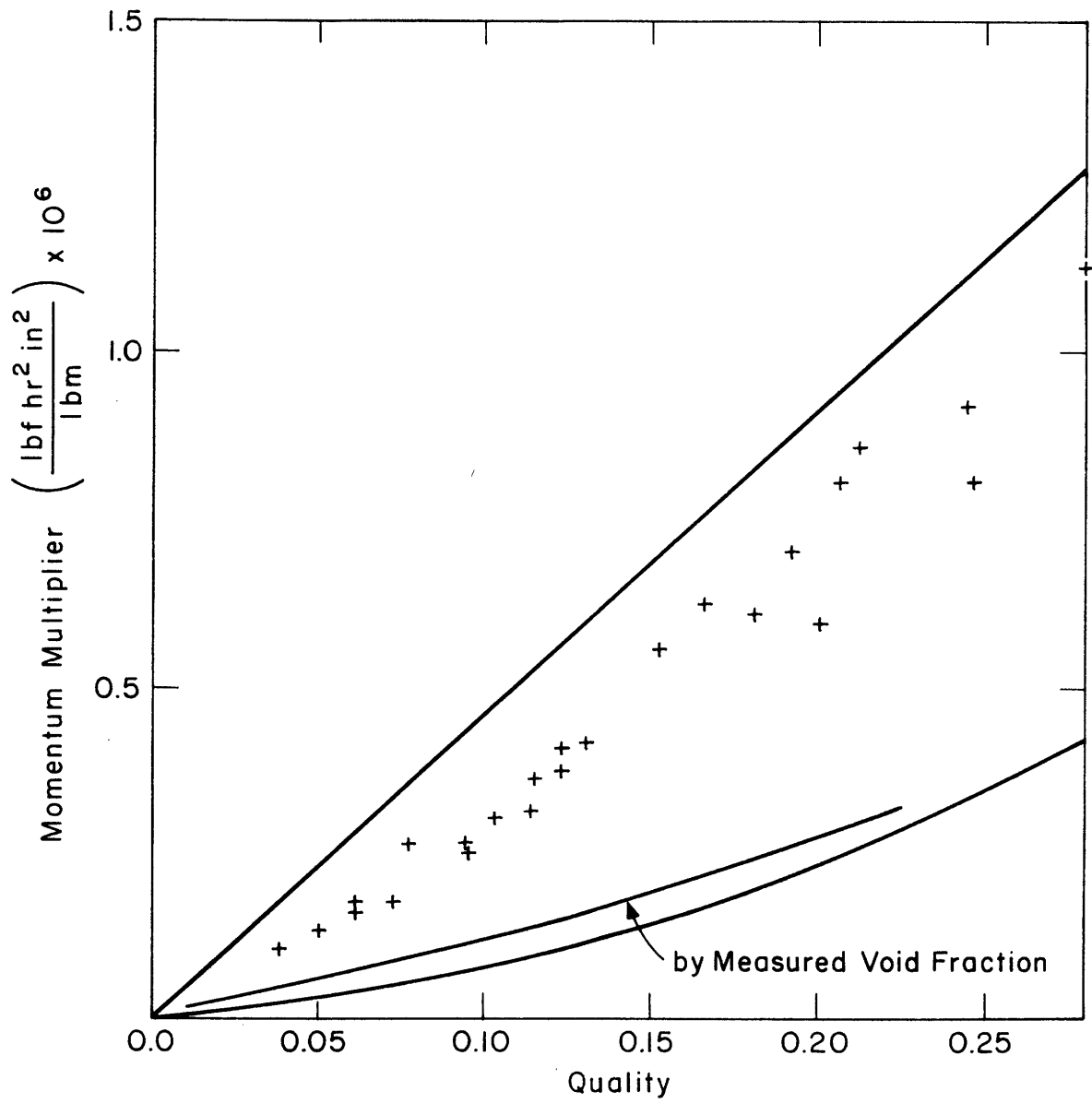


FIGURE 42. AIR - WATER 65 °F

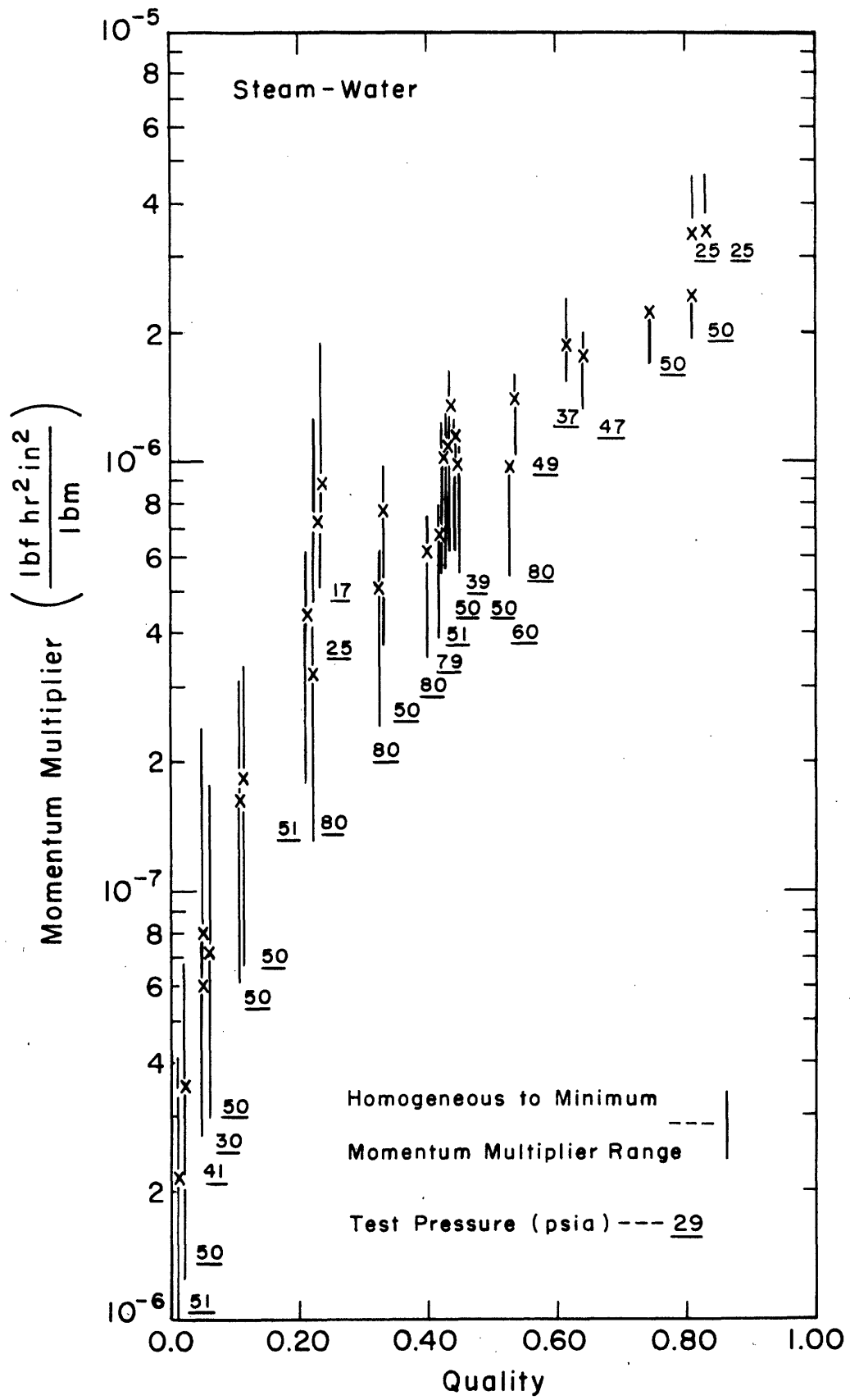


FIGURE 43. DATA OF VANCE

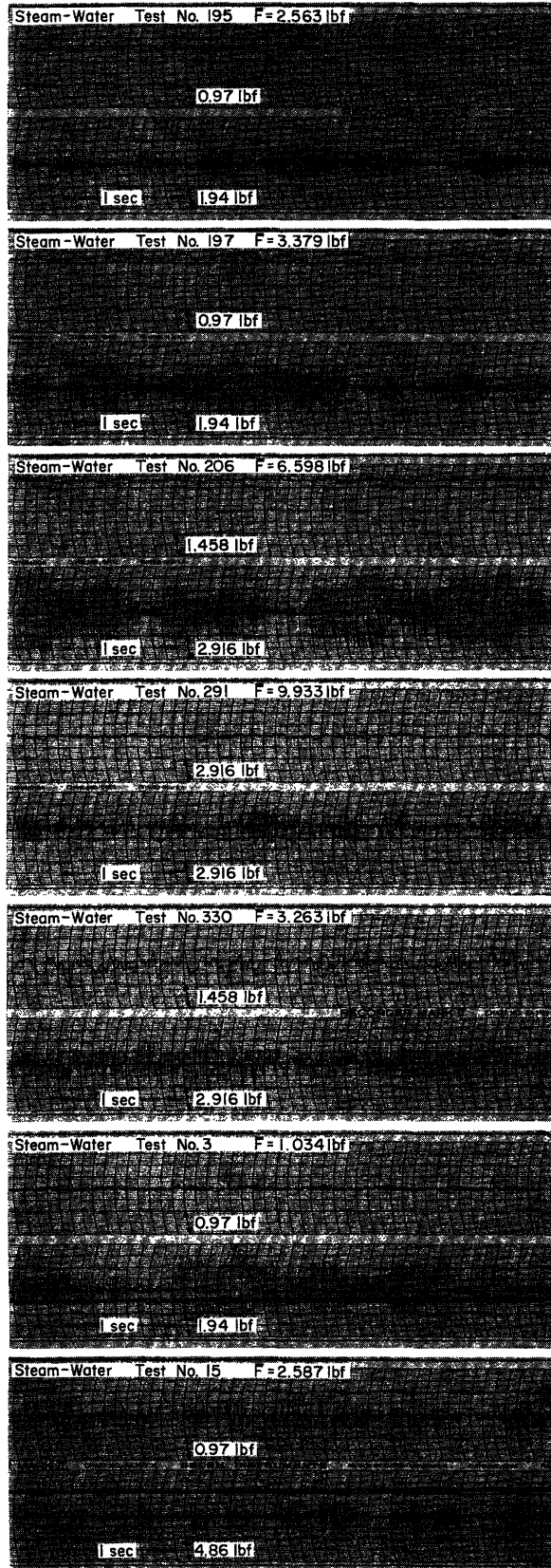


FIGURE 44 BRUSH RECORDINGS

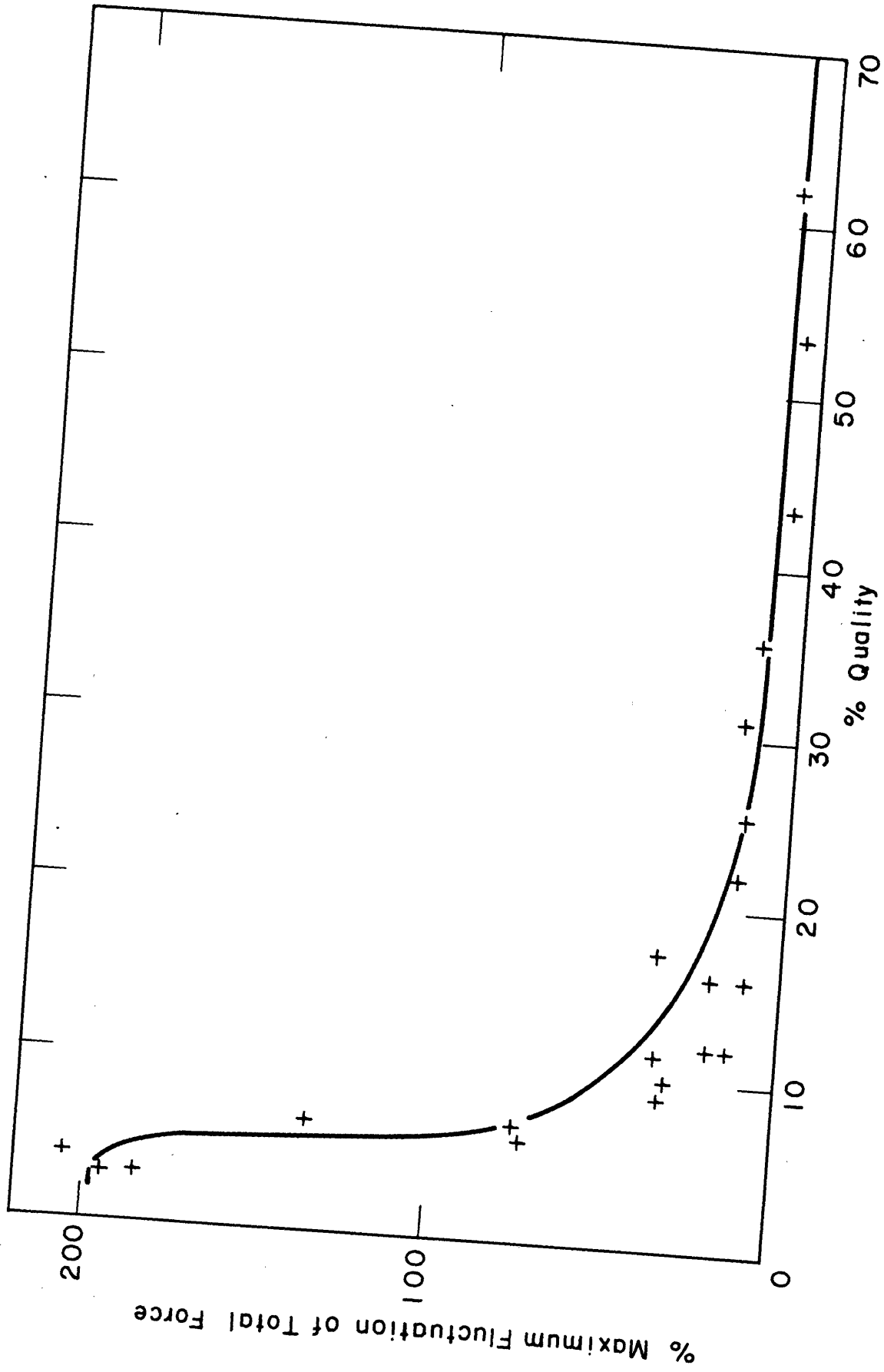


FIGURE 45. FLUCTUATION MAGNITUDE

Steam-Water, Atmospheric Pressure, One Inch Pipe

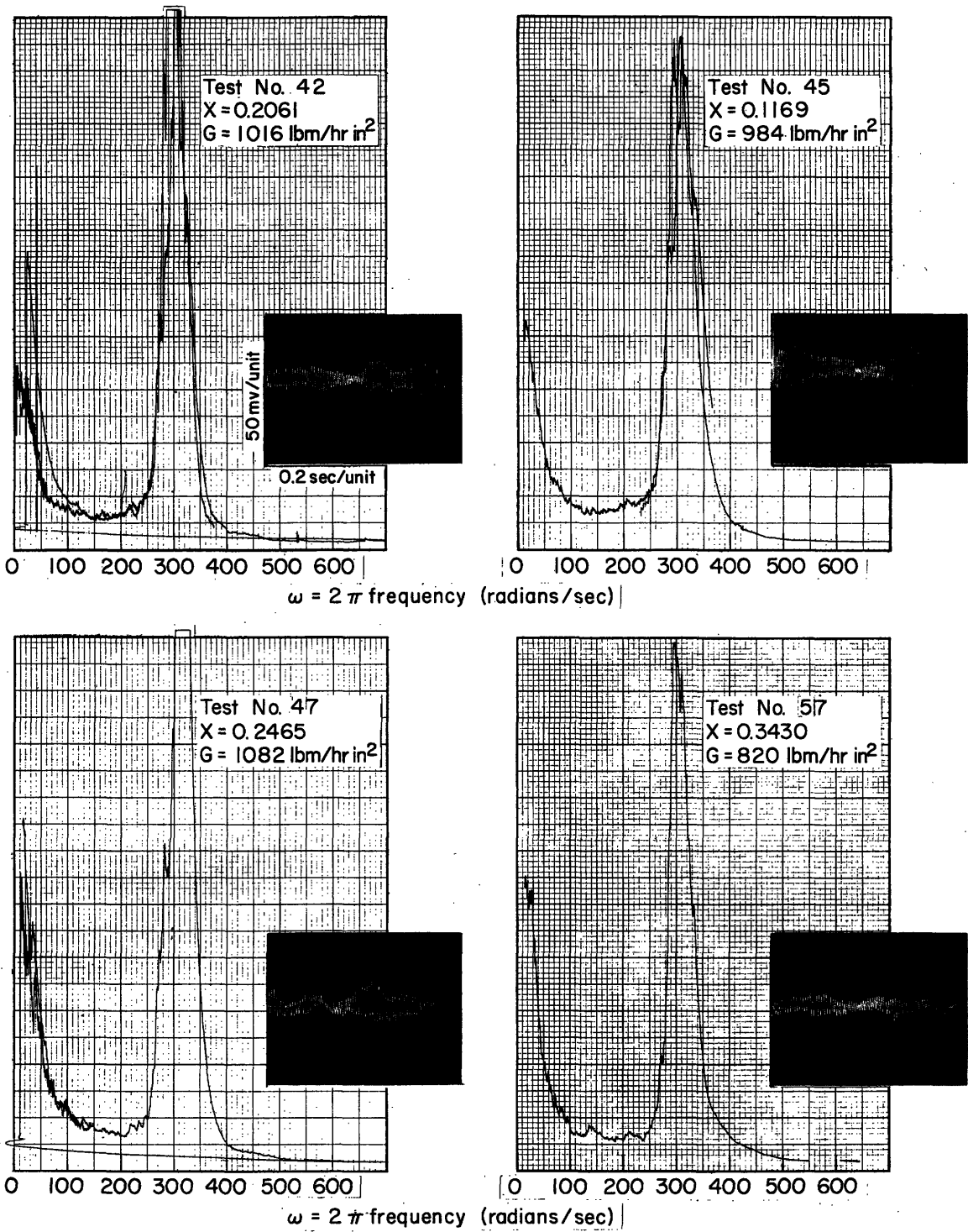


FIGURE 46. MOMENTUM FLUX SPECTRAL DENSITY

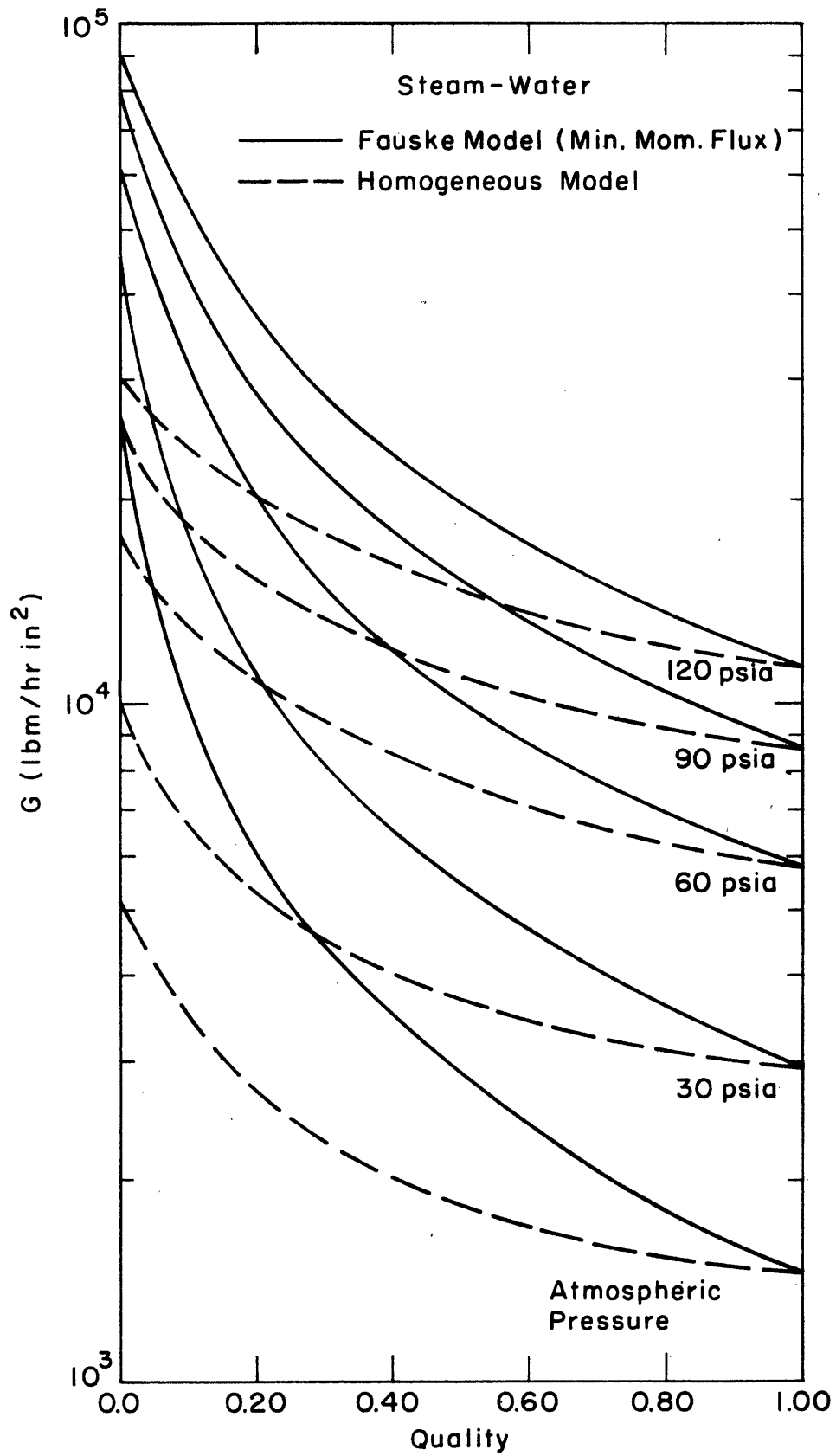


FIGURE 47. CRITICAL FLOW